CONSTRUCTION MATERIALS CONSULTANTS, INC.

Laboratory Analyses of Four Masonry Mortars & A Stucco Sample From The Georgetown Reservoir In Washington, D.C.

Georgetown Reservoir
Washington, D.C.

May 18, 2021
CMC 0421118

TABLE OF CONTENTS

LABORATORY ANALYSES OF FOUR MASONRY MORTARS & A STUCCO SAMPLE FROM THE GEORGETOWN RESERVOIR IN WASHINGTON, D.C.

ABSTRACT

The Georgetown Reservoir is a reservoir that is part of the water supply and treatment infrastructure for the District of Columbia. As part of the renovation process, four (4) masonry mortar samples and a stucco sample were provided for detailed laboratory investigations. Two mortar samples (#1 and 2) were retrieved from the exterior and interior of the Castle at east and north elevations, respectively, and, two additional mortar samples (#3 and 4) came from the North Dome and Interior of the Meigs Vault, respectively. Detailed laboratory testing were done to determine the types of mortars used, including compositions and grain-size distributions of sands, type(s) of the binder(s) added, and volumetric proportions of binder(s) to sands used in the mortars. The mortar samples were analyzed by comprehensive laboratory examinations, e.g., by following the methods of ASTM C 1324 and RILEM including optical microscopy, scanning electron microscopy and X-ray microanalyses (SEM-EDS), chemical analyses (gravimetry), X-ray diffraction (XRD), X-ray fluorescence (XRF), FTIR spectroscopy, and ion chromatography. Stucco sample (ST #1) collected from the upper west elevation of the Castle was analyzed mostly by optical microscopy to determine compositions and properties of the three coats detected.

Based on detailed laboratory studies, the mortar samples are determined to be made using natural cement, magnesian lime, and excessively fine sand (mostly < 0.2 mm in size, close to the silt size fractions). The determined compositions are not representative of the modern day mortars, but are similar to many historic mortars from the eastern regions of United States. Natural cements used in the mortars are close to the classic historic Rosendale cements except the original feed (argillaceous magnesian limestone) used in calcination of natural cement in these mortars are slightly different from the argillaceous dolomitic limestone of Rosendale Formation used in the production of Rosendale cements.

Optical microscopy of four mortar samples from the Castle and Meigs Vault have determined dominantly natural cement and magnesian lime compositions of mortars, particularly of the ones from the Castle and the interior of Meigs Vault. By contrast, severely altered and lime leached nature from the dominantly lime-based composition of the mortar is found in the North Dome of Meigs Vault. Sand compositions are similar, consistent between all four mortars, and are all excessively fine-grained, close to the silt-size fractions (mostly 0.2 mm or less of the entire sand size range of 2 mm and 0.05 mm), and made using major amount of quartz and suborinate amounts of quartzite, feldspar, and other siliceous components. Sand in the two mortars from the Meigs Vault contained muscovite and biotite flakes from use of micaceous schist grains that are not found in the mortar from the Caslte. The siliceous sand, natural cement, and lime compositions of all four mortars are determined from: (a) the characteristic mineralogies of sands and binders; (b) microstructures and compositions of paste having overall variably dense and carbonated paste having scattered grains of incompletely calcined residual raw feeds of natural cements showing the typical original argillaceous limestone composition of the natural cement feed; and (c) dominantly quartz-based compositions from optical microsocpy, XRD, and acid-insoluble residue content analyses. Sand was probably derived from the nearby Potomac river, which was excessively finer than the typical ASTM C 144 masonry sand. SEM-EDS analyses of interstitial paste fractions of mortars have confirmed the presence of a natural cement and a magnesian lime binder as well as the hydraulic nature of the binder from the silica contents of paste. XRD analysis has confirmed dominant quartz from quartz sand and subordinate calcite from carbonated lime paste along with phases contributed from natural cement. XRF studies of acid and alkali-digested filtrates of mortars showed detectable soluble silica from the hydraulic binders. Results obtained from microscopy and chemical analyses are all consistent, confirmatory to each other, and provided a comprehensive understanding of mortars, which was determined to be prepared from mixing natural cement, magnesian lime, and excessively fine-grained silica sand. Mortar from Castle is slightly different from that from Meigs Vault in lacking mica in sand and having an overall higher proportion of natural cement binder. The high lime and severely altered (leached) nature of Mortar #3 from North Dome of Meigs Vault is indicative of corrosive action of water in the mortar.

Contrary to the mortars, the stucco sample received is made using Portland cement and silica sand. Stucco contains three distinct layers: (a) an interior medium gray scratch coat, approximately 18 mm in nominal thickness applied over the brick masonry, which contains expanded metal lath reinforcement present as large voids (circled) mostly at the upper end of the scratch coat as opposed to the more common installation of mesh at the lower end, i.e. closest to the brick wall on which the coat was applied; (b) a thin dark gray intermediate brown coat, approximately 3 to 5 mm in nominal thickness, well-bonded to the scratch coat, but is noticeably denser and darker gray in color tone due to lower water-cement ratio of the coat compared to the underlying scratch coat; and, finally, (c) a thin finish coat, approximately 4 mm in nominal thickness, which is also well-bonded to the intermediate dark gray brown coat but is lighter gray in color tone, indicating an inherently higher water-cement ratio, more similar to the innermost scratch coat. The finish coat has a sand-texture finish. Contrary to reported cracking and delamination of stucco, the stucco sample received showed no evidence of cracking or de-bonding where all three coats are well-bonded and present in sound conditions. However, the detected differential water-cement ratios of three coats along with very different thickness of the scratch coat as opposed to similar thinner brown and finish coats (which are each less than half the thickness of scratch coat) can potentially lead to differential drying shrinkage and shrinkage-related cracking and debonding of the coats. There is no evidence of corrosion of any metal lath reinforcement in the scratch coat of stucco received.

Information obtained from microscopy and chemical analyses of mortars to determine the binder compositions, soluble silica contents, water contents, and insoluble residue contents, and, determination of use of natural cement and magnesian lime composition of binders in the mortars are useful for calculation of the natural cement and lime and sand contents, and, eventually, the volumetric proportions of ingredients of mortars. However, due to the extreme variability of compositions of natural cements, conventional calculations of mix proportions according to the procedures of ASTM C 1324 recommended for modern-day cement-lime or masonry cement mortars are not feasible. Therefore, the natural cement, lime, and sand contents are estimated from the combined approach of microstructural and chemical analyses, which indicate use of natural cement to lime to sand at 1 to $^1/_2$ to 5-7 proportions, respectively for the two mortars from Castle and 1 to $1^1/_2$ to 7 for the mortar from North Dome of Meigs Vault, and 1 to $^1/_2$ to 10 for the mortar from interior of Meigs Vault, which is essentially an over-sanded mortar.

Extensive leaching and carbonation is noticed for the Mortar #3 from the North Dome of Meigs Vault. Gypsum salt precipitation is found in Mortar #1 from the exterior of east elevation of Castle, which was also confirmed by excessively high sulfate in the water-soluble filtrate in ion chromatography. No freezing-related distress is found in the samples. Sand was present in sound condition without any deleterious reactions with the binder.

Based on: (i) the determined natural cement, lime, and siliceous sand compositions of mortars from microscopy and chemical analyses; and (ii) 'estimated' volumetric proportions, a possible replacement mortar mix for the Castle could be made using: (a) 1-part natural cement (e.g., similar to the 10C natural cement from Edison Coatings) to $^1/_2$ part magnesian lime or a natural hydraulic lime (e.g., NHL 3.5), and (b) a modern ASTM C 144 masonry sand at 2 $^1/_2$ to 3 times the sum of volumetric proportions of cement and lime. ASTM C 270 Type M, S, N cement-lime or masonry cement mortars should not be used since all these modern-day mortars contain Portland cement as the essential hydraulic phase, which is not detected in the mortars. Similar mix of the Castle mortar can be used for the Meigs Vault mortars even at the location of North Dome where a lime-rich highly altered (lime-leached) mortar was detected. Sand to be used should match in color to the color of sand in the present mortars, preferably from a similar source, free of any debris, certainly not of as fine-grained as found in the samples, sound, free of clay particles, or any potentially deleterious constituents, should conform to the size requirements of ASTM C 144 for masonry sand, and should be durable. Due to years of atmospheric weathering and alterations, an exact match in color to the existing mortars may not be possible, which, even if possible, could alter in future due to continued atmospheric weathering in the presence of oxygen, moisture, and other elements.

INTRODUCTION

The Georgetown Reservoir is a reservoir that is part of the water supply and treatment infrastructure for the District of Columbia. It is located in the Palisades neighborhood of Washington, D.C., approximately two miles downstream from the Maryland–D.C. boundary. The reservoir was built by the United States Army Corps of Engineers as part of the Washington Aqueduct project. It was partially completed by 1858, but work was suspended for lack of funds. Construction began again in 1862 and was complete in 1864. Additional construction and modifications to the reservoir were carried out through the 1860s and 1870s. Water from the Dalecarlia Reservoir is pumped to the Georgetown Reservoir for further sedimentation before being treated at the McMillan Reservoir. The reservoirs and the nearby Dalecarlia water treatment plant are operated by the Army Corps of Engineers. The treated water is distributed throughout the city in water mains managed by the D.C. Water and Sewer Authority. At the outlet of the Georgetown facility is a sluice gate building that controls the flow of water into Washington City Tunnel, which leads to the McMillan Reservoir. This structure, called the Georgetown Castle Gatehouse, was built by the Army (c. 1901) in the shape of a castle.

As part of the renovation process, four (4) masonry mortar samples and a stucco sample were provided for detailed laboratory investigations. Two mortar samples (#1 and 2) were retrieved from the exterior and interior of the Castle at east and north elevations, respectively, and, two additional mortar samples (#3 and 4) came from the North Dome and Interior of the Meigs Vault, respectively.

The purposes of the investigation are to determine:

a. The types, compositions, and microstructures of the mortars and stucco sample, including

b. The type, grain-size distribution, and mineralogical composition of sands used in the mortars,

c. Type(s), chemical, and mineralogical compositions of the binder(s) added in mortars and in the different coats of the stucco sample,

d. Microstructural evidence of any physical and/or chemical deterioration of mortars and stucco from prolonged exposures, and,

e. Volumetric proportions of binder(s) and sand ingredients in the mortar mixes, and, finally, suggestions for suitable mortar mixes to match with the existing mortars.

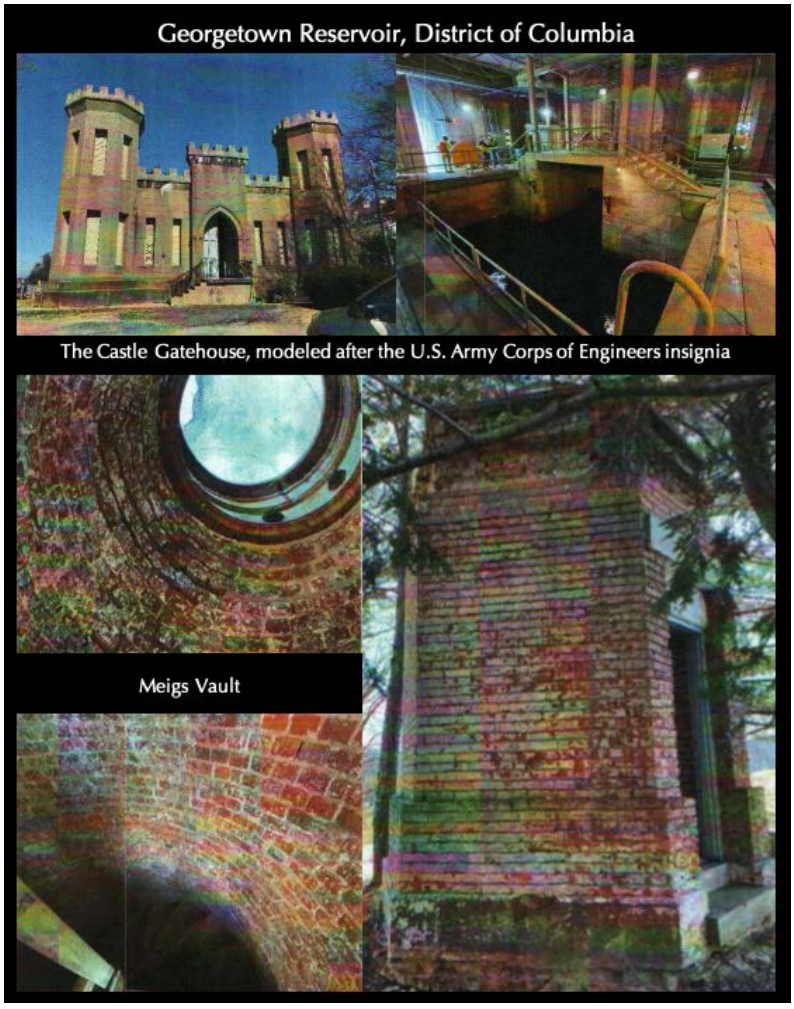

Figure 1: The Georgetown Reservoir in Washington, D.C.

The pieces were subsequently subdivided into multiple portions, and representative fragments were selected for optical microscopy of stucco, and, optical and electron microscopy and microanalyses, X-ray diffraction, X-ray fluorescence, wet chemical analyses (soluble silica content, insoluble residue, loss on ignition, and ion chromatography), and sand extraction and sieve analyses of four mortar samples. Figures 2 through 4 show the samples received.

Figure 2: Shown are fragments of mortar samples collected from the east elevation of the Castle exterior (#1, top) and north elevation of Castle interior (#2, bottom) both showing a dark beige color tone of mortar fragments, which, along with many other properties seen in the fragments (e.g., dense, hard natures compared to the softer and lighter toned historic lime mortars) are characteristic of many natural cement mortars.

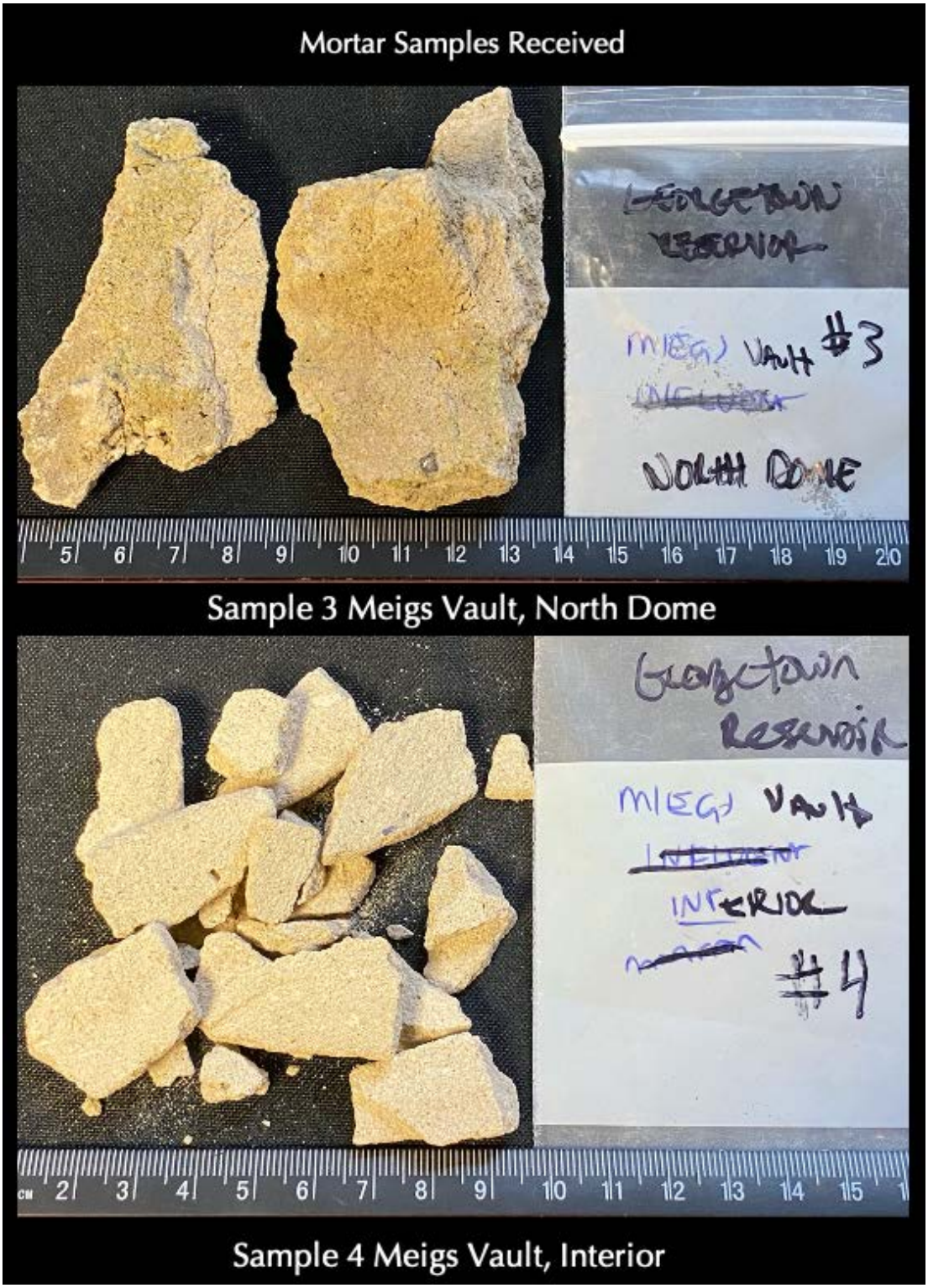

Figure 3: Shown are fragments of mortar samples collected from the Meigs Vault, North Dome (#3, top) and Meigs Vault, Interior (#4, bottom). Mortar #3 shows a dark beige color tone, which, along with many other properties seen in the fragments (e.g., dense, hard natures compared to the softer and lighter toned historic lime mortars) are characteristic of many natural cement mortars. Mortar #4 is relatively grayish and softer, dustier in nature than the other three mortars, which are reflected in subsequent analysis of the mortar.

Figure 4: Shown is the stucco sample of the Castle collected from the upper west elevation showing a red brick backing and sand-textured finish of the exterior face of the stucco.

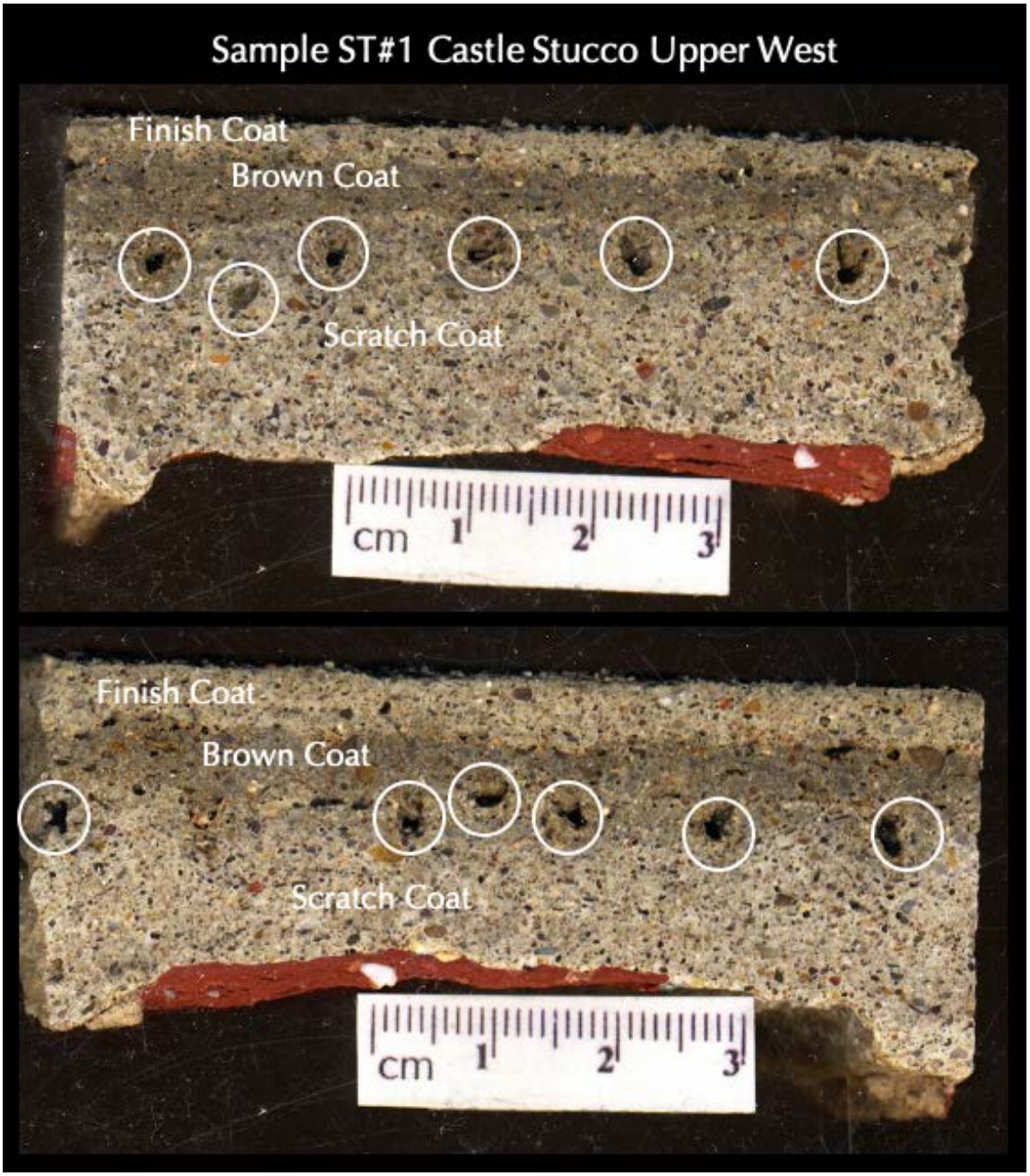

Figure 5: Lapped cross sections of the stucco sample showing three distinct layers: (a) an interior medium gray scratch coat, approximately 18 mm in nominal thickness applied over the brick masonry, which contains expanded metal lath reinforcement present as large voids (circled) mostly at the upper end of the scratch coat as opposed to the more common installation of mesh at the lower end, i.e. closest to the brick wall on which the coat was applied; (b) a thin dark gray intermediate brown coat, approximately 3 to 5 mm in nominal thickness, well-bonded to the scratch coat, but is noticeably denser and darker gray in color tone due to lower water-cement ratio of the brown coat compared to the underlying scratch coat; and, finally, (c) a thin finish coat, approximately 4 mm in nominal thickness, which is also well-bonded to the intermediate dark gray brown coat, but is lighter gray in color tone, indicating an inherently higher water-cement ratio, more similar to the innermost scratch coat. The finish coat has a sand-textured finish. Although all three coats are well-bonded to each other in the small fragment received, such differential water-cement ratios of three coats can potentially led to differential drying shrinkage and potential shrinkage-related cracking and debonding of the coats.

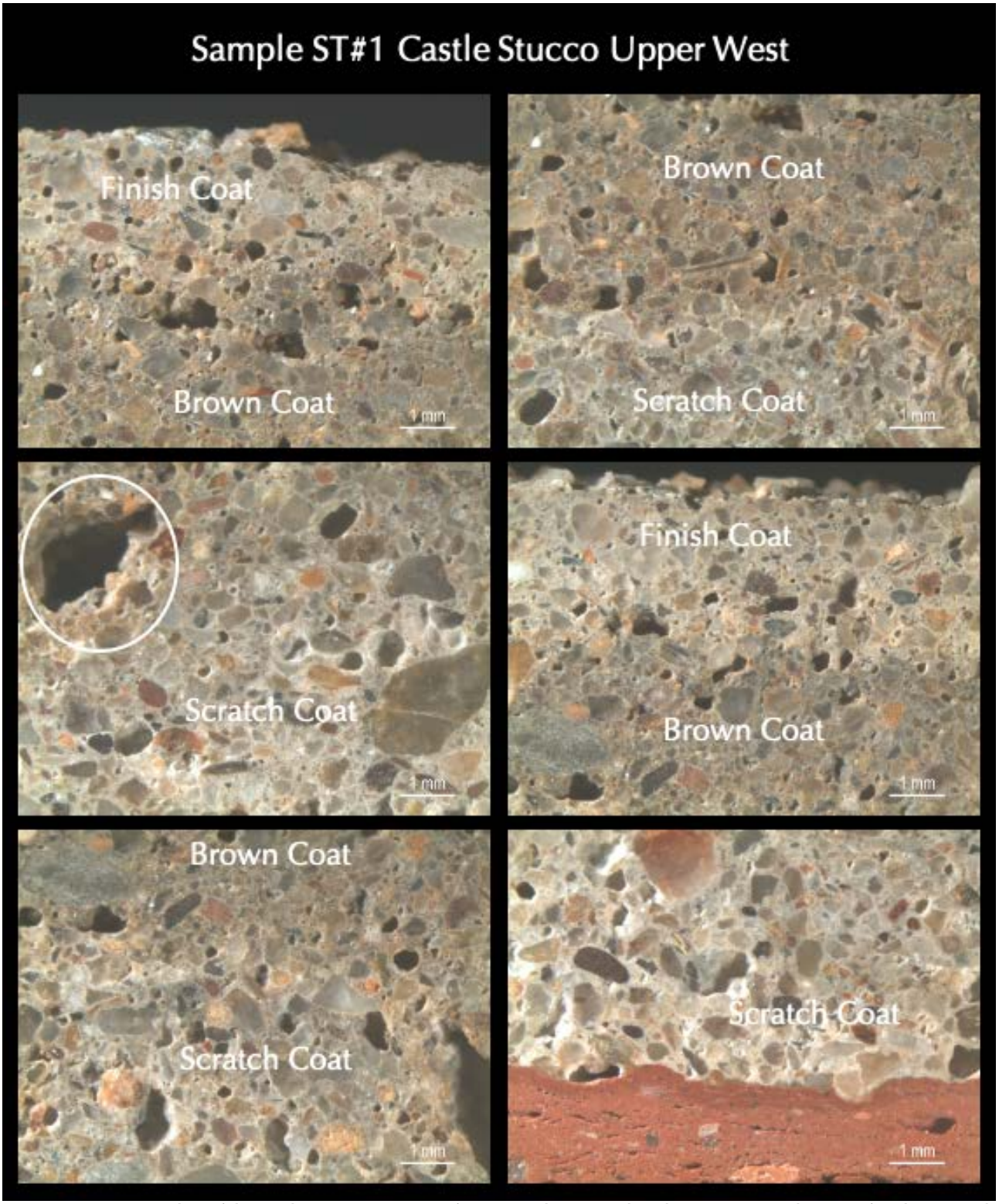

Figure 6: Micrographs of lapped cross sections of stucco showing the three coats – the top finish coat, the intermediate brown coat, and the bottom scratch coat where, the coats are differentiated at the first hand by the variations in color tones due to inherent variations in water-cement ratios of pastes. Notice intimate bonds between the coats. Also notice the lack of air entrainment in all three coats. The bottom right photo shows remains of brick masonry on which the stucco was applied.

METHODOLOGIES[1]

Until 1970-1980, characterization of masonry mortars were mostly based on traditional wet chemical analysis (Jedrzejewska, 1960, Stewart and Moore, 1981) where interpretation of results were often difficult if not impossible without a good knowledge of the nature of different ingredients. The majority of later characterization proposed optical microscopy (Erlin and Hime 1987, Middendorf et al. 2000, Elsen 2006) as the first step in identification of different components or mortar based on which other analytical techniques including wet chemistry are performed, e.g., scanning electron microscopy and X-ray microanalysis, X-ray diffraction, X-ray fluorescence, atomic absorption, thermal analysis, infrared spectroscopy, etc. (Bartos et al. 2000, Elsen 2006, Callebaut et al. 2000, Erlin and Hime 1987, Goins 2001, 2004, Groot et al. 2004, Doebley and Spitzer 1996, Chiari et al. 1996, Middendorf et al. 2000, 2004, 2005, Leslie and Hughes 2001, Martinet and Quenee 2000, Valek et al., 2012, Jana 2005, 2006). The choice of appropriate analytical technique depends mainly on the questions that have to be addressed, and, on the amount of material available.

Purposes of laboratory testing are: (a) to document a historic or modern masonry mortar by examining its sand and binder components, proportions of various ingredients, and their effects on properties and performance of the mortar, (b) evidence of any chemical or physical deterioration of mortar from unsoundness of its ingredients to effects of potentially deleterious agents from the environment (e.g., salts), (c) records of later repointing events and their beneficial or detrimental effects on the performance of the original mortar and masonry units, and finally, (d) an assessment of an appropriate restoration mortar to ensure compatibility with the existing mortar.

Currently there are two standardized procedures available that describe various laboratory techniques for analyses of masonry mortars with special emphases on historic mortars. One is ASTM C 1324 "Standard Test Method for Examination and Analysis of Hardened Masonry Mortar," which includes detailed petrographic examinations, followed by chemical analyses, along with various other analytical methods to test masonry mortars as described in various literatures, e.g., XRD, thermal analysis, and infrared spectroscopy. The second one is the RILEM method described in Middendorf et al. (2004, 2005).

The present mortar was tested by following these established methods of ASTM C 1324, and RILEM, which include detailed petrographic examinations i.e. optical and scanning electron microscopy and X-ray microanalyses (SEM-EDS), followed by chemical analyses (gravimetry, acid digestion), X-ray fluorescence (XRF), X-ray diffraction (XRD), and thermal analyses (TGA, DTG, and DSC). Mortar sample was first photographed with a digital camera, scanned on a flatbed scanner, and examined in a low-power stereomicroscope for the preliminary examinations, e.g., to screen any unusual pieces having different appearances, e.g., representing contaminants from prior pointing episodes.

Representative subset pieces of interest are then selected for: (a) optical microscopy and (b) scanning electron microscopy and X-ray microanalysis for chemical and mineralogical compositions, and microstructures of sand, paste, and overall mortar, (c) acid digestion, preferably from un-pulverized or lightly pulverized sample for sand extraction for grain size distribution, (d) loss on ignition from ambient to 950°C temperatures for free and hydrate water, and carbonate contents, (e) acid digestion for determination of insoluble residue content, (f) cold acid and hot alkali digestions for determination of soluble silica content from hydraulic binder if any, after pulverizing a subset to finer than 0.3 mm size, and, (g) ultra-fine pulverization (<44-micron) of a subset for XRD, XRF, FTIR, and thermal analysis. Any additional analyses, if needed, e.g., water digestion of mortar for determination of water-soluble salts by ion chromatography, or, Fourier-transform infrared spectroscopy of mortar for determining any organics added, etc. are done on as-needed basis from the remaining set.

Information obtained from petrographic examinations is crucial to devise appropriate guidelines for chemical methods, and, to properly interpret the results of chemical analyses. For example, detection of siliceous versus calcareous versus argillaceous components of aggregates in sample, or, the presence of any pozzolan in the binder

[1] For details on laboratory facilities for testing of masonry mortar, visit www.cmc-concrete.com.

(slag, fly ash, ceramic dusts, etc.) from petrography restricts which chemical method to follow, and how to interpret the results of such analyses, e.g., acid-insoluble residue contents.

Therefore, a direct chemical analysis e.g., acid digestion of a mortar without doing a prior petrographic examination to determine the types of aggregates and binder used could lead to highly erroneous results and interpretation. Armed with petrographic and chemical data, and based on assumed compositions and bulk densities of the sand and the binder(s) similar to the ones detected from petrographic examinations, volumetric proportions of sand and various binders present in the examined sample can be calculated. The estimated mix proportions from such calculations can provide a rough guideline to use as a starting mix for mock-up mix during formulation of a pointing mortar to match with the existing mortar.

Optical Microscopy

The main purposes of optical microscopy of masonry mortar are characterization of: (a) aggregates, e.g., type(s), chemical and mineralogical compositions, nominal maximum size, shape, angularity, grain-size distribution, soundness, alkali-aggregate reactivity, etc. (b) paste, e.g., compositions and microstructures to diagnose various type(s) of binder(s) used, (c) air, e.g., presence or absence of air entrainment, air content, etc., (d) alterations, e.g., lime leaching, carbonation, staining, etc. due to interactions with the environmental agents during service, and effects of such alterations on properties and performance of mortar; and (e) deteriorations, e.g., chemical and/or physical deteriorations during service, cracking from various mechanisms, salt attacks, possible reasons for the lack of bond if reported from the masonry unit, etc. Fragments selected from preliminary examinations for microscopy are sectioned, polished, and thin-sectioned (down to 25-30 micron thickness) preferably after encapsulating and impregnating with a dyed-epoxy (Fig. 3) to improve the overall integrity of the sample during precision sectioning and grinding, and to highlight porous areas, voids, and cracks. Prepared sections are then examined in a high-power (up to 100X) Stereozoom microscope having reflected and transmitted-light, and plane and crossed polarized-light facilities, and eventually in a high-power (up to 600X) petrographic microscope equipped with transmitted, reflected, polarized, and fluorescent-light facilities. Capturing high-resolution photomicrographs from these microscopes via digital microscope cameras with image analyses software are an integral part of documentations during petrographic examinations.

Therefore, four essential steps followed during optical microscopy are: (a) visual examination of as-received, fresh fractured, and sectioned surfaces of mortar in a stereo-microscope, (b) preparation of a large-area (50 × 75 mm) thin section of homogeneous thickness (25-30 micron), (c) observation of thin section in a transmitted-light stereo-zoom microscope from 5X to 100X preferably with polarized-light facilities to observe large-scale distribution of sand and mortar microstructure, and finally (d) observation of thin section in a polarized-light (petrographic) microscope from 40X to 600X equipped with transmitted and reflected, polarized and fluorescent-light facilities for examinations of sand and binder compositions and microstructures.

For thin section preparation, representative fragments are oven-dried at 40°C to a constant mass and placed in a flexible (e.g., molded silicone) sample holder, then encapsulated with a colored dye-mixed (e.g., blue dye commonly used in sedimentary petrography, or, fluorescent dye, Elsen 2006) low-viscosity epoxy resin under vacuum to impregnate the capillary pore spaces of mortar, improve the overall integrity of sample during sectioning by the cured epoxy, highlight porous areas of mortar, alterations, cracks, voids, reaction products, etc. The epoxy-encapsulated cured solid block of sample is then de-molded, sectioned if needed, and processed through a series of coarse to fine grinding on metal and resin-bonded diamond grinding discs with water or a lubricant, eventually a perfectly flat clean ground surface is glued to a frosted large-area (50 × 75 mm) glass slide. Careful precision sectioning and precision grinding of the sample is then done in a thin-sectioning machine till the thickness is down to 50 to 60 micron. Final thinning down to 25 to 30 micron thickness is done on a glass plate with fine (5-15 micron) alumina abrasive. Thin section is eventually polished with various fine (1 micron to 0.25 micron size) diamond abrasives on polishing wheels suitable for examinations in a petrographic microscope, and eventually in SEM-EDS. Sample preparation steps are described in Jana (2006).

More elaborate steps followed during optical microscopy include: (a) visual examinations of sample as-received to select fragments for detailed optical microscopy; initial digital and flatbed scanner photography of sample as-received; (b) low-power stereomicroscopic examinations of saw-cut and freshly fractured sections of sample for evaluation of variations in color, grain-size and appearances of sand, and the nature of the paste; (c) examinations of oil immersion mounts for special features and materials in a petrographic microscope; (d) examinations of colored (blue or fluorescent) dye-mixed epoxy-impregnated polished thin sections in a transmitted-light Stereozoom microscope for determination of size, shape, angularity, and distribution of sand, as well as abundance and distribution of void and pore spaces that are highlighted by the colored dye-mixed epoxy; (e) image analyses of photomicrographs of thin sections for estimations of pores, voids, intergranular open spaces, and shrinkage microcracks by using Image J or other image analysis software where multiple photomicrographs are collected in plane polarized light mode by using a high-resolution Stereozoom microscope equipped with transmitted and polarizing light facilities and stitched to get an adequate representative coverage; (f) examinations of colored (blue or fluorescent) dye-mixed epoxy-impregnated polished thin sections in a petrographic microscope for detailed compositional, mineralogical, textural, and microstructural analyses of aggregates and binders, along with diagnoses of evidence of any deleterious processes and alterations (e.g., lime leaching, precipitation of secondary deposits and alteration products, salts); (g) examinations of polished thin or solid section in reflected-light (epi-illumination) mode of petrographic microscope after etching the surface with acids to identify various non-hydrated hydraulic phases (e.g., C_2S, C_3S, C_3A, etc., Middendorf et al., 2005); (h) examinations of any physical or chemical deterioration or signs of improper construction practices from microstructural evidences; (i) stereo-microscopical examinations of size, shape, and color variations of sand extracted after hydrochloric acid digestion; and finally (j) selection of areas of interest to be examined by scanning electron microscopy.

Scanning Electron Microscopy & Microanalysis by Energy-Dispersive X-ray Spectroscopy (SEM-EDS)

Methods followed in SEM-EDS include: (a) secondary electron imaging (SEI) to determine the microstructure and morphology of the examined surface of sample, (b) backscatter electron (BSE) imaging to determine compositions of various phases from various shades of darkness/grayness/brightness from average atomic numbers of phases from the darkest pore spaces to brightest iron minerals (e.g., thaumasite, periclase, ettringite, quartz, dolomite, monosulfate, gypsum, calcite, C-S-H, aluminate, calcium hydroxide, belite, alite, free lime, and ferrite having progressively increasing average atomic numbers and brightness in BSE image), (c) X-ray elemental mapping (dot mapping) of an area of interest to differentiate various phases, (d) point-mode or area (raster)-mode analysis of specific area/phase of interest on a polished thin or solid section, and (e) average compositional analysis of a specific phase or an area on a polished thin or solid section or small subset of a sample.

The main purposes of SEM-EDS studies are to: (a) observe the morphologies and microstructures of various phases of sand and binder, (b) characterize the typical fine-grained microstructure of hydrated, carbonated, and hydraulic components of binder that are too fine to be examined by optical microscopy and are not well crystallized to be detected by XRD; (c) determine major element oxide compositions, and compositional variations of paste, and from that determine the type of binder(s) used, especially to differentiate non-hydraulic calcitic and dolomitic lime mortars from hydraulic lime varieties (e.g., from silica contents of paste), natural cements (e.g., from silica and magnesia contents), pozzolans, slag cements, Portland cements, etc. all from their characteristic differences in compositions and hydraulicities (e.g., cementation index of Eckel 1922); (d) determine composition of residual hydraulic phases to assess the raw feed and calcination processes used in manufacturing of binder; (e) assess hydration, carbonation, and alteration products of binders, (f) investigate effects of various alterations of paste during service and its role on properties and performance of mortar, (g) detect salts and other potentially deleterious constituents, (h) detect pigments and fillers, (i) examine compositional variations across multiple mortars installed, etc.; and eventually (j) complement and confirm the results of optical microscopy.

Due to characteristic difference in compositions of pastes made using various binders, e.g., non-hydraulic lime (CaO dominates over all other oxides), variably hydraulic lime (CaO with variable SiO_2 contents depending on degree of hydraulicity), dolomitic lime (high CaO and MgO), natural cement (CaO, SiO_2, Al_2O_3, and MgO contents are high, high MgO and FeO contents are characteristic), and Portland cement (CaO and SiO_2 contents are higher than all other oxides), SEM-EDS analysis of paste is a powerful method for detection of the original binder

components in the sample. Effects of chemical alterations and various chemical deteriorations of a mortar (e.g., lime leaching, secondary calcite precipitates, gypsum deposits, etc.) can also be detected by SEM-EDS.

SEM-EDS analysis was done in a CamScan Series 2 scanning electron microscope equipped with a high-resolution column 40Å tungsten, 40 kV electron optics zoom condenser 75° focusing lens operating at 20 kV, equipped with a variable geometry secondary electron detector, backscatter electron detector, EDS detector for observations of microstructures at high-resolution, compositional analysis, and quantitative determinations of major element oxides from various areas of interest, respectively. Revolution 4Pi software was used for digital storage of secondary electron and backscatter electron images, elemental mapping, and compositional analysis along a line, or on a point or an area of interest. Portion(s) of interest on the polished 50 mm × 75 mm size thin section used for optical microscopy were subsequently coated with carbon or gold-palladium film and placed on a custom-made aluminum sample holder to fit inside the large multiported chamber of CamScan SEM equipped with the eucentric 50 × 100 mm motorized stage. Usually, features of interest from optical microscopy are marked on the thin section with a fine-tipped conductive marker pen for further observations in SEM. Alternately, solid polished section or grain mount from phases or areas of interest can also be examined. Procedures for SEM examinations are described in ASTM C 1723 and Sarkar et al. (2000).

Acid Digestion

Acid digestion is perhaps the most commonly used test of masonry mortar, which is done to: (a) extract sand from sample by dissolving out the binder fractions so that grain-size distribution of sand can be done by sieve analysis, and (b) assess insoluble sand content in the sample. Sand content after acid digestion is determined both from: (a) 1.00 gram of pulverized sample (finer than 0.3 mm size) digested in 50-ml dilute (1+3) HCl (heated rapidly but below boiling), and, (b) from digesting a representative bulk sample *per se* (for harder mortars or mortars perhaps with light pulverization) in multiple fresh batches of (1+3) HCl at ambient temperature. The former usually gives better result due to small amount, pulverization to easily remove the binder fraction for digestion, and use of rapidly heated acid, whereas latter method requires multiple episodes of digestion in fresh acid and is time-consuming. Acid digestion is also done as the first step to determine soluble silica content in a sample as described below, which is contributed from the hydraulic components in binder.

All these goals of acid digestion depend on the assumptions that: (i) sand is siliceous in composition and does not contain any acid-soluble constituents (e.g., carbonates), and, (ii) binder entirely dissolves in acid and does not contain any acid-insoluble constituents (gypsum, clay, etc.). Applicability of acid digestion to assess these tasks should therefore be first verified by optical microscopy to confirm the siliceous nature of sand without any appreciable acid-soluble constituents, and calcareous nature of binder, and none without any appreciable argillaceous (clay) constituents.

For grain-size distribution of sand (for sample found from optical microscopy to contain siliceous sand), a few representative fragments of (preferably not pulverized or lightly pulverized in a porcelain mortar and pestle for harder mortars to break down to smaller size fraction without crushing the sand to retain the original sand size) are selected for digestion in multiple fresh batches of (1+3) dilute hydrochloric acid to dissolve away all binder fractions and extract, wash, and oven-dry the acid-insoluble component of aggregate. Usually multiple episodes of acid digestion in fresh batches of acid and filtration of residues are needed to entirely remove the binder fractions without losing the finer fractions of sand. Sand particles thus extracted are washed, oven-dried, and sieved in an automatic mini sieve shaker through various U.S. Sieves from No. 4 (4.75 mm) through 8 (2.36 mm), 16 (1.18 mm), 30 (0.6 mm), 50 (0.3 mm), 100 (0.15 mm), and 200 (0.075 mm) for determination of the size, shape, angularity, and color of sands retained on various sieves. Grain-size distribution of sand is then compared with ASTM C 144 specifications for masonry sand. Photomicrographs of sand retained on each sieve are then taken with a stereomicroscope to record the sand size, shape, and color variations. For low amount of sample, or, for sample having calcareous sand, image analysis (e.g., ImageJ) on stitched photomicrographs of thin sections taken from multiple areas can be done to determine the sand-size distribution (Elsen et al. 2011).

Soluble Silica from Cold Acid & Hot Alkali Digestion

Digestion of a pulverized sample of mortar in a cold acid followed by further digestion of residue in a hot alkali hydroxide solution are done to determine the soluble silica content contributed from the hydraulic component of binder, where cold acid digestion usually dissolves most of the binder without affecting the sand, followed by hot alkali hydroxide digestion to dissolve remaining soluble silica from calcium silicate hydrate component of paste or in mortars containing hydraulic binders. The soluble silica content corresponds to the silica mostly contributed from the hydraulic binder components (and a minor amount from any soluble silica component in the aggregates).

For determination of soluble silica content (modified from ASTM C 1324), 5.00 grams of pulverized sample (finer than 0.3 mm size, without excessive fines) is first digested in 100-mL cold (at 3 to 5°C) HCl and filtered through two 2.5-micron filter papers (filtrate #1). The residue with filter papers is then digested again in hot (below boiling) 75-ml NaOH, and filtered through two 2.5-micron filter papers (filtrate# 2). The two filtrates from acid and alkali digestions are then combined, re-filtered twice with 2.5-micron and then through 0.45-micron filter paper to remove any suspended silica fines, brought to 250 ml volume with distilled water, and then used for soluble silica determination by an analytical method, such as atomic absorption spectroscopy (AAS), inductive coupled plasma optical emission spectroscopy (ICP-OES), or X-ray fluorescence spectroscopy (XRF). Multiple steps of filtrations from 2.5-micron to submicron filter papers are necessary to remove any suspended silica from sand that can skew the result. Instrument to be used for such determination must be calibrated with several silica standards in matrices similar to the one used in mortar analysis. An XRF unit calibrated with filtrates from acid-and-alkali-digested series of laboratory-prepared standards of Portland cement and silica sand mortars (moist cured at *w/c* of 0.50 for 30 days) having various proportions of Portland cements (SiO_2 contents of standards ranging from 1 to 10%) were used for determining SiO_2 Kα X-ray intensities from known stoichiometric silica (cement) contents of standards (using exact 5.00 grams as samples) prepared by the same procedure of cold HCl-digestion/filtration/hot NaOH-digestion/2nd filtration/combination of two filtrates/re-filtration steps as followed for mortars or mortars.

Hydraulic binder content is calculated as: [(soluble SiO_2, weight percent in sample as calculated) divided by assumed soluble SiO_2 content in binder] ×100, where assumed SiO_2 contents of binders varies with binder types, e.g., 21% in Portland cement, 20% in natural cement, 27% in slag cement, 7 to 10% in hydraulic lime, etc., or, more preferably, from the average paste-SiO_2 content determined from SEM-EDS.

Weight Losses on Ignition

Losses in weight of a mortar on step-wise heating from ambient to 110°C, 550°C, and 950°C temperatures liberate free water from capillary pore spaces by 110°C, combined water from dehydroxylation of various hydrous phases (calcium silicate hydrate, calcium hydroxide, etc.) by 550°C, and liberation of carbon dioxide from decomposition of carbonated paste and carbonate minerals by 950°C. Such losses in weight are measured by following the procedures of ASTM C 1324 by heating 1.00 gram of pulverized mortar (finer than 0.3 mm) in an alumina crucible in a muffle furnace in a controlled step-wise heating at a heating rate of 10ºC/min. Mortars having hydraulic binders and hydration products of such provide measurable combined water contents after calcination to 550°C, whereas those having high calcareous components (high-calcium lime mortar or mortar having calcareous sand) produce higher weight losses during ignition to 950°C. Usually, a good correlation is found between weight losses at 550°C from dehydration of combined water, and, soluble silica contents contributed from hydraulic binders amongst series of mortars containing variable amounts of hydraulic phases.

X-ray Diffraction (XRD)

X-ray diffraction (XRD) is useful for: (a) determination of bulk mineralogical composition of mortar, including its aggregate and binder mineralogies (e.g., quartz in sand from major diffraction peaks at 26.65º, 20.85º, 50.14º 2θ, or calcite in sand or carbonated lime binder from major peaks at 29.41º, 39.40º, 43.15º 2θ, or Portlandite in binder from major peaks at 34.09º, 18.09º, 47.12º 2θ); (b) individual primary mineralogies and alteration products of

aggregates at various size fractions, and binder phases; (c) detection of dolomitic lime binder from brucite in the sample from major peaks at 38.02º, 18.59º, 50.86º 2θ; (d) detection of use of lime (portlandite), gypsum (11.59º, 20.72º, 29.11º 2θ), or cement binders from their characteristic mineralogies; (e) detection of any potentially deleterious constituents, e.g., deleterious salts, or efflorescence deposits; (f) detection of a mineral oxide-based pigment in sample; and (g) detection of components difficult to detect by microscopical methods.

X-ray diffraction can be done on: (i) pulverized (to finer than 45 micron) portion of bulk sample, or (ii) on the sand extracted from mortar by acid digestion, if sand has a complex mineralogy, or also (iii) on the binder-fraction by separating sand from the binder from a carefully ground sample (in a mortar and pestle) and passing the ground mass through US 200 sieve (75 micron) to collect the fraction rich in binder. XRD pattern of a sample containing silica sand typically shows quartz as the dominant phase that surpasses peaks for all other phases (e.g., calcite, dolomite, clay, secondary deposits); hence binder separation is sometimes useful to detect minor minerals of interest (e.g., salts or pigments). For mortars containing marine shell fragments as sand, aragonite appears with calcite as two calcium carbonate phases from the shell fragments and paste. For binder mineralogy, sample is first dried at 40°C to a constant mass, then carefully crushed without pulverizing the sand, and sieved through a 75-micron opening screen to retain sand-rich fraction on the sieve and obtain the passed binder-rich fraction for further pulverization down to finer than 45 micron. Salts and other soft components can be analyzed from binder fraction. Efflorescence salts on masonry walls are also analyzed routinely in XRD.

For sample preparation, a Rocklab (Sepor Mini-Thor Ring) pulverizer is used to grind sample down to finer than 100 microns. Usually, a few drops of anhydrous alcohol are added to reduce decomposition of hydrous phases from the heat generated from grinding. Approximately 10 grams of sample is ground first in the pulverizer, from which about 8.0 grams of sample is selected, mixed with an appropriate binder (e.g., three Herzog grinding aid pellets from Oxford Instruments having a total binder weight of 0.6 gram for 8 grams of sample for a fixed binder proportion of 7.5 percent); the mixture is then further ground in Rocklab pulverizer and in a McCrone micronizing mill with anhydrous alcohol down to finer than 44 micron size. Approximately 7.0 grams of binder-mixed pulverized sample thus prepared is weighed into an aluminum sample cup and inserted in a stainless steel die press to prepare the sample pellet. A 25-ton Spex X-press is used to prepare 32 mm diameter pellet from the pulverized sample. The pressed pellet is then placed in a custom-made circular sample holder for XRD and excited with the copper radiation of 1.54 angstroms. Sample holders made with quartz or silicon are best for working with very small quantities of sample because these holders create no diffraction peaks between 2° and 90° 2θ (Middendorf et al. 2005).

XRD is carried out in a Siemens D5000 Powder diffractometer (θ-2θ goniometer) employing a long line focus Cu X-ray tube, divergent and anti-scatter slits fixed at 1 mm, a receiving slit (0.6 mm), diffracted and incident beam Soller slits (0.04 rad), a curved graphite diffracted beam monochromator, and a sealed proportional counter. Siemens D 5000 is equipped with (a) a horizontal stage (fixed), (b) an X-ray generator with CuKα, fine focus sealed tube source, (c) large diameter goniometer (600 mm), low divergence collimator, and Soller slits, (d) fixed detector slits 0.05, 0.2, 0.6, 1.0, 2.0, and 6.0, and (e) Scintillation detector. Generator settings used are 40 kV and 30 mA. Tests are usually run at 2θ from 4° to 64° with a step scan of 0.02° and a dwell time of one second. The resulting diffraction patterns are collected by DataScan 4 software of Materials Data, Inc. (MDI), analyzed by Jade software of MDI with ICDD PDF-4 (Minerals 2017) diffraction data. Phase identification, and quantitative analyses were carried out with MDI's Search/Match, Easy Quant, and Rietveld modules, respectively.

X-ray Fluorescence (XRF)

X-ray fluorescence (XRF) is used for determining: (a) major element oxide composition of sample, and, (b) soluble silica content of filtrate after digestion of sample in cold-HCl and hot-NaOH. Major element oxide compositions provide clues about the siliceous sand content of mortar from silica content, type of binder used (e.g., a dolomitic lime or natural cement based binder gives a characteristically higher magnesia than a calcitic lime or Portland cement based binder), calculation of lime content in a cement-lime mortar from bulk CaO content from XRF, effect of alterations and deteriorations (e.g., salt ingress in a mortar from marine environment can be diagnosed from excessive sodium, sulfate, and chlorine, etc.), etc. A series of standards from Portland cements, lime, gypsum, to

various rocks, and masonry cements of certified compositions (e.g., from USGS, GSA, NIST, CCRL, Brammer, or measured by ICP) are used to calibrate the instrument for various oxides, and empirical calculations are done from such calibrations to determine oxide compositions of mortars. For mortars with highly unusual compositions (e.g. severely salt-contaminated or a gypsum-based mortar) a standard-less FP calculation is done to determine the best possible composition.

An energy-dispersive bench-top X-ray fluorescence unit from Rigaku Americas Corporation (NEX-CG) is used. Rigaku NEX-CG delivers rapid qualitative and quantitative determination of major and minor atomic elements in a wide variety of sample types with minimal standards. Unlike conventional EDXRF analyzers, the NEX-CG was engineered with a unique close-coupled Cartesian Geometry (CG) optical kernel that dramatically increases signal-to-noise. By using monochromatic secondary target excitation, instead of conventional direct excitation, sensitivity is further improved. The resulting dramatic reduction in background noise, and simultaneous increase in element peaks result in a spectrometer capable of routine trace element analysis even in difficult sample types. The instrument is calibrated by using various certified (CCRL, NIST, GSA, and Brammer) reference standards of cements and rocks. The same pressed pellet used for XRD for mineralogical compositions is used for XRF to determine the chemical composition.

Thermal Analyses (TGA, DTG, and DSC)

Thermal analyses encompass: (1) thermogravimetric analysis (TGA), which measures the weight loss in a sample as it is heated, where weight loss can be related to specific physical decomposition of a phase of interest at a specific temperature that is characteristic of the phase from which both the phase composition and the abundance can be determined; (2) differential thermal analysis (DTA, or first derivative of TGA i.e. DTG) measuring temperature difference between the sample and an inert standard (Al_2O_3) both are heated at the same rate and time where endothermic peaks are recorded when the standard continues to increase in temperature during heating but the sample does not due to decompositions (e.g., dehydration of hydrous or decarbonation of carbonate phases); the endothermic or exothermic transitions are characteristic of particular phase, which can be identified and quantified using DTA (or DTG); and (3) differential scanning calorimetry (DSC), which follows the same basic principle as DTA, whereas temperature differences are measured in DTA, during heating using DSC energy is added to maintain the sample and the reference material (Al_2O_3) at the same temperature; this energy use is recorded and used as a measure of the calorific value of the thermal transitions that the sample experiences; this is useful for detection of quartz that undergoes polymorphic (α to β form) transitions and no weight loss.

Thermal analyses are done to determine the presence and quantitative amounts of: (a) hydrates (e.g., combined water liberated from paste dehydration during decomposition of calcium-silicate-hydrate component in paste at 180-190ºC); (b) sulfates (gypsum from decompositions at 125ºC, and 185-200ºC, ettringite at 120-130ºC, thaumasite at 150ºC); (c) brucite from its dehydroxylation at 300-400ºC to confirm the presence of dolomitic lime; (d) hydrate water from decomposition of Portlandite component of paste at 400-600ºC; (e) quartz from polymorphic transformation (α to β form) at 573ºC; (f) cryptocrystalline calcite in the carbonated lime matrix from decomposition at 620-690ºC, or magnesite at 450-520ºC, or (g) coarsely crystalline calcite e.g., in limestone by decomposition at 680-800ºC or (h) dolomite at 740-800ºC and 925ºC, and (i) phase transition of belite (C_2S) at 693ºC, etc. Phases are determined from their characteristic decomposition temperatures occurring mostly as endothermic peaks or polymorphic transition temperatures as for quartz.

Simultaneous TGA and DSC analyses are done in a Mettler Toledo TGA/DSC 1 unit on 30-70 mg of finely ground (<0.6 mm) sample in alumina crucible (70 µl, no lid) from 30°C to 1000°C at a heating rate of 10°C/min with high purity nitrogen as purge gas at a flow rate of 75.0 ml/min. TGA/DSC 1 simultaneously measures heat flow in addition to weight change. The instrument offers high resolution (ultra-microgram resolution over the whole measurement range), efficient automation (with a reliable sample robot for high sample throughput), wide measurement range (measure small and large sample masses and volumes) broad temperature scale (analyze samples from ambient to 1100°C), superior ultra-micro balance, simultaneous DSC heat flow measurement (for simultaneous detection of thermal events, e.g., polymorphic alpha-to-beta transition of quartz and quartz content), and a gastight cell (ensures a properly defined measurement environment).

Fourier Transform Infra-red Spectroscopy (FT-IR)

Fourier-transform infrared spectroscopy (FT-IR) measures interaction between applied infrared radiation and the molecules in the compounds of interest (Middendorf et al. 2005). FT-IR is particularly useful for detection of admixture, additives, and polymer resins, mainly to identify various organic components (functional groups) in mortar (e.g., methyl CH_3, organic acids CO-OH, carbonates CO_3) from their characteristic spectral fingerprints in FT-IR spectrum. FT-IR can also be used for detection of main mineral phases in a hydraulic binder, CSH, carbonates, gypsum, and clays (Middendorf et al. 2005). Organic compounds such as synthetic (e.g., acrylics, polyesters) and natural resins, carbohydrates, colorants, oils and fats, proteins, waxes as well as inorganic compounds, e.g., corrosion products, minerals, pigments, paints, fillers, stone, glass, and ceramics can be detected by this technique.

FT-IR measurements are done in a Perkin Elmer Spectrum 100 FT-IR spectrophotometer running with Spectrum 10 software. Sample is measured using attenuated total reflection (ATR) on a single bounce diamond/ZnSe ATR crystal between a frequency range of 4000 to 650 cm^{-1}. Each run is collected at 4 cm^{-1} resolution with Strong Beer-Norton apodization. Data are collected with a temperature-stabilized deuterated triglycine sulfate (DTGS) detector by placing the sample in contact with the ATR crystal and by applying force from the pressure applicator supplied with the ATR accessory. The application of pressure enables the sample to be in intimate contact with the ATR crystal, ensuring achievement of a high-quality spectrum. Additionally, more conventional KBr pellet is also sometimes used for samples on as-needed basis.

Ion Chromatography

Salts can cause various deteriorations from: (a) mere aesthetic issues of surface efflorescence by precipitation from evaporation of leachates on the surfaces followed by atmospheric carbonation of the precipitates where salts deposit as individual crystals or as crust to (b) more serious internal distress in mortar from crystallization inside the pores (sub-fluorescence or crypto-fluorescence) from expansive forces associated with crystallization of salt from supersaturated solutions. Some common salts are calcium carbonates (e.g., calcite, vaterite), magnesium carbonate (magnesite), sodium carbonate hydrate and bicarbonate (thermonatrite, trona, nahcolite), sulphates (gypsum, thenardite, epsomite, melanterite, mirabilite, glauberite, or ettringite and thaumasite from oxidation of sulfides or cement hydrates), and chlorides (halite, sylvite, calcium oxychloride from deicing salts, salt-bearing aggregates, ground water). X-ray diffraction and SEM-EDS can determine many of these salts as long as they are present in detectable amounts. Ion chromatography is an established technique used for analyses of various water-soluble anions and cations in salts (e.g., chloride, sulfate, and nitrate anions, and magnesium, calcium, alkali, ammonium cations) to assess magnitude of environmental impacts on masonry units and mortars, and subsequent effects of such salt ingress. Samples are pulverized, digested in deionized water to remove all water-soluble salts, then solid residues are filtered out and the water-digested filtrates are analyzed by an ion chromatograph.

Ion chromatography methods are described in ASTM D 4327 “Standard Test Method for Anions in Water by Chemically Suppressed Ion Chromatography.” Briefly, an aliquot of 1 gram of pulverized sample (passing No. 50 sieve) was digested in 50 ml distilled water for 6 to 8 hours on a magnetic stirrer at a temperature below boiling point of water; then the digested sample was filtered through two 2.5-micron filter papers using vacuum, followed by a second filtration through micro-filter (0.45 micron) paper, then the filtrate was either used directly or diluted to 100 to 250 ml with distilled water depending on the concentration of anions, and used for analysis to get ppm-level fluoride, chloride, nitrite, bromide, nitrate, phosphate, and sulfate in the water-digested sample in Metrohm 861 Advanced Compact IC. The instrument was calibrated against six different custom-made Metrohm anion standard solutions having all these anions from 0.1-ppm to 100-ppm levels. To check the accuracy of the instrument, a 50-ppm standard solution was run first prior to the analyses of samples.

Laboratory Analyses of Masonry Mortars

Initial Mortar (50 to 100 grams) [Photographed with digital camera & flat-bed scanner, As-received condition, total weight, and dimensions of largest piece are documented]

Intact Pieces (20+ g)

1. *Optical Microscopy*

I. Perform visual examination of mortar as received, then saw-cut and fractured surfaces and with a low-power stereomicroscope,
II. Take digital and flat bed scanner photos of intact piece(s),
III. Encapsulate the piece for thin section microscopy in a flexible mold with a low-viscosity colored or fluorescent dye-mixed epoxy to highlight voids, pores, cracks, etc.,
IV. Prepare thin section (< 30 micron thickness) and polish the thin section for optical and SEM-EDS analyses,
V. Scan the thin section on a flat-bed scanner with the thin section residue,
VI. Take transmitted light high-power stereo-zoom photomicrographs of thin sections from different areas to be stitched to determine volumes and size distributions of pore spaces and sand grains by Image J,
VII. Take plane and crossed polarized-light photomicrographs of sand and binder fractions in thin section from a petrographic microscope and determine areas for further studies by SEM-EDS,
VIII. Do detailed petrographic examinations to determine the sand and binder compositions, sand mineralogy and texture, binder phases, residual binders, alterations, and products of any deleterious reactions, immersion mounts of specific areas of interest, etc.

2. *SEM-EDS*

I. Put conductive coating only on the portion of polished thin section intended for SEM-EDS studies from optical microscopy,
II. Take backscatter and/or secondary electron images, and if needed X-ray elemental maps,
III. Select multiple areas on paste to determine oxide compositions and Eckel's cementation indices,
IV. Tabulate the paste composition variations across the backscatter/secondary electron image.
V. Determine chemical compositions of resides left from the original components of the binders, as well as the hydration and carbonation and other alteration products

Lightly hand-ground in a Mortar & Pestle (30+ g)

3. *Acid Digestion - Sand Color & Sand Size Distribution* (10 g)

I. Take 10 g. of mortar lightly ground in mortar & pestle and digest in HCl (1+3) in a 250 ml beaker on a magnetic stirrer until all sand separates and settles at the bottom of beaker,
II. Filter all through two 2.5 micron filter paper, wash the beaker, filter paper, and all sand residue with dist. water,
III. Dry the residue at 110°C in an oven for 10 min., gently brush out from the filter paper and collect, then sieve the entire sand residue through No. 4 through 200 sieves in a mini sieve shaker (e.g., from Gilson),
IV. Determine the mass retained on each sieve, and on the pan (finer than No. 200 sieve),
V. Take photomicrographs of sand particles retained on each sieve for sand color variations in a stereomicroscope.

4. *Acid & Alkali Digestion – Soluble Silica for Hydraulic Binder* (5 g)

I. Grind 5-6 g of lightly ground fraction from mortar & pestle in a WC pulverizer for 30 sec.
II. Sieve thru. No. 50 sieve, collect the fraction passing the sieve,
III. Re-grind the residue retained on sieve for 15 sec. and mix thoroughly with the previous fraction;
IV. Use 5.000 g of thus prepared powder (passing No. 50 sieve) for digestion in 100 ml cold (3-5°C/38-41°F) HCl (1+4) in a 250 ml beaker for 15 min. on a magnetic stirrer,
V. Filter thru. two 2.5 micron filter paper and keep the filtrate# 1,
VI. Digest the residue with filter paper in 75 ml hot NaOH (below boiling) on hot plate for 15 min. on magnetic stirrer,
VII. Cool down to room temp. and filter thru. two 2.5 micron filter paper and collect filtrate# 2,
VIII. Combine these two filtrates, filter the combined filtrates thru. two 2.5 micron filter paper to remove any suspended silica (especially for sand-rich mortars, or if mortar is grounded too long); then dilute to 250 ml in a volumetric flask with dist. water, an aliquot (about 10 ml) is then used for XRF for soluble silica determination against the calibrations with standard PC mortars of known soluble silica contents prepared in the same way.

5. *Acid Digestion – Acid-Insoluble Residue Content for Siliceous Sand Content* (2 g)

I. Take 1-2 g of prepared mortar powder from Step 4 iii (passing No. 50 sieve) and digest in 50 ml HCl (1+3) in a 250 ml beaker (covered) on a hot pate rapidly near boiling, then 15 min. at a temp. below boiling, then cool down to room temperatures,
II. Filter thru. two pre-weighed 2.5 micron filter papers, washing the beaker, paper, and residue thoroughly with hot water,
III. Dry the filter paper at 110C for 10 min, cool in a desiccator to room temp. and measure the weight.
IV. Subtract from mass of dry filter paper to determine acid-insoluble residue content.

6. *Chemical Analysis – Loss On Ignition for Free and Combined Water Content, and Carbonate plus Carbonation* (2 g)

I. Take 1-2 g (W_1) of prepared mortar powder from Step 3 iii (passing No. 50 sieve) in a tarred porcelain crucible (keep a record of mass of the empty crucible),
II. Dry at 110°C for 15 min in a muffle furnace pre-set to 110°C, cool in a desiccator to room temp. and measure the mass (W_2) by subtracting the empty crucible mass from the total mass,
III. Ignite at 550°C for 15 min. in the muffle furnace pre-set to 550°C, cool in a desiccator to room temp. and measure the mass (W_3) by subtracting the empty crucible mass from the total mass,
IV. Ignite at 950°C for 15 min. in the muffle furnace pre-set to 950°C, cool in a desiccator to room temp. and measure the mass (W_4) by subtracting the empty crucible mass from the total mass,
V. Calculate the losses on ignition at 110°C, 550°C, and 950°C for free water, combined water, and carbonate plus degree of carbonation, respectively.

7. *Mineralogy of Bulk Mortar, Extracted Sand, Extracted Binder, or Salt from XRD* (at least 8 g)

I. Weigh 8.00 g of mortar (or extracted sand or binder as needed) lightly ground in a mortar & pestle, add three grinding/pelletizing aid tablets (e.g., from Oxford Instruments) and pulverize in a suitable mill to minimize contamination (e.g., Rocklab pulverizer with WC bowl or McCrone Micronizing Mill with agate) for 3 min. with anhydrous alcohol to get <45 micron size particles passing U.S. No. 325 sieve,
II. Take 6.8 to 7.0 g. of ground <45 micron prepared mass in an aluminum sample holder inside a stainless steel die to prepare a 32 mm pellet with 25 ton pressure for 1 min,
III. Use the prepared pellet for XRD and then use the same pellet for XRF.
IV. Do XRD on the binder-rich fraction, or salt either on a shallow-depth sample holder or preferably on a zero background quartz plate for small volume of sample.

8. *Bulk Mortar's Composition from X-Ray Fluorescence (XRF)* (same pellet used in XRD)

I. Use the same pellet prepared for XRD in the XRF, or, use a fused bead if sample volume is low to prepare a pellet. In either method, have calibrations of measured oxides with adequate standard.
II. XRF can also be used with proper calibrations for soluble silica determination on the filtrates after acid and alkali digestions, as described in Section 4.

9. *Thermal Analyses* (0.1 g), TGA, DTG, DSC, DTA, for quantitative analysis of various hydrous, sulfate, and carbonate phases in mortar, content of dolomitic lime added from the brucite content in mortar as determined from TGA or DSC, etc.

I. Simultaneous TGA and DSC analyses can be done on 30-70 mg of finely ground (<0.6 mm) mortar in alumina crucible (70 µl, no lid) from 30°C to 1000°C at a heating rate of 10°C/min with high purity nitrogen as purge gas at a flow rate of 75.0 ml/min .

10. *Infrared Spectroscopy,* for determination of various organic additives, paint, and clays in mortar

I. Take an aliquot of powder prepared for thermal analysis, or peel a paint and use that in Universal ATR of FTIR.
II. Alternately, digest a pulverized mortar in acetone to extract the organic additive and analyze the liquid in FTIR for characteristic functional groups.

11. *Ion Chromatography of Water-Soluble Salts* (1 g)

I. Take an aliquot of 1.00 gram powder prepared for chemical analysis (i.e. passing U.S. No. 50 sieve), digest in hot (below boiling) 50 ml distilled or deionized water for at least 6 hours in a beaker on a magnetic stirrer covered with watch glass, filter the solid residues out to collect the filtrate and analyze the final 100 ml of filtrate for soluble salts (chloride, sulfate, nitrate, nitrite, phosphate, etc.) by ion chromatography.

Figure 7: Outline of step-by-step procedures of various laboratory analyses of a masonry mortar, many of which were followed for the present mortar sample.

RESULTS

Grain-size Distribution of Sand in Mortar #1

Figure 8 shows grain-size distribution of sand extracted after digestion of Mortar #1 from exterior east elevation of Castle in dilute (1+3) hydrochloric acid. Due to extremely fine grain size of sand (silty sand) in the mortar, effective separation of sand from the binder after dissolving all binder components was impossible, even after 10 days of continuous acid digestion and magnetic stirring of the acid-soaked sample. As a result, lumps of undigested mortar were left mostly in the coarsest fractions after sieve analysis. Results of sieve analysis, therefore, do not indicate the true grain size distribution of the coarsest size fractions of sand *per se*.

Also shown are micrographs of extracted sand particles taken with a stereomicroscope retained on various sieves including size, shape, angularity, and color variations of sand particles. Many sand particles in the coarsest fractions are still agglomerated due to incomplete separation of binder from silty sand particles despite repeated acid digestion. It is important to remember that argillaceous sand particles, if any, have broken down during acid digestion and hence are present mostly in the finest fractions instead of intact grains, and calcareous particles, if present, are mostly dissolved out in acid. Hence, photos of particles retained on each sieve are mostly from the siliceous component of sand.

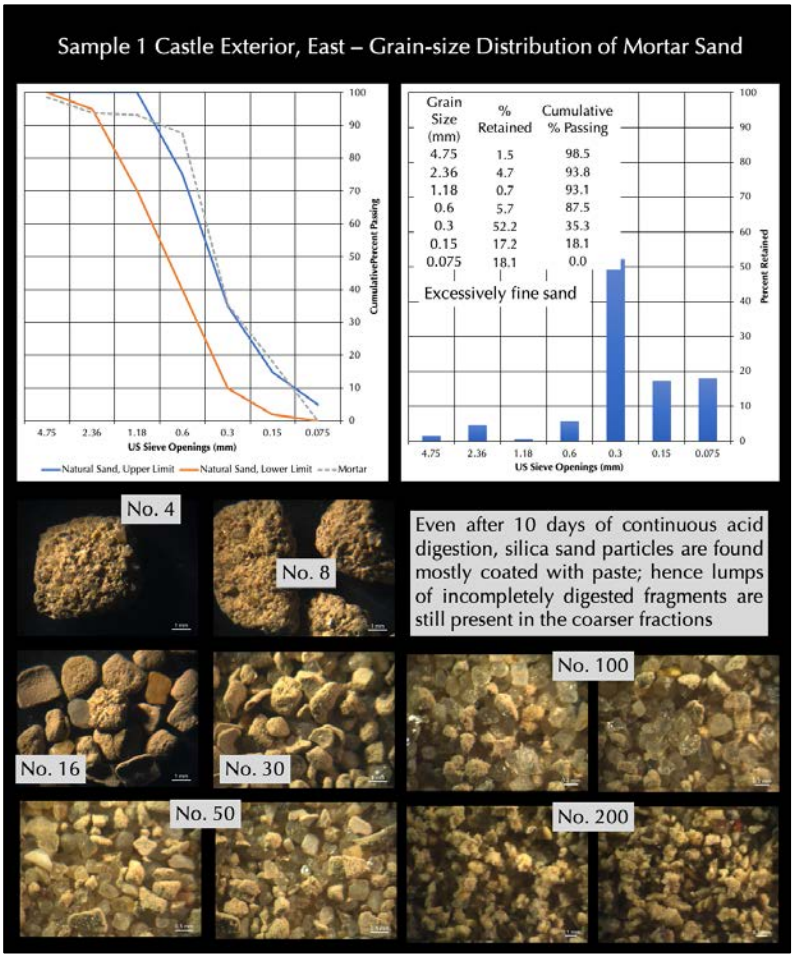

Figure 8: Grain-size distribution of sand extracted from the mortar after acid digestion. In the top left plot, size distribution of sand is compared with upper and lower limit of natural sand in ASTM C 144 (blue and red lines). Top right plot shows distribution of sand (inset Table shows percent retained and cumulative percent passing through each sieve). Bottom photos show stereo-micrographs of sand particles retained on various sieves.

Size distribution of sand in the mortar is compared with the ASTM C 144 specification of natural sand for unit masonry, which shows that for all size fractions, sand is noticeably finer than the upper limit of ASTM C 144 size gradation for natural sand indicating a finer particle size than C 144 sand in the silty sand category. The 'percent retained' histogram plot shows the abundance of fines in sand which is detrimental for the overall water demand of mortar. Therefore, sand is judged to be excessively finer than a modern ASTM C 144 masonry sand, rich mostly in close to silt-size fractions (silt, however, by definition, is < 0.05 mm in size, sand is between 2 and 0.05 mm in size).

Subsequent optical microscopical examinations of sand determined its **siliceous composition**. Therefore, materials extracted from acid digestion are determined to be majority of the sand.

Grain-size Distribution of Sand in Mortar #2

Figure 9 shows grain-size distribution of sand extracted after digestion of Mortar #2 from interior north elevation of Castle in dilute (1+3) hydrochloric acid. Due to extremely fine grain size of sand (silty sand) in the mortar, effective separation of sand from the binder after dissolving all binder components was impossible, even after 10 days of continuous acid digestion and magnetic stirring of the acid-soaked sample. As a result, lumps of undigested mortar were left mostly in the coarsest fractions after sieve analysis. Results of sieve analysis, therefore, do not indicate the true grain size distribution of the coarsest size fractions of sand *per se*.

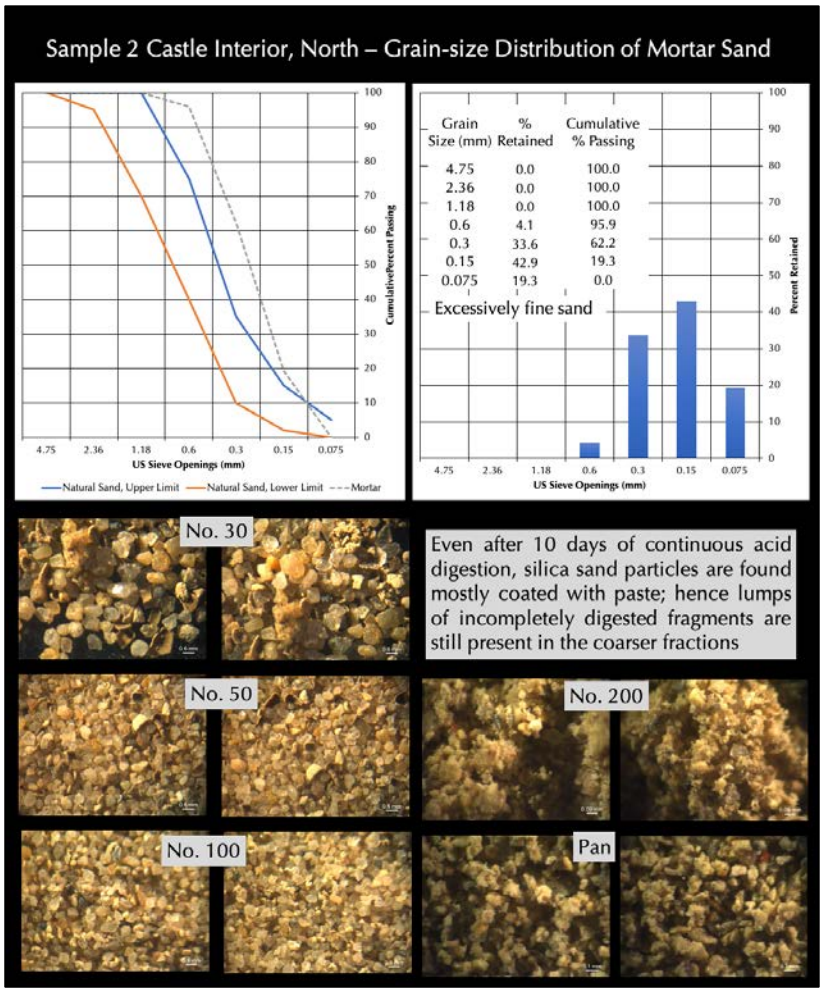

Figure 9: Grain-size distribution of sand extracted from the mortar after acid digestion. In the top left plot, size distribution of sand is compared with upper and lower limit of natural sand in ASTM C 144 (blue and red lines). Top right plot shows distribution of sand (inset Table shows percent retained and cumulative percent passing through each sieve). Bottom photos show stereo-micrographs of sand particles retained on various sieves.

Also shown are micrographs of extracted sand particles taken with a stereomicroscope retained on various sieves including size, shape, angularity, and color variations of sand particles. Many sand particles in the coarsest fractions are still agglomerated due to incomplete separation of binder from silty sand particles despite repeated acid digestion. It is important to remember that argillaceous sand particles, if any, have broken down during acid digestion and hence are present mostly in the finest fractions instead of intact grains, and calcareous particles, if present, are mostly dissolved out in acid. Hence, photos of particles retained on each sieve are mostly from the siliceous component of sand.

Size distribution of sand in the mortar is compared with the ASTM C 144 specification of natural sand for unit masonry, which shows that for all size fractions, sand is noticeably finer than the upper limit of ASTM C 144 size gradation for natural sand indicating a finer particle size than C 144 sand in the silty sand category. The 'percent retained' histogram plot shows the abundance of fines in sand which is detrimental for the overall water demand of mortar. Therefore, sand is judged to be excessively finer than a modern ASTM C 144 masonry sand, rich mostly in close to silt-size fractions (silt, however, by definition, is < 0.05 mm in size, sand is between 2 and 0.05 mm in size).

Subsequent optical microscopical examinations of sand determined its **siliceous composition**. Therefore, materials extracted from acid digestion are determined to be majority of the sand.

Grain-size Distribution of Sand in Mortar #3

Figure 10 shows grain-size distribution of sand extracted after digestion of Mortar #3 from North Dome of Meigs Vault in dilute (1+3) hydrochloric acid. Due to extremely fine grain size of sand (silty sand) in the mortar, effective separation of sand from the binder after dissolving all binder components was impossible, even after 10 days of continuous acid digestion and magnetic stirring of the acid-soaked sample. As a result, lumps of undigested mortar were left mostly in the coarsest fractions after sieve analysis. Results of sieve analysis, therefore, do not indicate the true grain size distribution of the coarsest size fractions of sand *per se*.

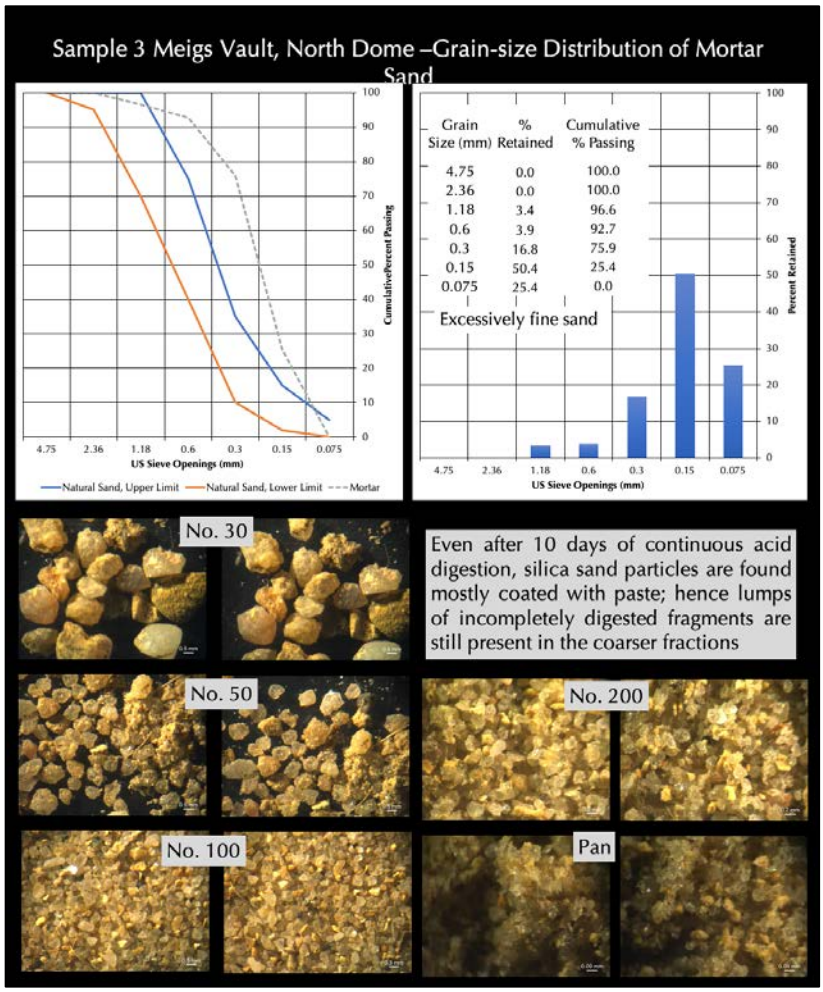

Figure 10: Grain-size distribution of sand extracted from the mortar after acid digestion. In the top left plot, size distribution of sand is compared with upper and lower limit of natural sand in ASTM C 144 (blue and red lines). Top right plot shows distribution of sand (inset Table shows percent retained and cumulative percent passing through each sieve). Bottom photos show stereo-micrographs of sand particles retained on various sieves.

Also shown are micrographs of extracted sand particles taken with a stereomicroscope retained on various sieves including size, shape, angularity, and color variations of sand particles. Many sand particles in the coarsest fractions are still agglomerated due to incomplete separation of binder from silty sand particles despite repeated acid digestion. It is important to remember that argillaceous sand particles, if any, have broken down during acid digestion and hence are present mostly in the finest fractions instead of intact grains, and calcareous particles, if present, are mostly dissolved out in acid. Hence, photos of particles retained on each sieve are mostly from the siliceous component of sand.

Size distribution of sand in the mortar is compared with the ASTM C 144 specification of natural sand for unit masonry, which shows that for all size fractions, sand is noticeably finer than the upper limit of ASTM C 144 size gradation for natural sand indicating a finer particle size than C 144 sand in the silty sand category. The 'percent retained' histogram plot shows the abundance of fines in sand which is detrimental for the overall water demand of mortar. Therefore, sand is judged to be excessively finer than a modern ASTM C 144 masonry sand, rich mostly in close to silt-size fractions (silt, however, by definition, is < 0.05 mm in size, sand is between 2 and 0.05 mm in size).

Subsequent optical microscopical examinations of sand determined its **siliceous composition**. Therefore, materials extracted from acid digestion are determined to be majority of the sand.

Grain-size Distribution of Sand in Mortar #4

Figure 11 shows grain-size distribution of sand extracted after digestion of Mortar #4 from interior of Meigs Vault in dilute (1+3) hydrochloric acid. Due to extremely fine grain size of sand (silty sand) in the mortar, effective separation of sand from the binder after dissolving all binder components was impossible, even after 10 days of continuous acid digestion and magnetic stirring of the acid-soaked sample. As a result, lumps of undigested mortar were left mostly in the coarsest fractions after sieve analysis. Results of sieve analysis, therefore, do not indicate the true grain size distribution of the coarsest size fractions of sand *per se*.

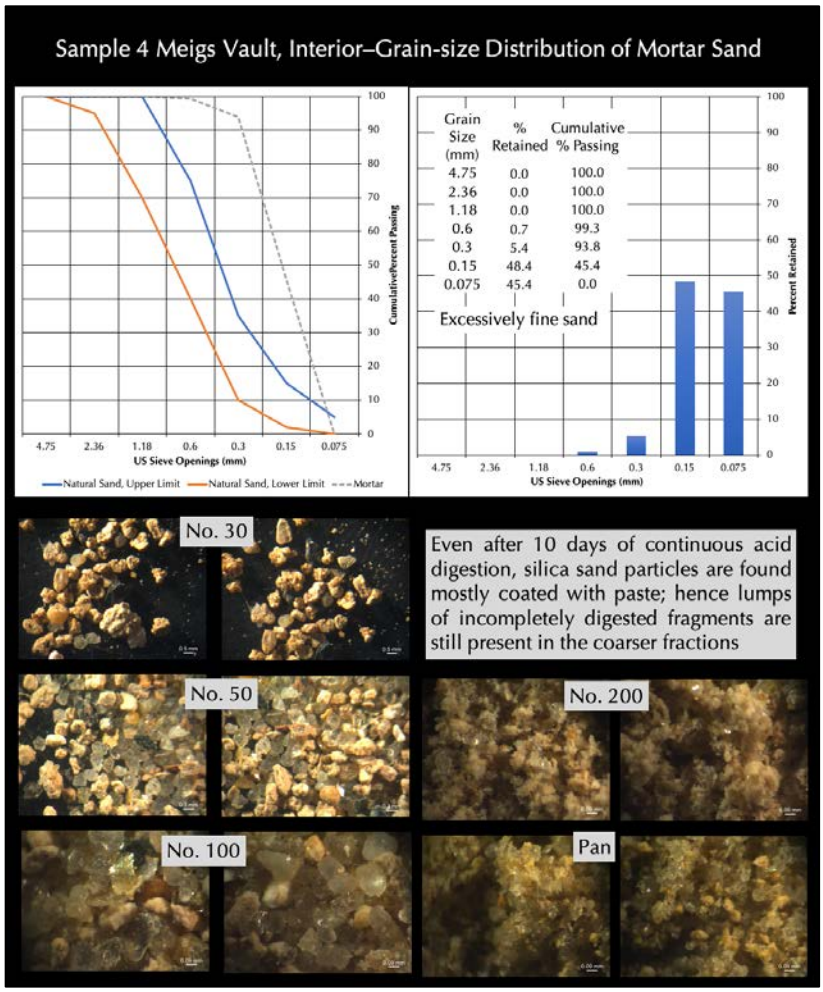

Figure 11: Grain-size distribution of sand extracted from the mortar after acid digestion. In the top left plot, size distribution of sand is compared with upper and lower limit of natural sand in ASTM C 144 (blue and red lines). Top right plot shows distribution of sand (inset Table shows percent retained and cumulative percent passing through each sieve). Bottom photos show stereo-micrographs of sand particles retained on various sieves.

Also shown are micrographs of extracted sand particles taken with a stereomicroscope retained on various sieves including size, shape, angularity, and color variations of sand particles. Many sand particles in the coarsest fractions are still agglomerated due to incomplete separation of binder from silty sand particles despite repeated acid digestion. It is important to remember that argillaceous sand particles, if any, have broken down during acid digestion and hence are present mostly in the finest fractions instead of intact grains, and calcareous particles, if present, are mostly dissolved out in acid. Hence, photos of particles retained on each sieve are mostly from the siliceous component of sand.

Size distribution of sand in the mortar is compared with the ASTM C 144 specification of natural sand for unit masonry, which shows that for all size fractions, sand is noticeably finer than the upper limit of ASTM C 144 size gradation for natural sand indicating a finer particle size than C 144 sand in the silty sand category. The 'percent retained' histogram plot shows the abundance of fines in sand which is detrimental for the overall water demand of mortar. Therefore, sand is judged to be excessively finer than a modern ASTM C 144 masonry sand. Sand in this mortar is finest of all four mortars received, rich mostly in close to silt-size fractions (silt, however, by definition, is < 0.05 mm in size, sand is between 2 and 0.05 mm in size).

Subsequent optical microscopical examinations of sand determined its **siliceous composition**. Therefore, materials extracted from acid digestion are determined to be majority of the sand.

Optical Microscopy of Sand

Figures 12 through 19 show size, shape, angularity, gradation, and distribution of siliceous sand particles in four mortar samples, which are all compositionally similar, excessively fine-grained as determined from sieve analyses of extracted sands, mostly made using quartz and quartzite particles. Figures 20 to 22 show similar sand particles in the three coats of stucco. These are scanned photos of thin sections of mortar fragments and stucco impregnated with a blue dye-mixed epoxy and scanned on a flatbed office scanner with film scanning capability where thin section was placed with one or two perpendicular polarizing filters to create plane-polarized light (PPL) and crossed-polarized light (XPL) views of scanned thin sections. PPL images show distribution of sand and voids whereas XPL images show dominantly siliceous (variably strained quartz, quartzite) composition of sand.

Sands in all mortar and stucco samples show excessively fine grain size where the dominant population of particles are less than 0.20 mm in nominal size, which is consistent with the results of grain-size distribution analyses of sand extracted from the mortars. Sand used was siliceous (mostly <0.2 mm quartz) noticeably finer than the modern equivalent of ASTM C 144 masonry sand, indicating potential use of close to the silt-sized fraction of the nearby Potomac river sand.

Figures 23 to 37 show micrographs of thin sections of mortars and the stucco sample taken with a petrographic microscope showing the overall siliceous compositions of sands in all samples examined. Sand particles contain major amounts of variably strained quartz sand, subordinate amounts of variably strained quartzite, fine-grained microcrystalline silica or chert, and feldspar particles. Sand particles are present in sound conditions without any evidence of potentially deleterious physical or chemical reactions in the mortars or in the three coats of stucco.

A major difference in sand between the samples #1 and 2 from the Castle and #3 and 4 from Meigs Vault, however, are detection of many mica (muscovite) flakes in the sand from Meigs Vault, which are not detected in the Castle sand. Mica in the sand was also not detected in the three coats of stucco sample.

Optical Microscopy of Paste

Mortar #1, 2, and 4 show many residual calcined argillaceous limestone raw feed particles of sizes less than 0.5 mm scattered throughout the variably carbonated hydraulic cement-lime matrix, which are indicative of use of natural cement as a main binder component in the mortars.

Mortar #3 does not show as many such particles as found in other samples, although a few such particles are detected indicating a potential low abundance of natural cement in that mortar from North Dome of Meigs Vault compared to the amounts added in three other samples.

Mortar #3 shows abundant leaching and carbonation of paste, deposition of secondary calcium carbonation in voids, porous leached gelatinous deposits in paste, etc., indicating more extensive water infiltration through this mortar compared to three other types.

Interstitial paste in all four mortars are variably carbonated, non-air-entrained, variably dense to porous, and indicative of the use of lime along with natural cement. The porous carbonated areas of paste were originally more enriched in lime compared to denser areas rich in natural cement.

Many typical microstructural features of natural cement are present in the incompletely calcined residual leftover argillaceous limestone raw feed particles. For example, detection of reddish rims around some dolomite rhombs in residual calcined raw feed particles (e.g., see Figures 25 and 27) indicate a dolomitic limestone composition of raw feed where iron diffusion towards the rims of dolomite during calcination is a common microstructural feature of many natural cement mortars. However, abundance of such red rimmed dolomite rhombs or pseudomorphs of such rhombs are limited indicating the original raw feed was not as magnesian or dolomitic as the raw feeds, for example used in the production of the classic Rosendale natural cements.

Absence of lime putty, fine carbonation shrinkage microcracks, and many other microstructural features of historic lime mortar are absence of porous areas obliterated by the denser patches of paste from hydration of natural cement.

Figures 25, and 33 to 36 show many individual residual calcined particles of the original argillaceous limestone raw feed of natural cement which are helpful to detect the compositions of the feed used in the production of natural cements.

Paste shows overall variably carbonated and non-carbonated natures along with leached areas due to prolonged interactions with the elements in the environment.

There is no evidence of any residual Portland cement particles found in the paste in any mortar samples, indicating lack of any Portland cement component in the binder, consistent with its reported history of construction.

Based on optical microscopy, therefore, the four mortar samples are determined to have natural cement and lime components where lime is more abundant in Mortar #3 than the other three mortars, which also showed the maximum leaching and alteration of the lime paste.

Like natural cement, the lime component was also derived from calcination of an impure limestone, which, however, had lesser silica, alumina, iron impurities to prevent formation of hydraulic component from calcination as in the case of natural cement.

Subsequent SEM-EDS studies of paste (Figures 38 to 41) determined the magnesian composition of paste which is characteristic of natural cement binder along with potential use of a magnesian lime binder as a subordinate component.

Air

All four mortar samples as well as the stucco sample are non-air-entrained.

Figure 12: Blue dye-mixed epoxy-impregnated thin section of Mortar #1 from exterior east elevation of Castle scanned on a film scanner in plane-polarized light (PPL) mode, by placing one polarizing filter with the thin section during scanning so that sand particles and interstitial binder phases can be distinguished by their characteristic optical properties. Sand particles are mostly < 0.2 mm in size, siliceous in composition having major amounts of quartz sand, subordinate amounts of variably strained quartzite, fine-grained microcrystalline silica, and feldspar particles.

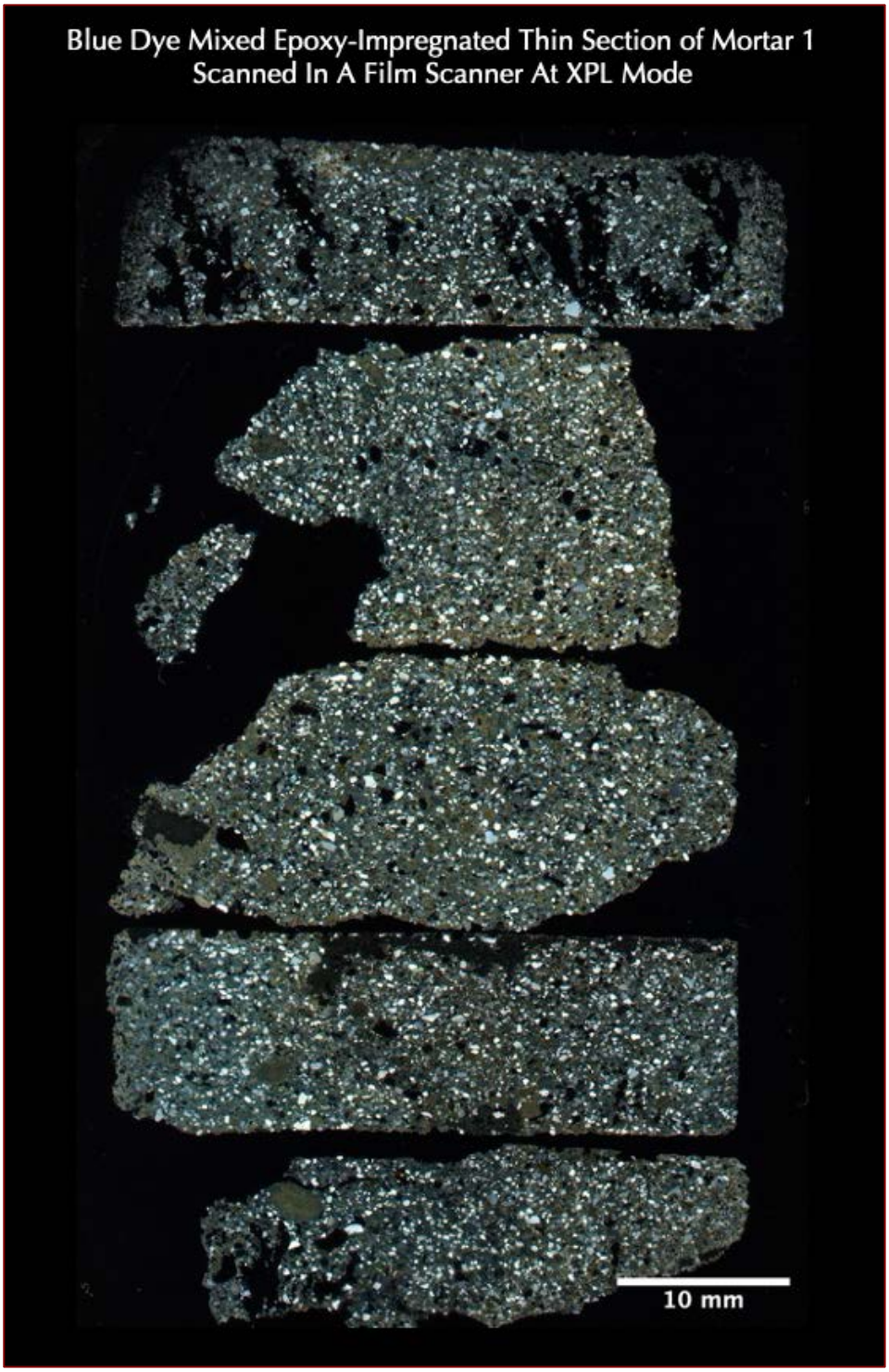

Figure 13: Blue dye-mixed epoxy-impregnated thin section of Mortar #1 from exterior east elevation of Castle scanned on a film scanner in crossed polarized light (XPL) mode, by placing two perpendicular polarizing filters with the thin section during scanning so that sand particles and interstitial binder phases can be distinguished by their characteristic optical properties. Sand particles are < 0.2 mm in size, siliceous in composition having major amounts of quartz sand, subordinate amounts of variably strained quartzite, fine-grained microcrystalline silica, and feldspar particles. Interstitial paste is variably dense and carbonated, and, non-air-entrained.

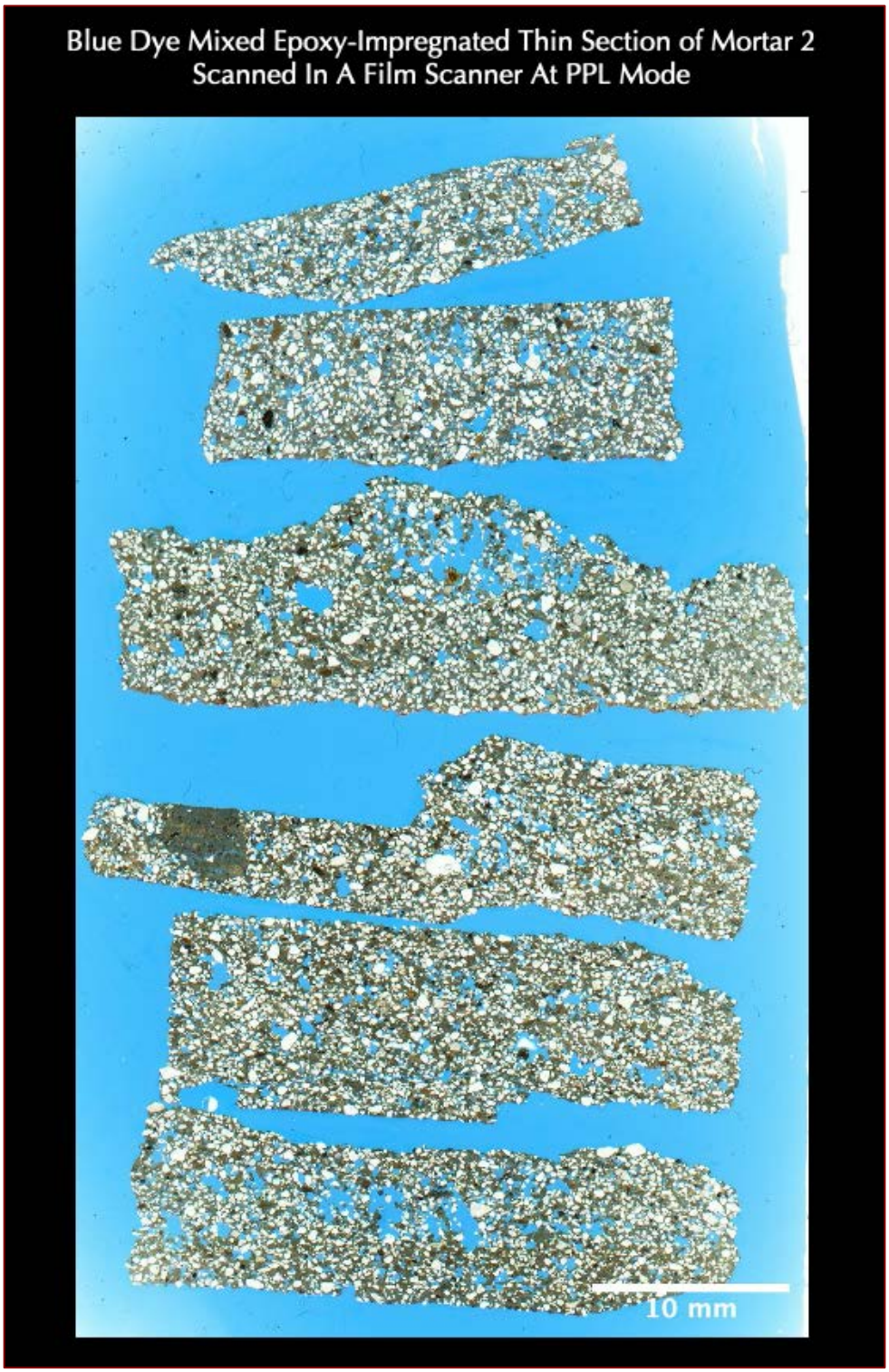

Figure 14: Blue dye-mixed epoxy-impregnated thin section of Mortar #2 from interior north elevation of Castle scanned on a film scanner in plane-polarized light (PPL) mode, by placing one polarizing filter with the thin section during scanning so that sand particles and interstitial binder phases can be distinguished by their characteristic optical properties. Sand particles are mostly < 0.2 mm in size, siliceous in composition having major amounts of quartz sand, subordinate amounts of variably strained quartzite, fine-grained microcrystalline silica, and feldspar particles.

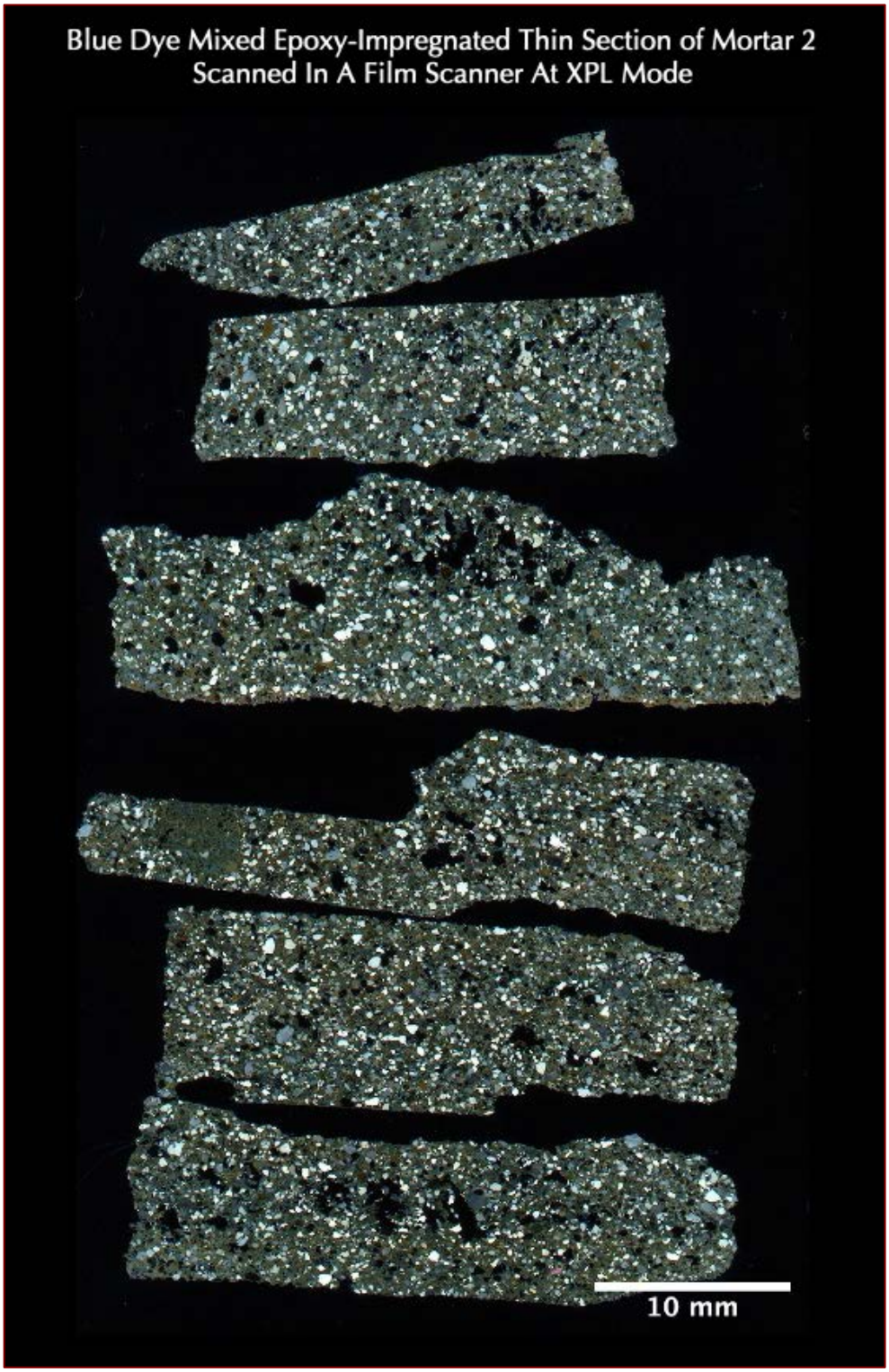

Figure 15: Blue dye-mixed epoxy-impregnated thin section of Mortar #2 from interior north elevation of Castle scanned on a film scanner in crossed polarized light (XPL) mode, by placing two perpendicular polarizing filters with the thin section during scanning so that sand particles and interstitial binder phases can be distinguished by their characteristic optical properties. Sand particles are < 0.2 mm in size, siliceous in composition having major amounts of quartz sand, subordinate amounts of variably strained quartzite, fine-grained microcrystalline silica, and feldspar particles. Interstitial paste is variably dense and carbonated, and, non-air-entrained.

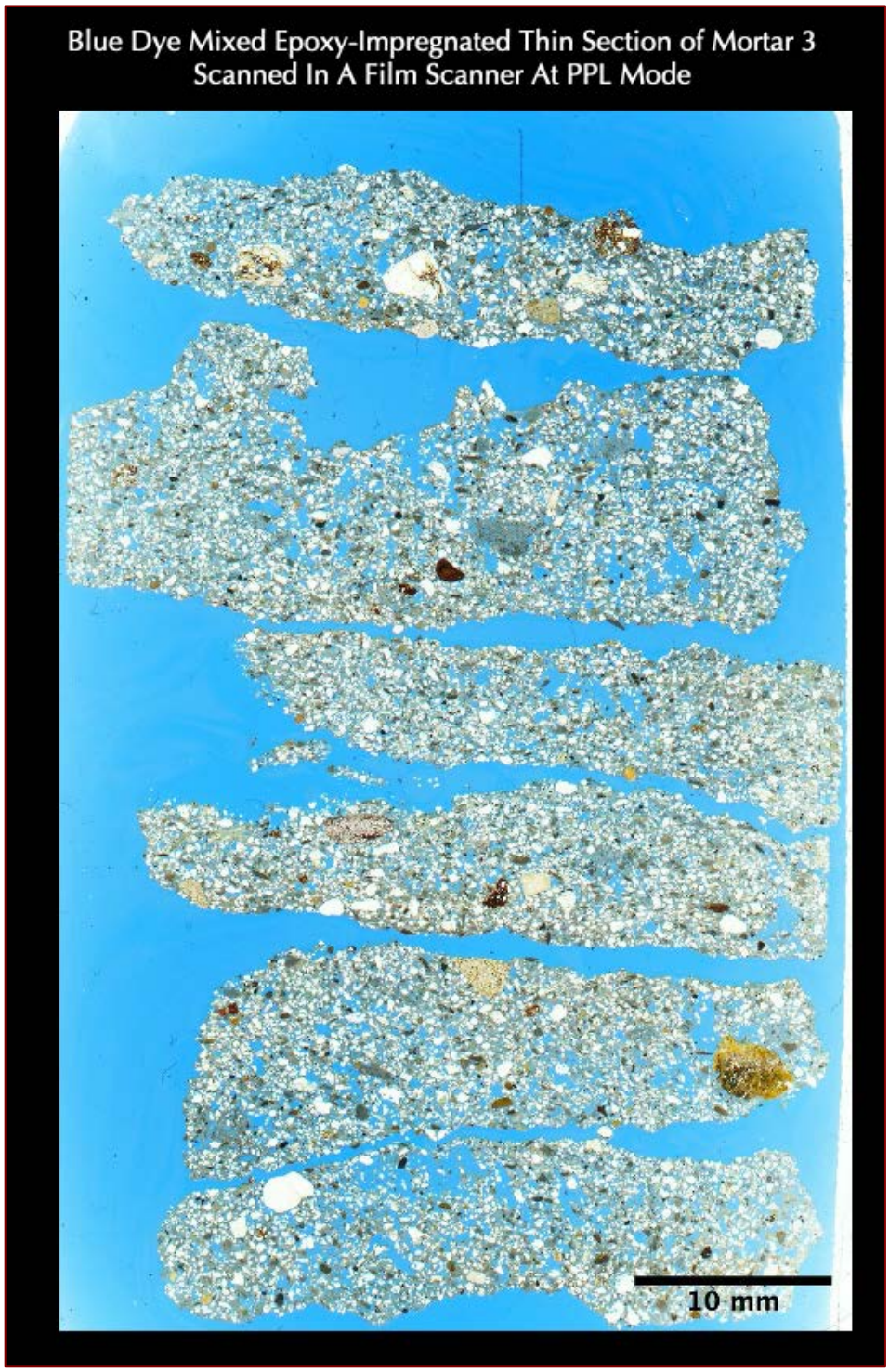

Figure 16: Blue dye-mixed epoxy-impregnated thin section of Mortar #3 from North Dome of Meigs Vault scanned on a film scanner in plane-polarized light (PPL) mode, by placing one polarizing filter with the thin section during scanning so that sand particles and interstitial binder phases can be distinguished by their characteristic optical properties. Sand particles are mostly < 0.2 mm in size, siliceous in composition having major amounts of quartz sand, subordinate amounts of variably strained quartzite, fine-grained microcrystalline silica, and feldspar particles.

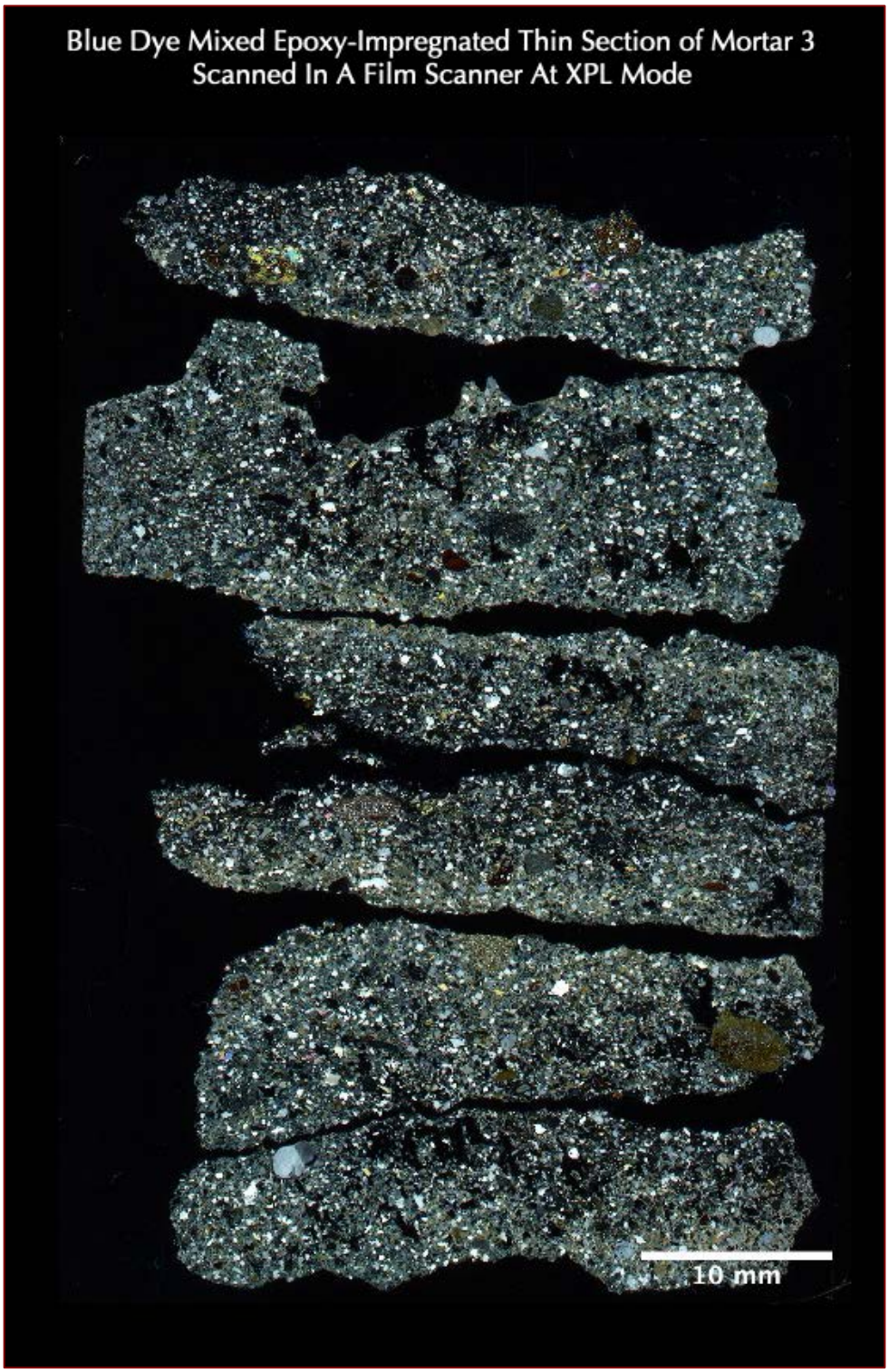

Figure 17: Blue dye-mixed epoxy-impregnated thin section of Mortar #3 from North Dome of Meigs Vault scanned on a film scanner in crossed polarized light (XPL) mode, by placing two perpendicular polarizing filters with the thin section during scanning so that sand particles and interstitial binder phases can be distinguished by their characteristic optical properties. Sand particles are < 0.2 mm in size, siliceous in composition having major amounts of quartz sand, subordinate amounts of variably strained quartzite, fine-grained microcrystalline silica, and feldspar particles. Interstitial paste is variably dense and carbonated, and, non-air-entrained.

Figure 18: Blue dye-mixed epoxy-impregnated thin section of Mortar #4 from interior of Meigs Vault scanned on a film scanner in plane-polarized light (PPL) mode, by placing one polarizing filter with the thin section during scanning so that sand particles and interstitial binder phases can be distinguished by their characteristic optical properties. Sand particles are mostly < 0.2 mm in size, siliceous in composition having major amounts of quartz sand, subordinate amounts of variably strained quartzite, fine-grained microcrystalline silica, and feldspar particles.

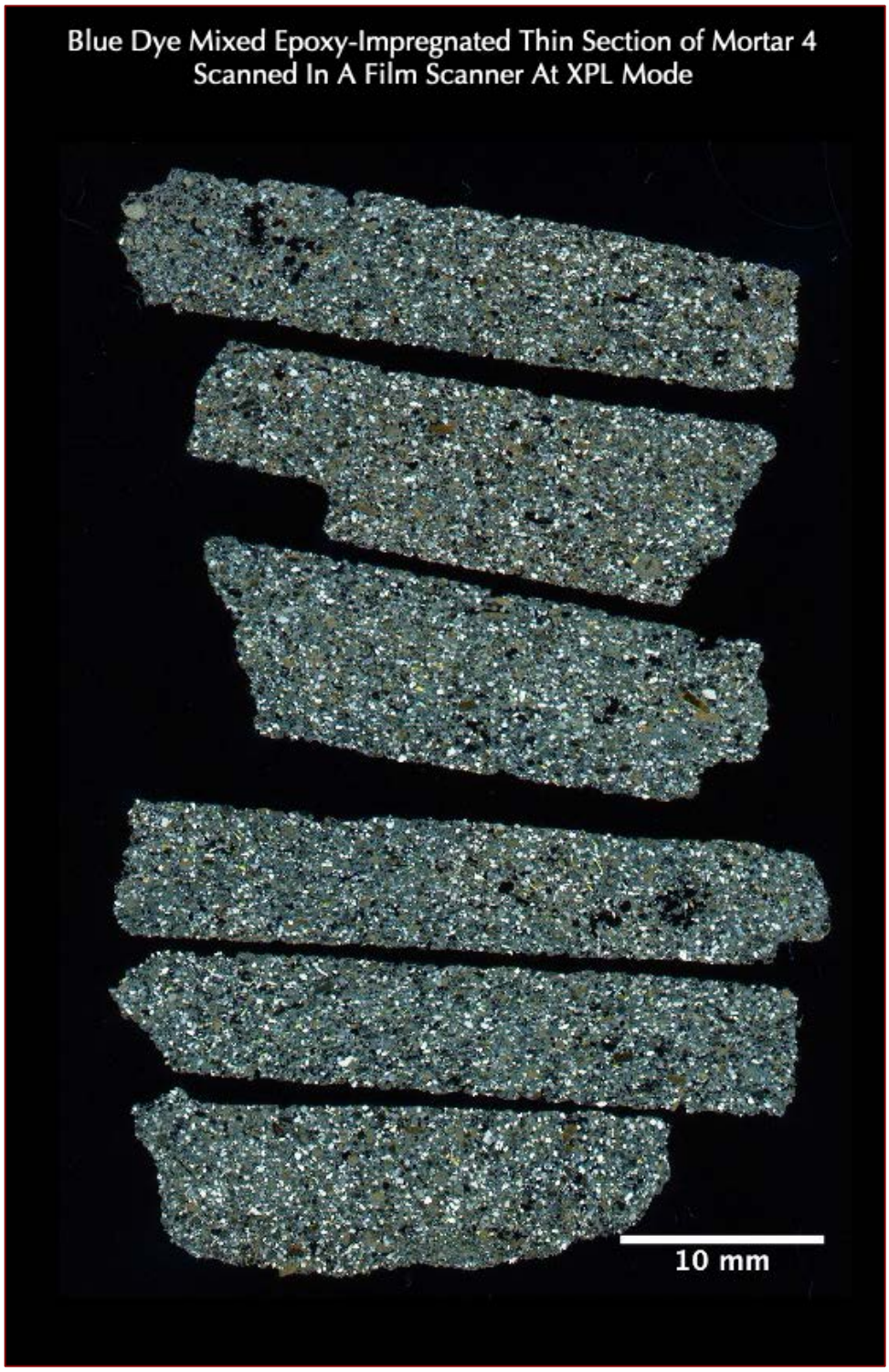

Figure 19: Blue dye-mixed epoxy-impregnated thin section of Mortar #4 from interior of Meigs Vault scanned on a film scanner in crossed polarized light (XPL) mode, by placing two perpendicular polarizing filters with the thin section during scanning so that sand particles and interstitial binder phases can be distinguished by their characteristic optical properties. Sand particles are < 0.2 mm in size, siliceous in composition having major amounts of quartz sand, subordinate amounts of variably strained quartzite, fine-grained microcrystalline silica, and feldspar particles. Interstitial paste is variably dense and carbonated, and, non-air-entrained.

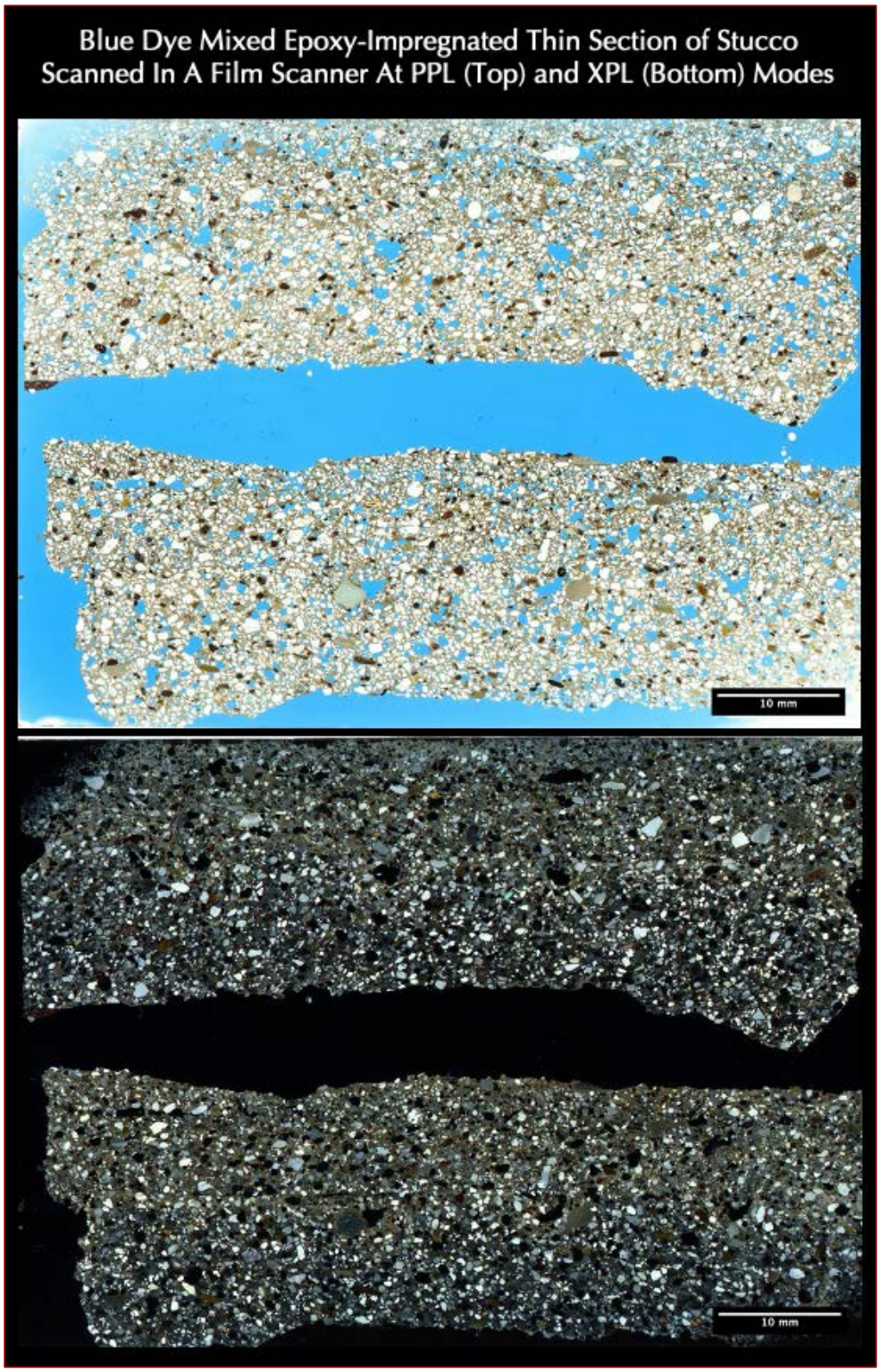

Figure 20: Blue dye-mixed epoxy-impregnated thin section of stucco sample scanned on a film scanner in plane (top) and crossed (bottom) polarized light (PPL and XPL) modes so that sand particles and interstitial binder phases can be distinguished by their characteristic optical properties. Sand particles are < 0.2 mm in size, siliceous in composition having major amounts of quartz sand, subordinate amounts of variably strained quartzite, fine-grained microcrystalline silica, and feldspar particles. Interstitial paste is variably dense and carbonated, and, non-air-entrained. The finish and brown coats show more carbonation of paste in the XPL image than the scratch coat.

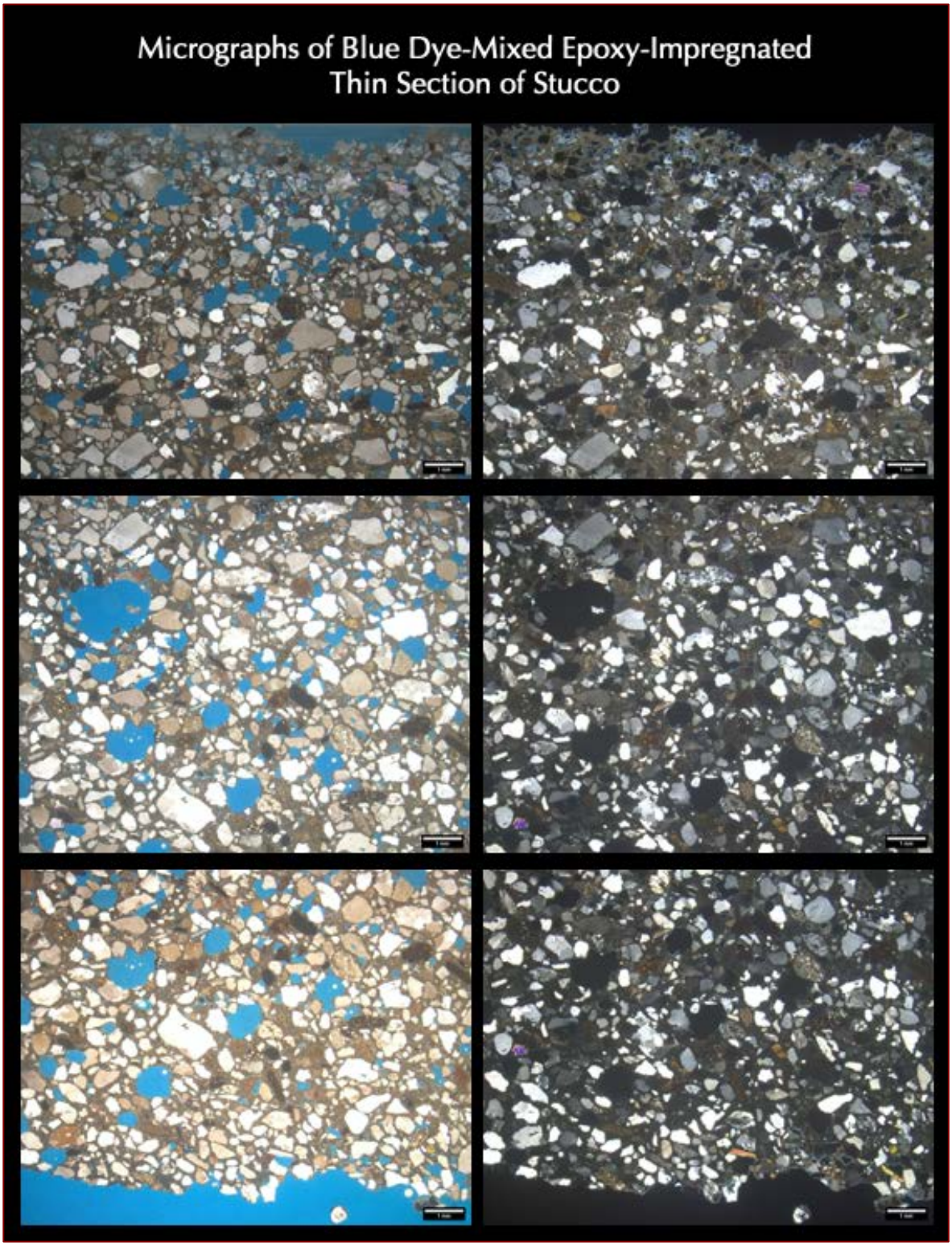

Figure 21: Micrographs of blue dye-mixed epoxy-impregnated thin section of stucco taken with a petrographic microscope in PPL (left) and corresponding XPL (right) modes, showing size, shape, angularity, gradation, and distribution of siliceous sand particles and variably carbonated Portland cement paste.

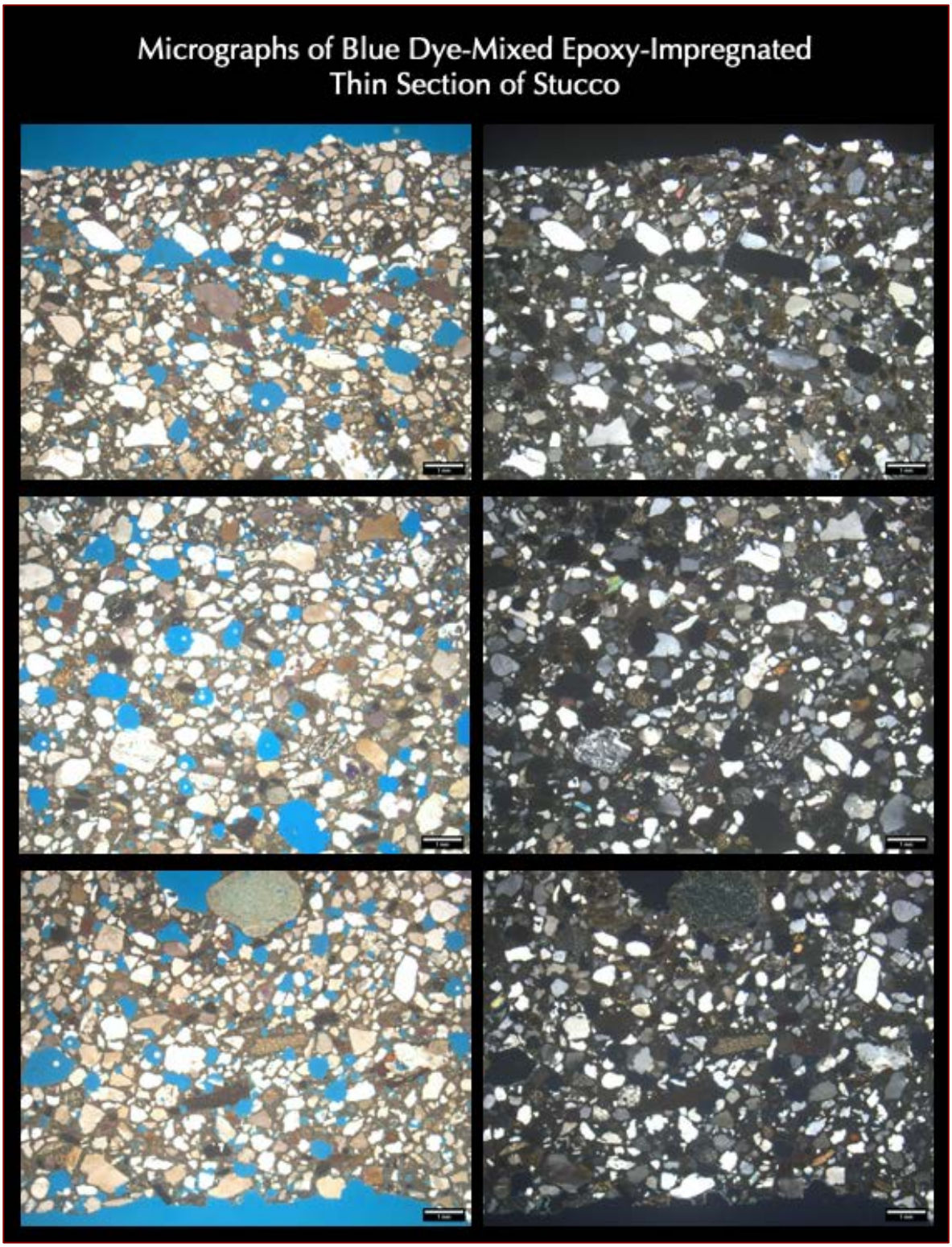

Figure 22: Micrographs of blue dye-mixed epoxy-impregnated thin section of stucco taken with a petrographic microscope in PPL (left) and corresponding XPL (right) modes, showing size, shape, angularity, gradation, and distribution of siliceous sand particles and variably carbonated Portland cement paste.

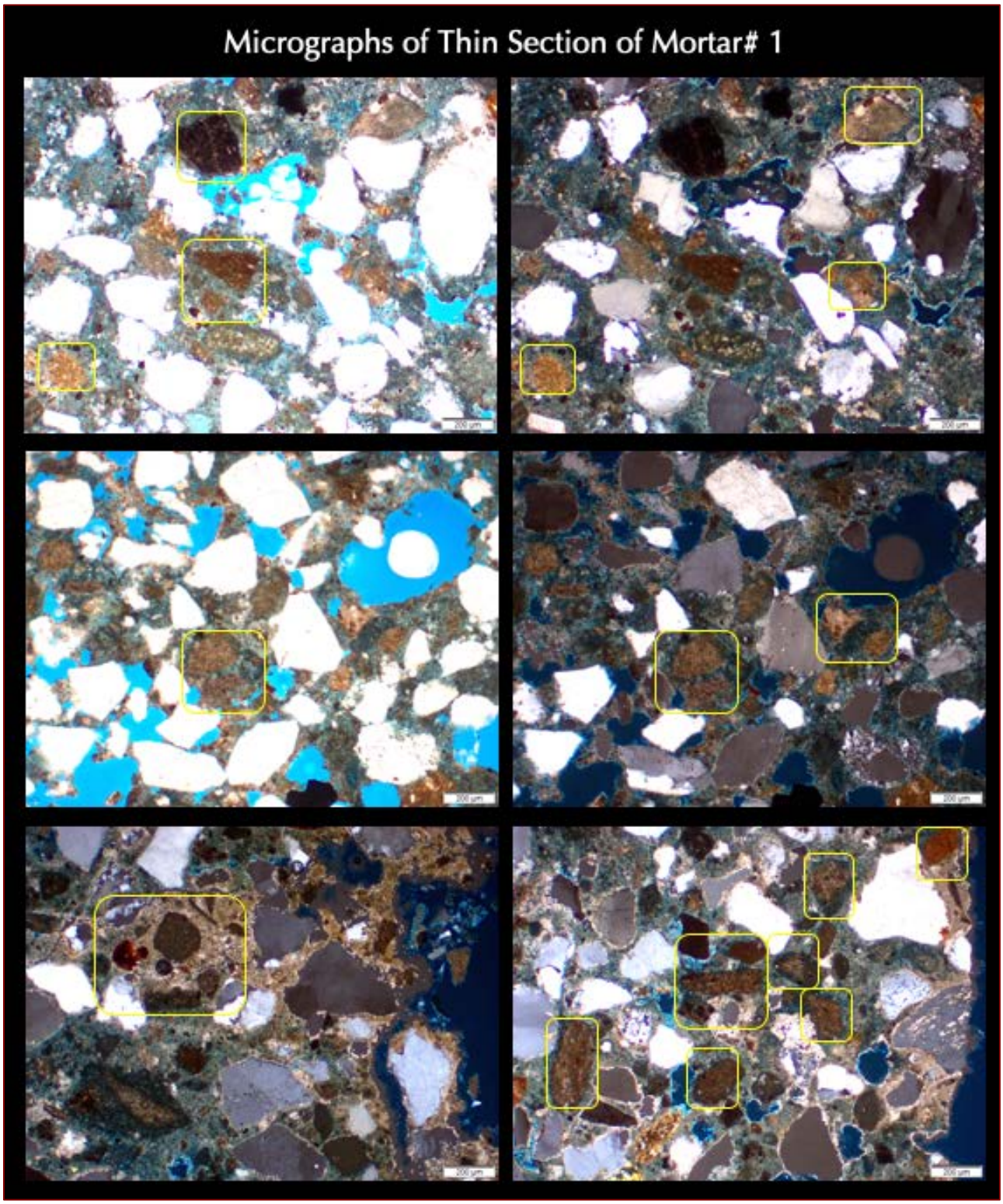

Figure 23: Micrographs of blue dye-mixed epoxy-impregnated thin section of Mortar #1 from exterior at east elevation of Castle taken with a petrographic microscope in PPL (left) and corresponding XPL (right) modes, showing size, shape, angularity, gradation, and distribution of siliceous sand particles and carbonated natural cement and lime paste having many residual incompletely calcined original argillaceous limestone raw feed particles (boxes) indicating use of natural cement as the main binder.

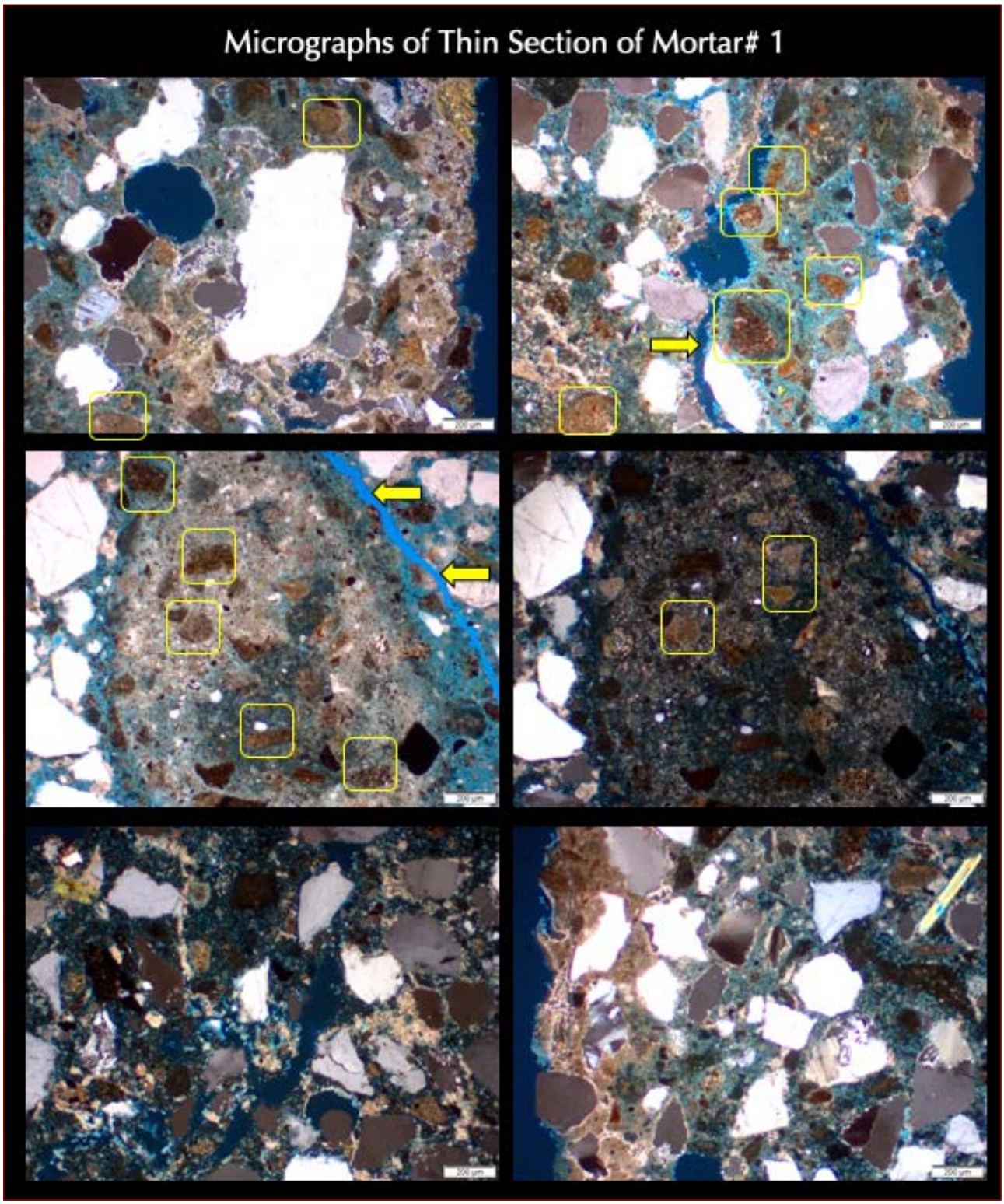

Figure 24: Micrographs of blue dye-mixed epoxy-impregnated thin section of Mortar #1 from exterior at east elevation of Castle taken with a petrographic microscope in PPL (left) and corresponding XPL (right) modes, showing size, shape, angularity, gradation, and distribution of siliceous sand particles and carbonated natural cement and lime paste having many residual incompletely calcined original argillaceous limestone raw feed particles (boxes) indicating use of natural cement as the main binder. Notice a denser carbonated area above a less dense carbonated surface of mortar in the top and bottom right photos.

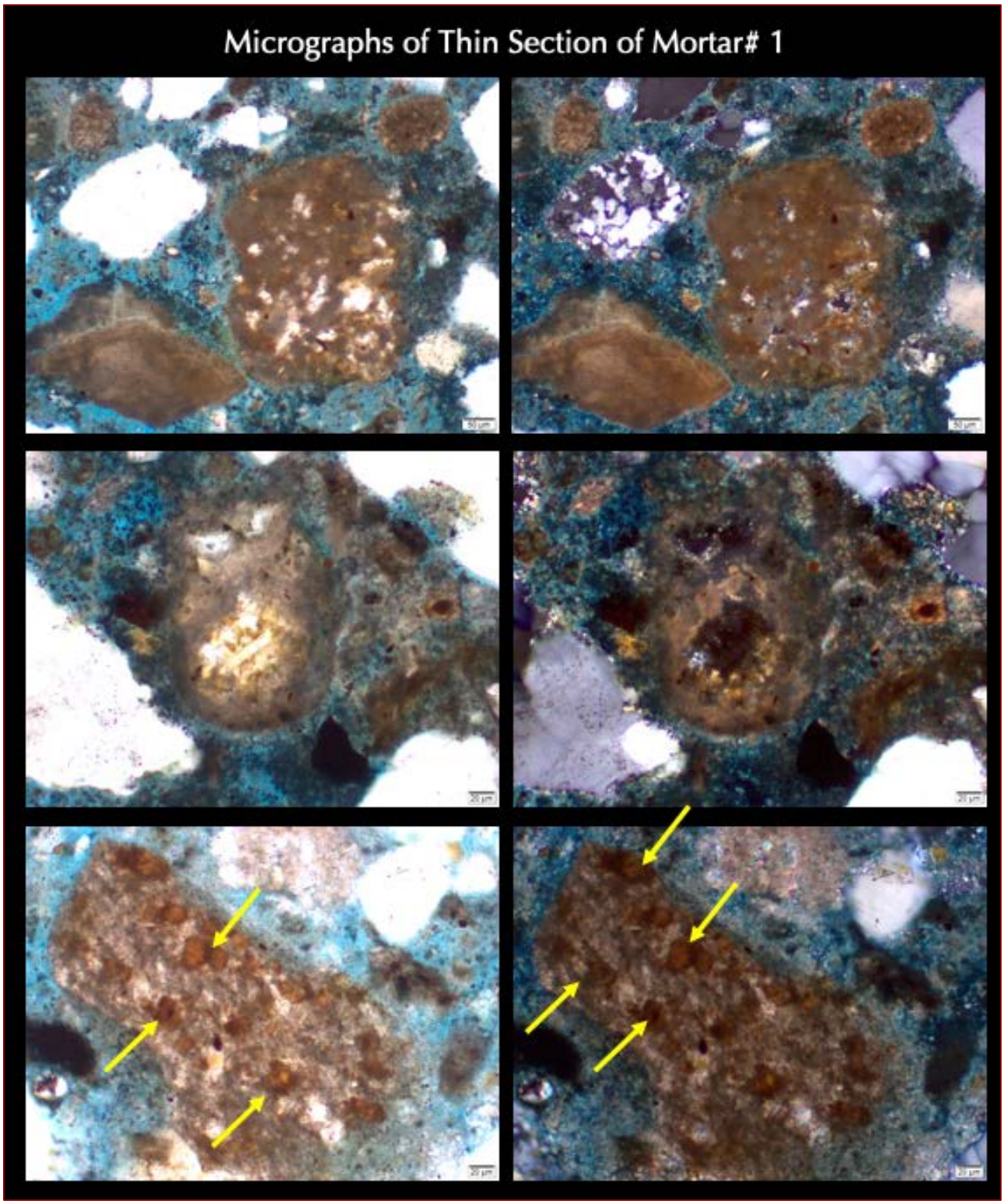

Figure 25: Micrographs of blue dye-mixed epoxy-impregnated thin section of Mortar #1 from the exterior at east elevation of Castle taken with a petrographic microscope in PPL (left) and corresponding XPL (right) modes, showing residual, incompletely calcined original argillaceous limestone raw feeds of natural cement productions leaving many telltale signatures of original microstructures of feed that have not been completely obliterated by the calcination process, or have been modified by calcination, e.g., as development of red oxidation rims from iron diffusion from the core to the rims of dolomite rhombs in the original particle which are marked with arrows.

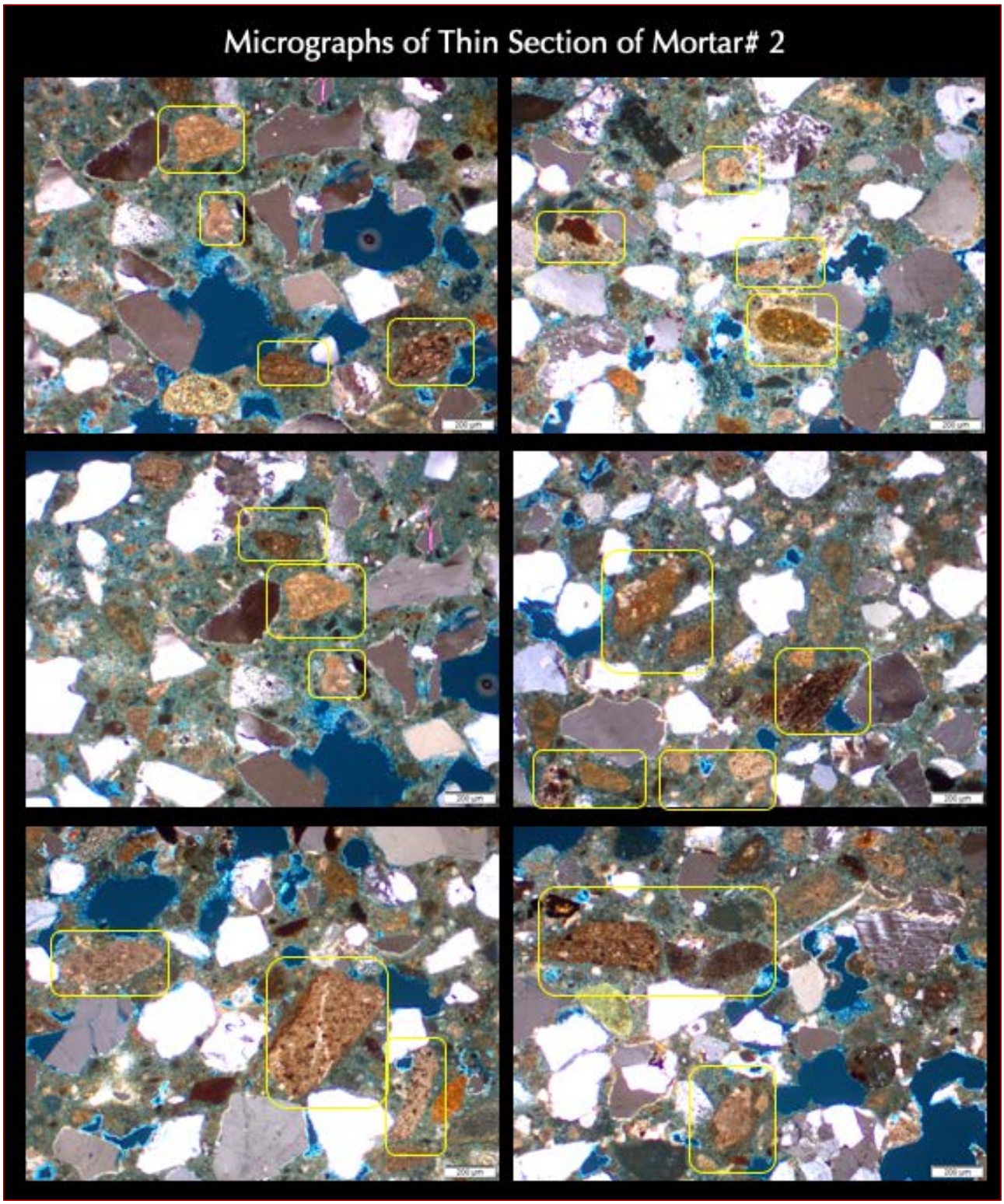

Figure 26: Micrographs of blue dye-mixed epoxy-impregnated thin section of Mortar #2 from interior at north elevation of Castle taken with a petrographic microscope, showing size, shape, angularity, gradation, and distribution of siliceous sand particles and carbonated natural cement and lime paste having many residual incompletely calcined original argillaceous limestone raw feed particles (boxes) indicating use of natural cement as the main binder.

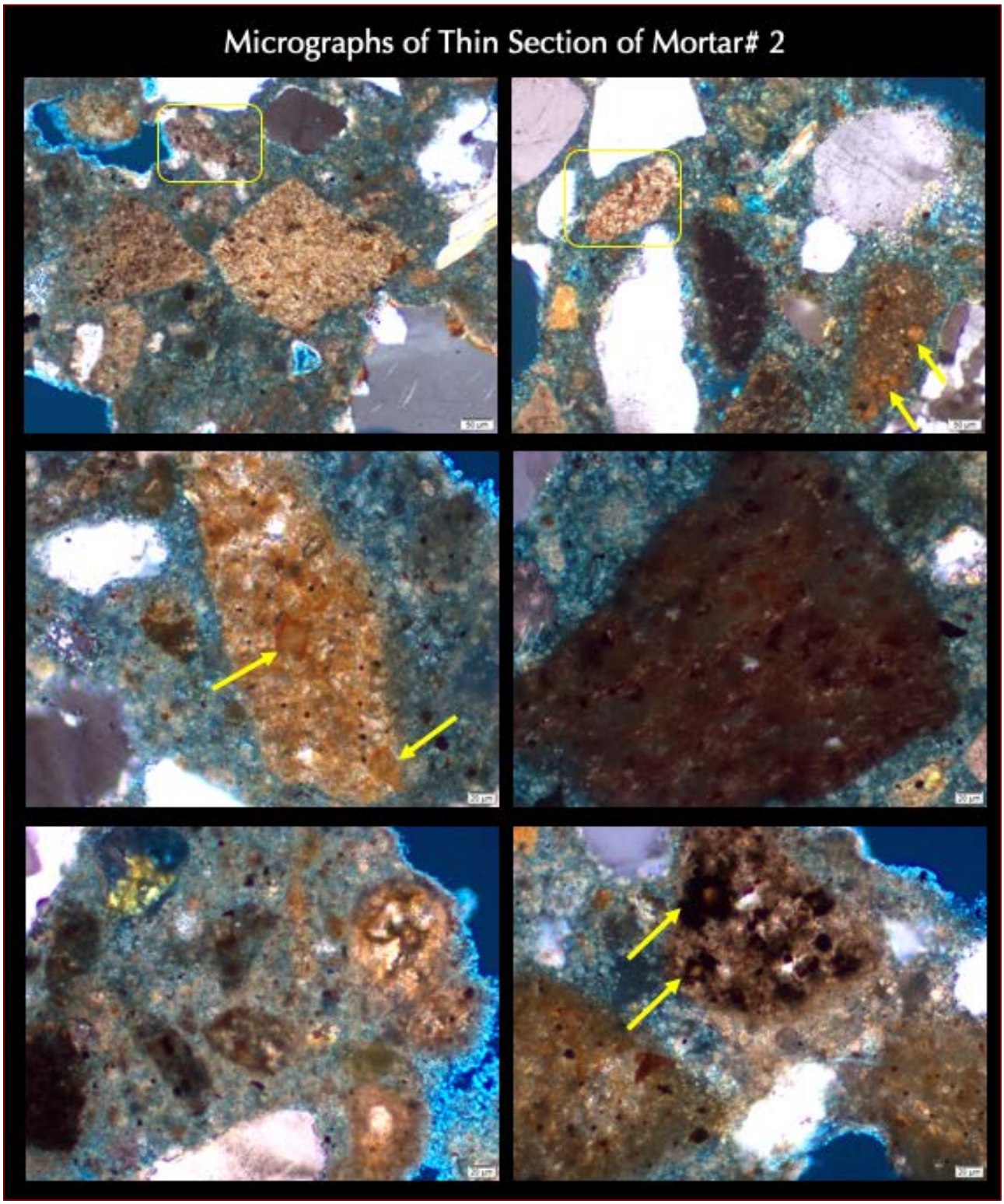

Figure 27: Micrographs of blue dye-mixed epoxy-impregnated thin section of Mortar #2 from interior at north elevation of Castle taken with a petrographic microscope, showing residual, incompletely calcined original argillaceous limestone raw feeds of natural cement productions leaving many telltale signatures of original microstructures of feed that have not been completely obliterated by the calcination process, or have been modified by calcination, e.g., as development of red oxidation rims from iron diffusion from the core to the rims of dolomite rhombs in the original particle which are marked with arrows.

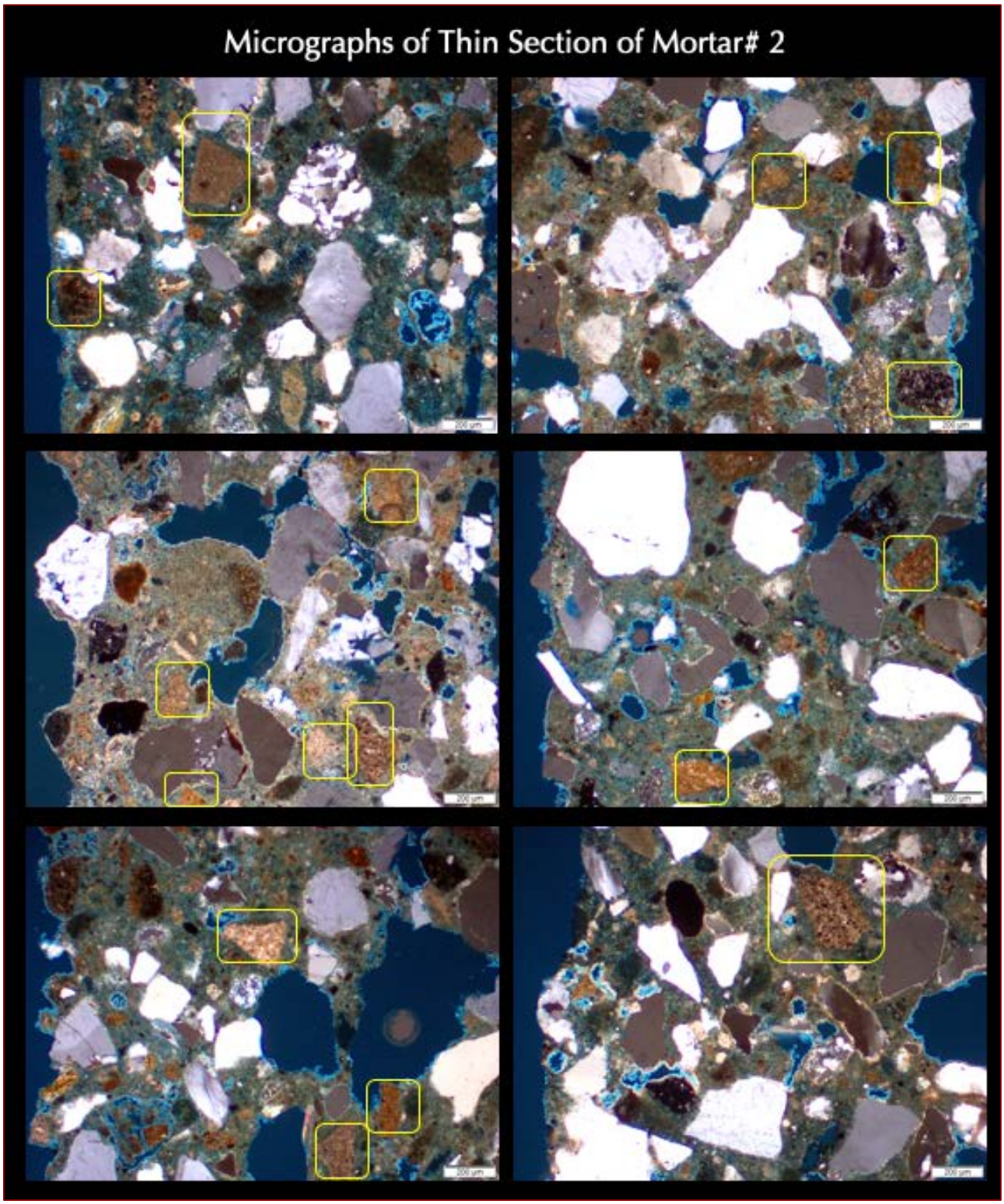

Figure 28: Micrographs of blue dye-mixed epoxy-impregnated thin section of Mortar #2 from interior at north elevation of Castle taken with a petrographic microscope, showing size, shape, angularity, gradation, and distribution of siliceous sand particles and carbonated natural cement and lime paste having many residual incompletely calcined original argillaceous limestone raw feed particles (boxes) indicating use of natural cement as the main binder.

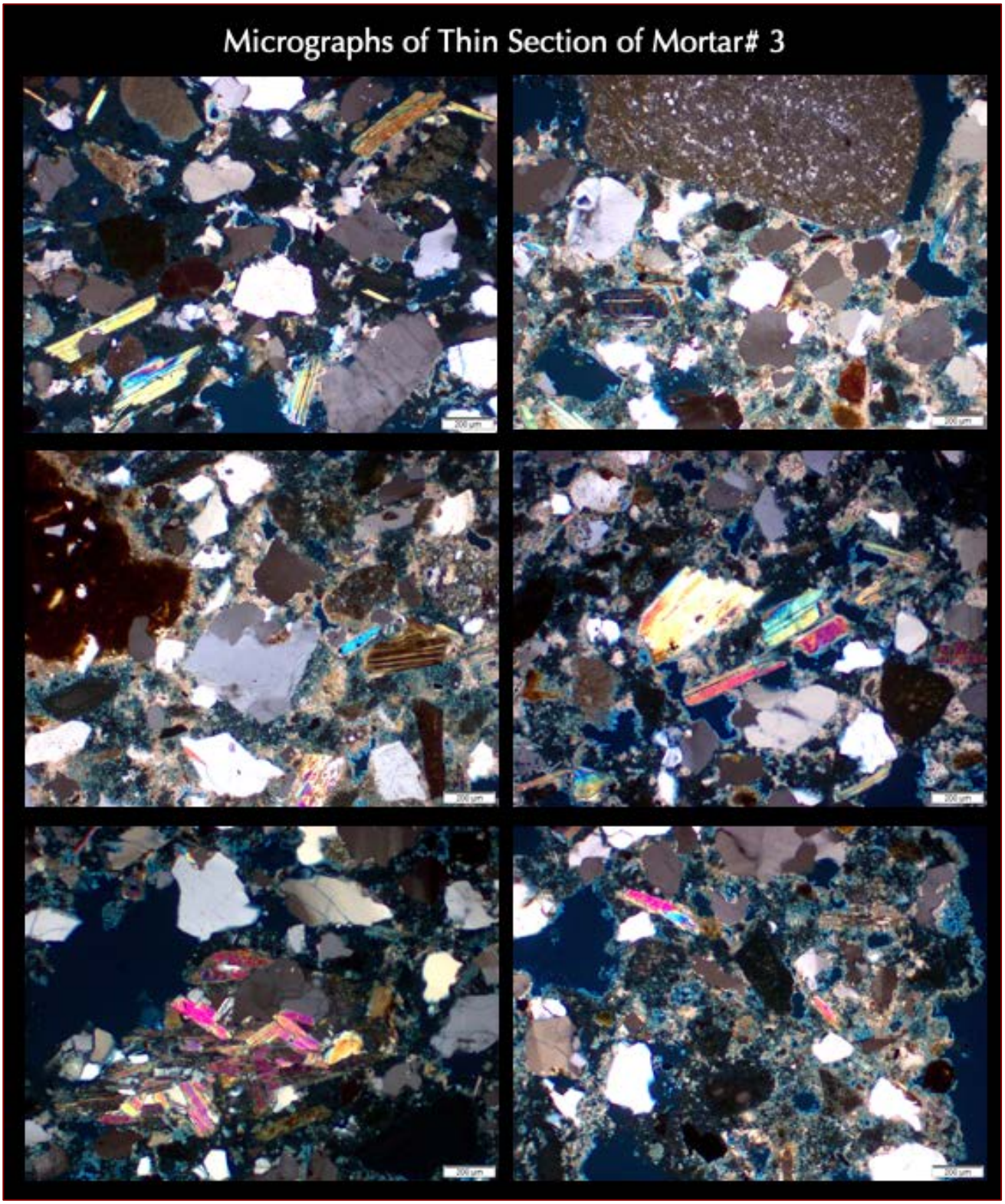

Figure 29: Micrographs of blue dye-mixed epoxy-impregnated thin section of Mortar #3 from North Dome of Meigs vault taken with a petrographic microscope, showing size, shape, angularity, gradation, and distribution of siliceous sand particles, many muscovite flakes in sand, and porous, carbonated, leached lime-rich paste.

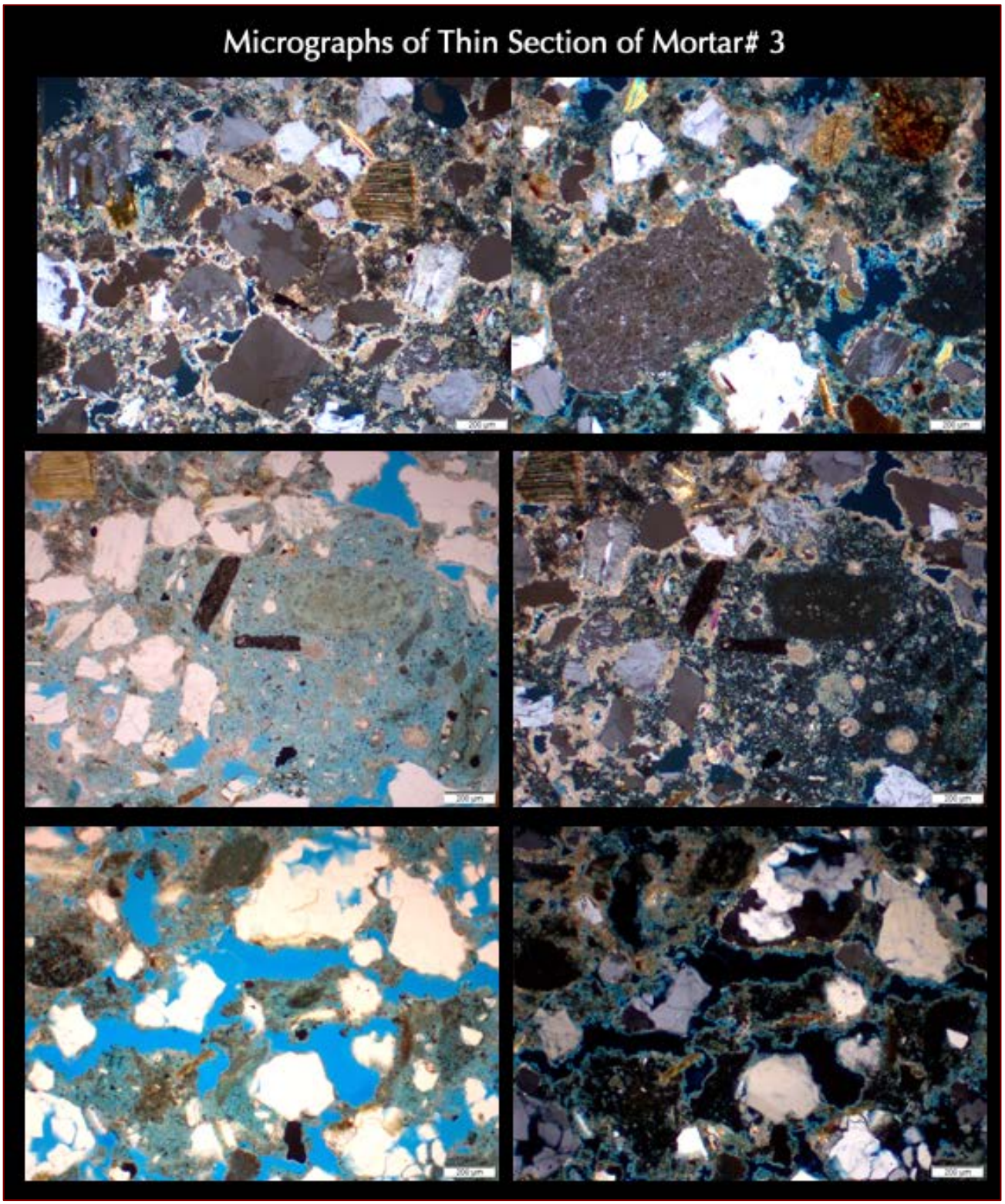

Figure 30: Micrographs of blue dye-mixed epoxy-impregnated thin section of Mortar #3 from North Dome of Meigs vault taken with a petrographic microscope, showing size, shape, angularity, gradation, and distribution of siliceous sand particles, many muscovite flakes in sand, and porous, carbonated, leached lime-rich paste.

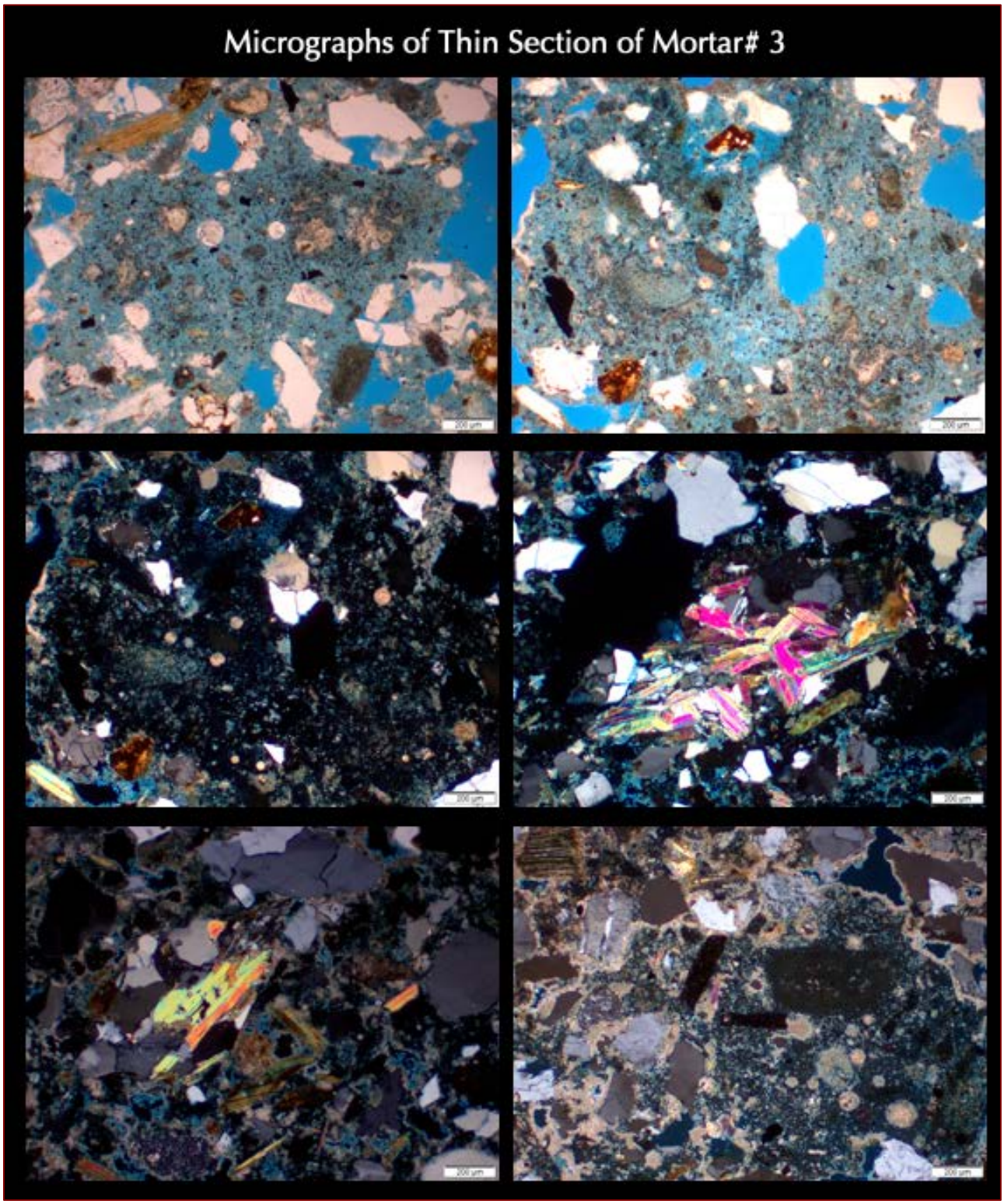

Figure 31: Micrographs of blue dye-mixed epoxy-impregnated thin section of Mortar #3 from North Dome of Meigs vault taken with a petrographic microscope, showing size, shape, angularity, gradation, and distribution of siliceous sand particles, many muscovite flakes in sand, and porous, carbonated, leached lime-rich paste.

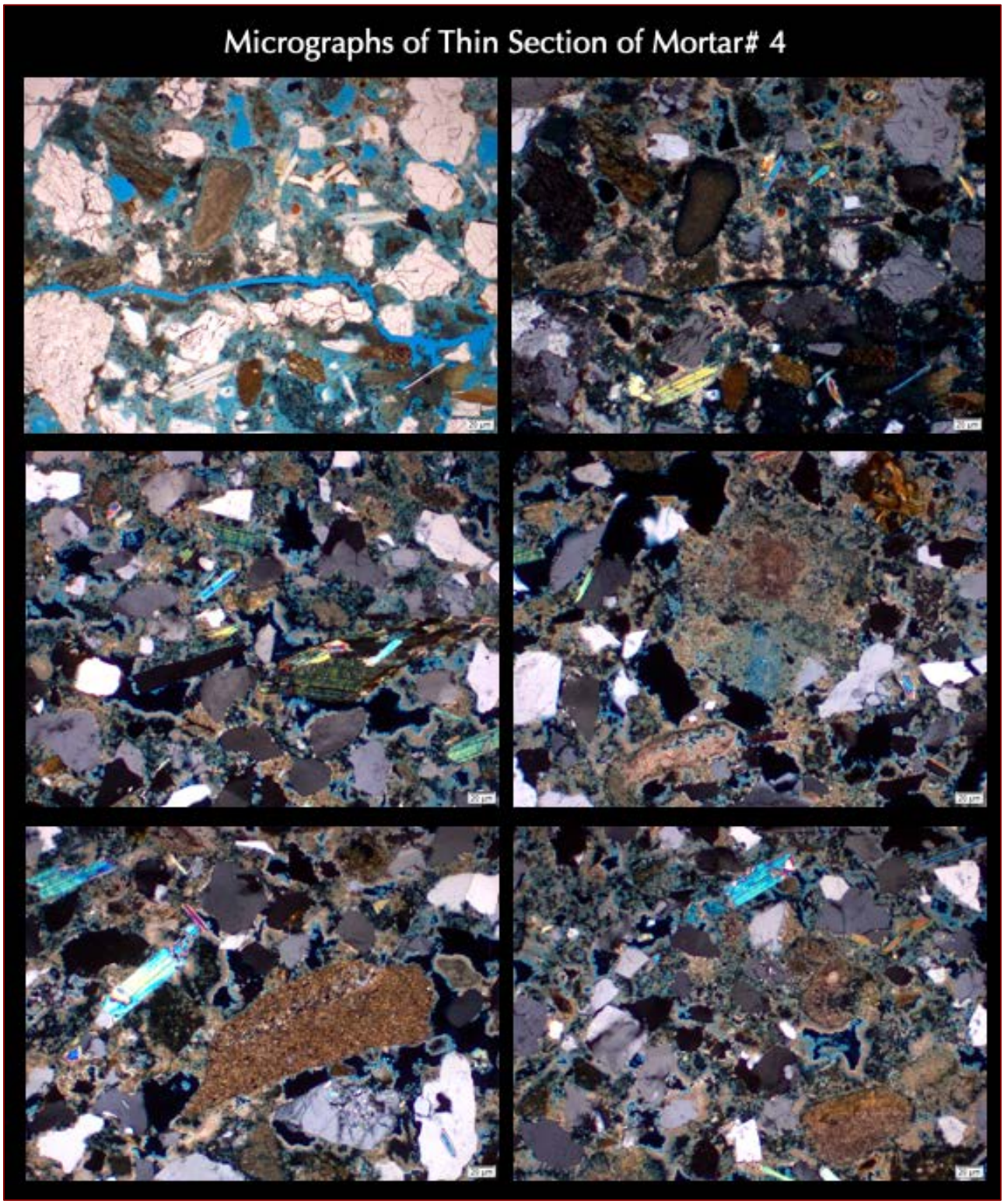

Figure 32: Micrographs of blue dye-mixed epoxy-impregnated thin section of Mortar #4 from the interior of Meigs Vault taken with a petrographic microscope showing size, shape, angularity, gradation, and distribution of siliceous sand particles, many muscovite flakes in sand, and variably carbonated and porous natural cement and lime paste having many residual incompletely calcined original argillaceous limestone raw feed particles indicating use of natural cement and lime as the binders.

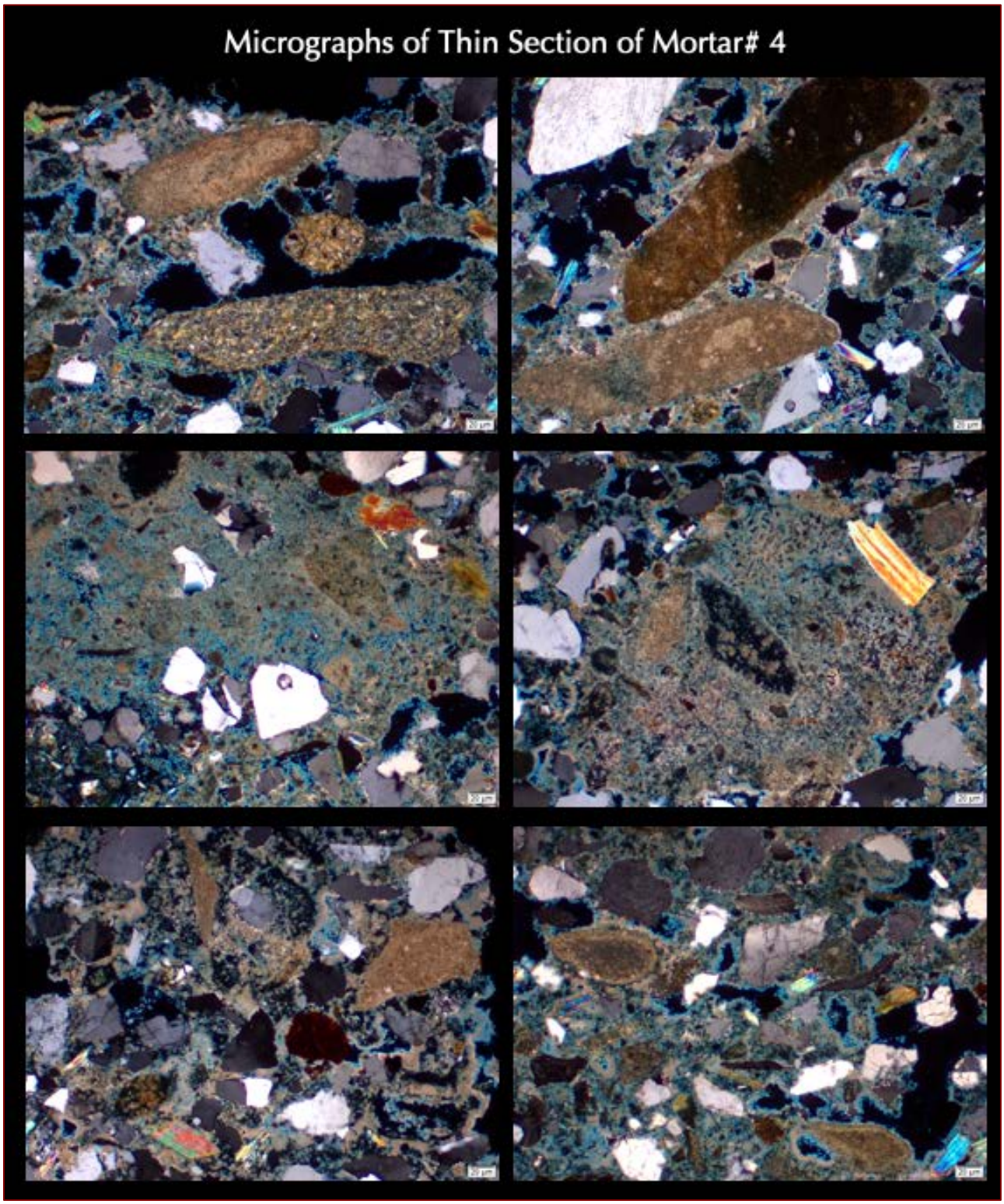

Figure 33: Micrographs of blue dye-mixed epoxy-impregnated thin section of Mortar #4 from the interior of Meigs Vault taken with a petrographic microscope showing size, shape, angularity, gradation, and distribution of siliceous sand particles, many muscovite flakes in sand, and variably carbonated and porous natural cement and lime paste having many residual incompletely calcined original argillaceous limestone raw feed particles indicating use of natural cement and lime as the binders.

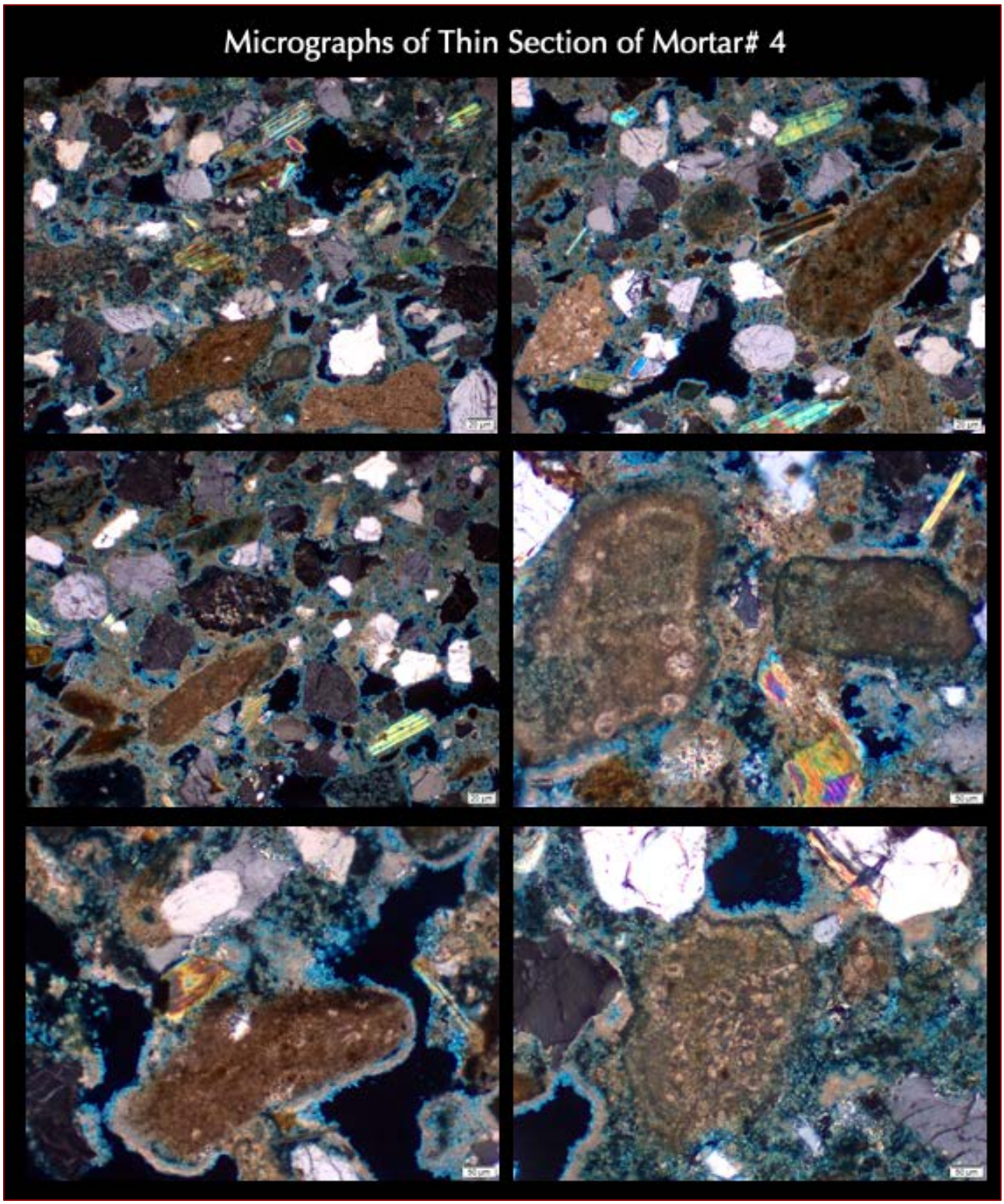

Figure 34: Micrographs of blue dye-mixed epoxy-impregnated thin section of Mortar #4 from the interior of Meigs Vault taken with a petrographic microscope showing size, shape, angularity, gradation, and distribution of siliceous sand particles, many muscovite flakes in sand, and variably carbonated and porous natural cement and lime paste having many residual incompletely calcined original argillaceous limestone raw feed particles indicating use of natural cement and lime as the binders.

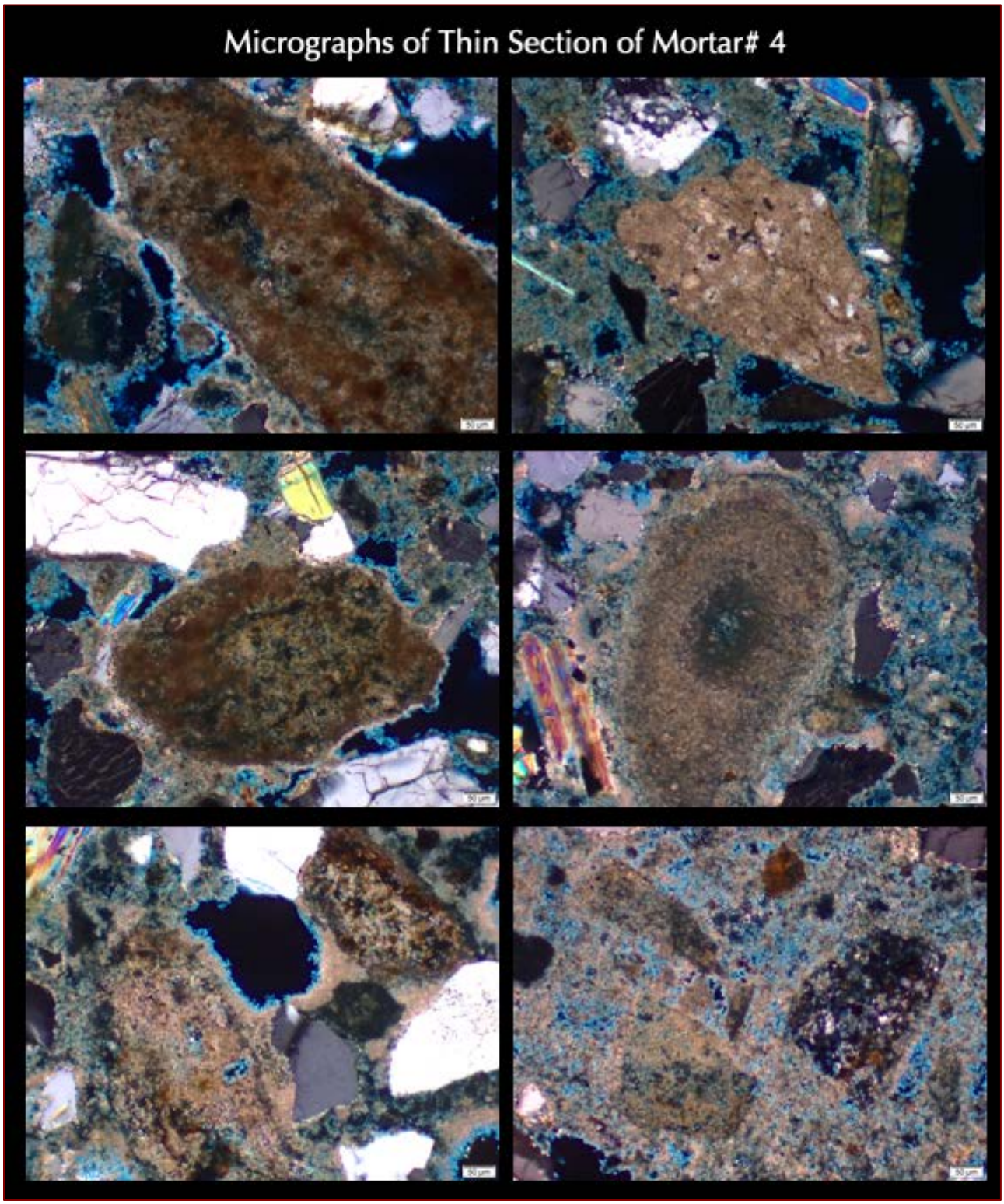

Figure 35: Micrographs of blue dye-mixed epoxy-impregnated thin section of Mortar #4 from the interior of Meigs Vault showing residual, incompletely calcined original argillaceous limestone raw feeds of natural cement productions leaving many telltale signatures of original microstructures of feed that have not been completely obliterated by the calcination process, or have been modified by calcination.

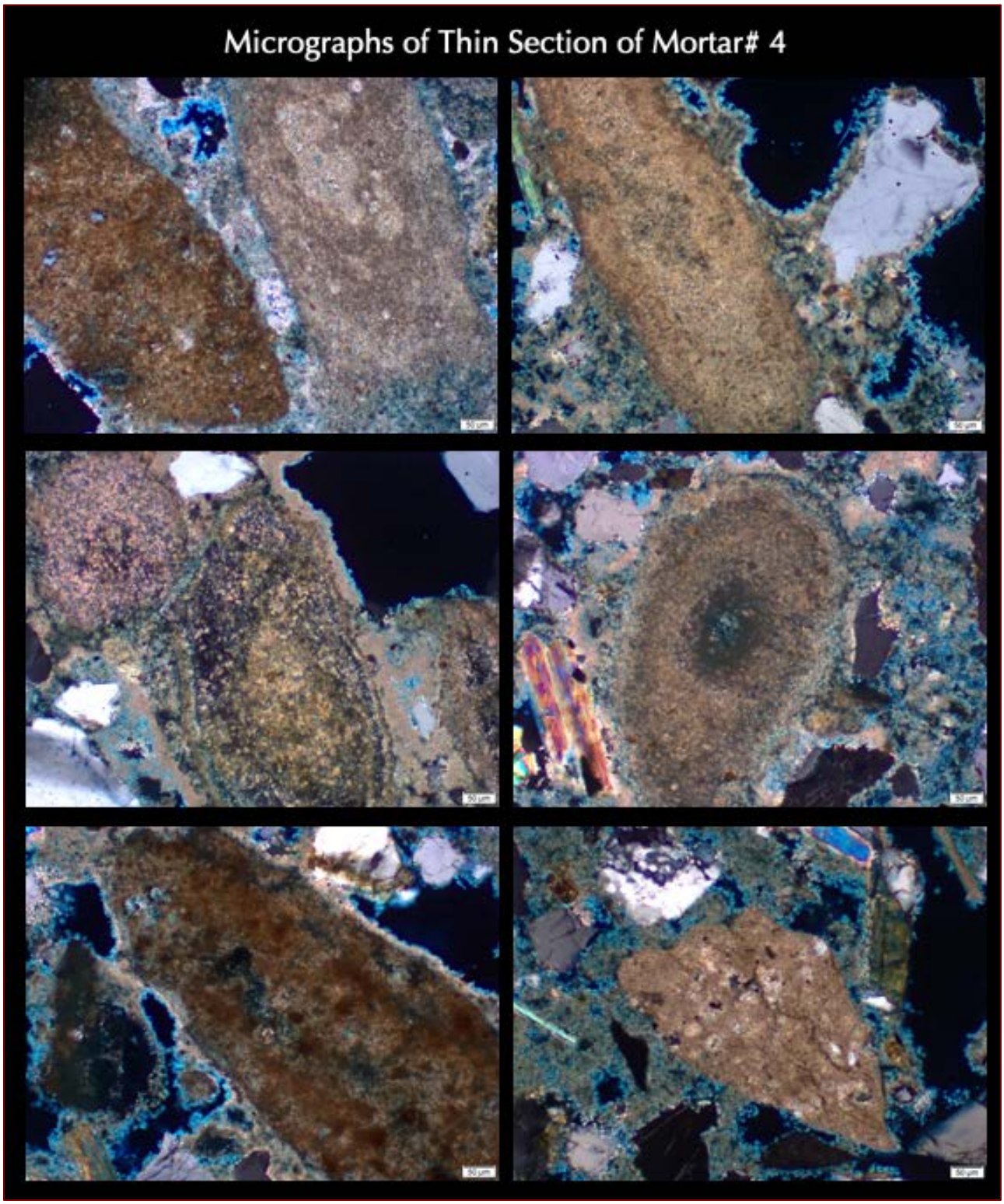

Figure 36: Micrographs of blue dye-mixed epoxy-impregnated thin section of Mortar #4 from the interior of Meigs Vault showing residual, incompletely calcined original argillaceous limestone raw feeds of natural cement productions leaving many telltale signatures of original microstructures of feed that have not been completely obliterated by the calcination process, or have been modified by calcination.

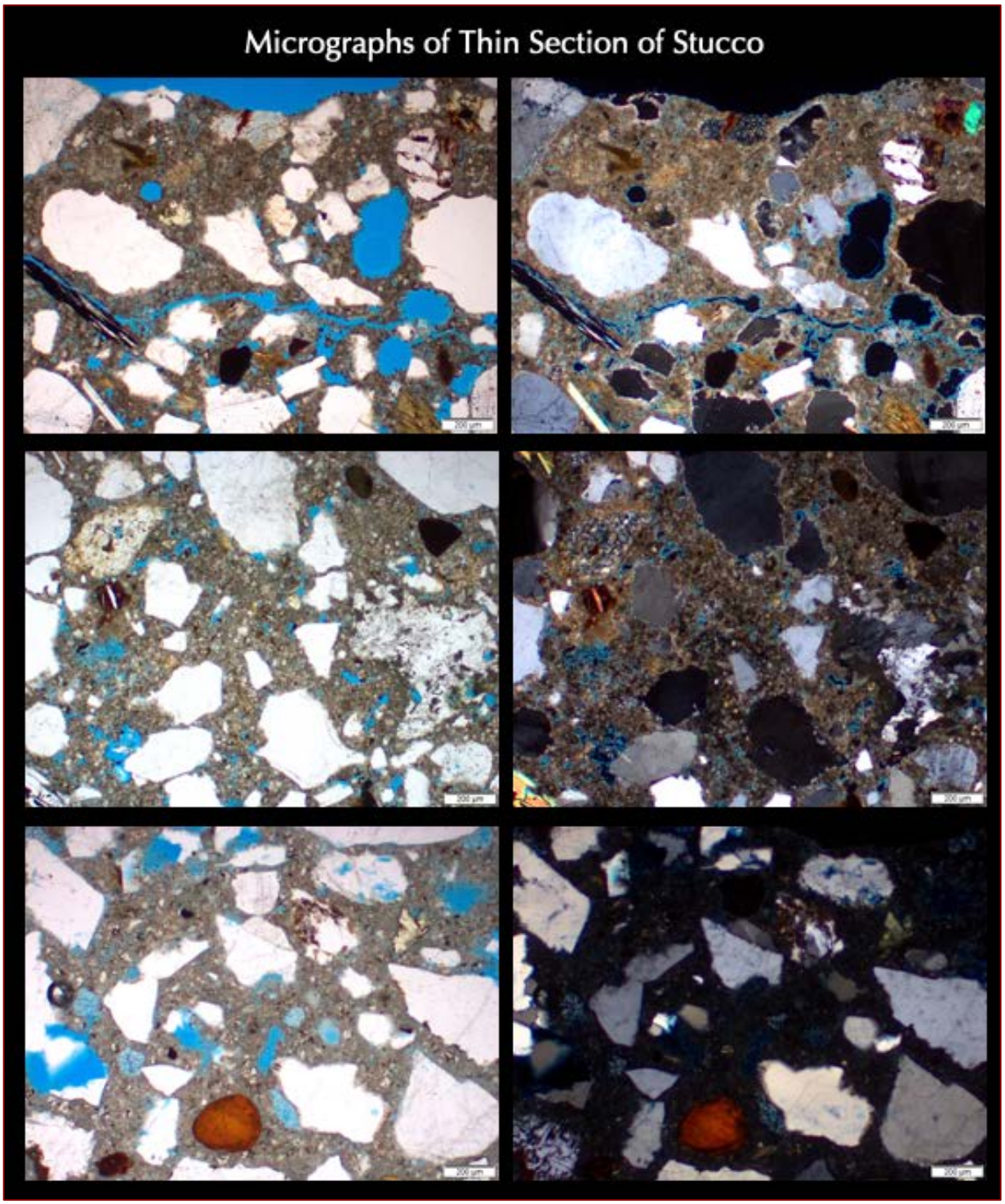

Figure 37: Micrographs of blue dye-mixed epoxy-impregnated thin section of three coats of stucco showing size, shape, angularity, gradation, and distribution of siliceous sand particles across the coats, and Portland cement paste across the coats. Notice some carbonation and shrinkage microcracks at the exposed sand finish end of finish coat in the top row photos. Middle row shows some carbonation of dense darker gray intermediate brown coat. Bottom row from innermost scratch coat shows lack of carbonation of Portland cement paste. Therefore, atmospheric carbonation has engulfed both two exterior finish and brown coats of stucco but not necessarily penetrated deep inside the innermost scratch coat.

Paste Compositions and Microstructure of Mortars From SEM-EDS

Figure 38 shows backscatter electron image (BSE, top), and, X-ray elemental analyses (as oxide weight percentages) of paste in Mortar #1 from exterior east elevation of the Castle where paste compositions provided in the Table are from various areas across the image measured at the tips of callouts.

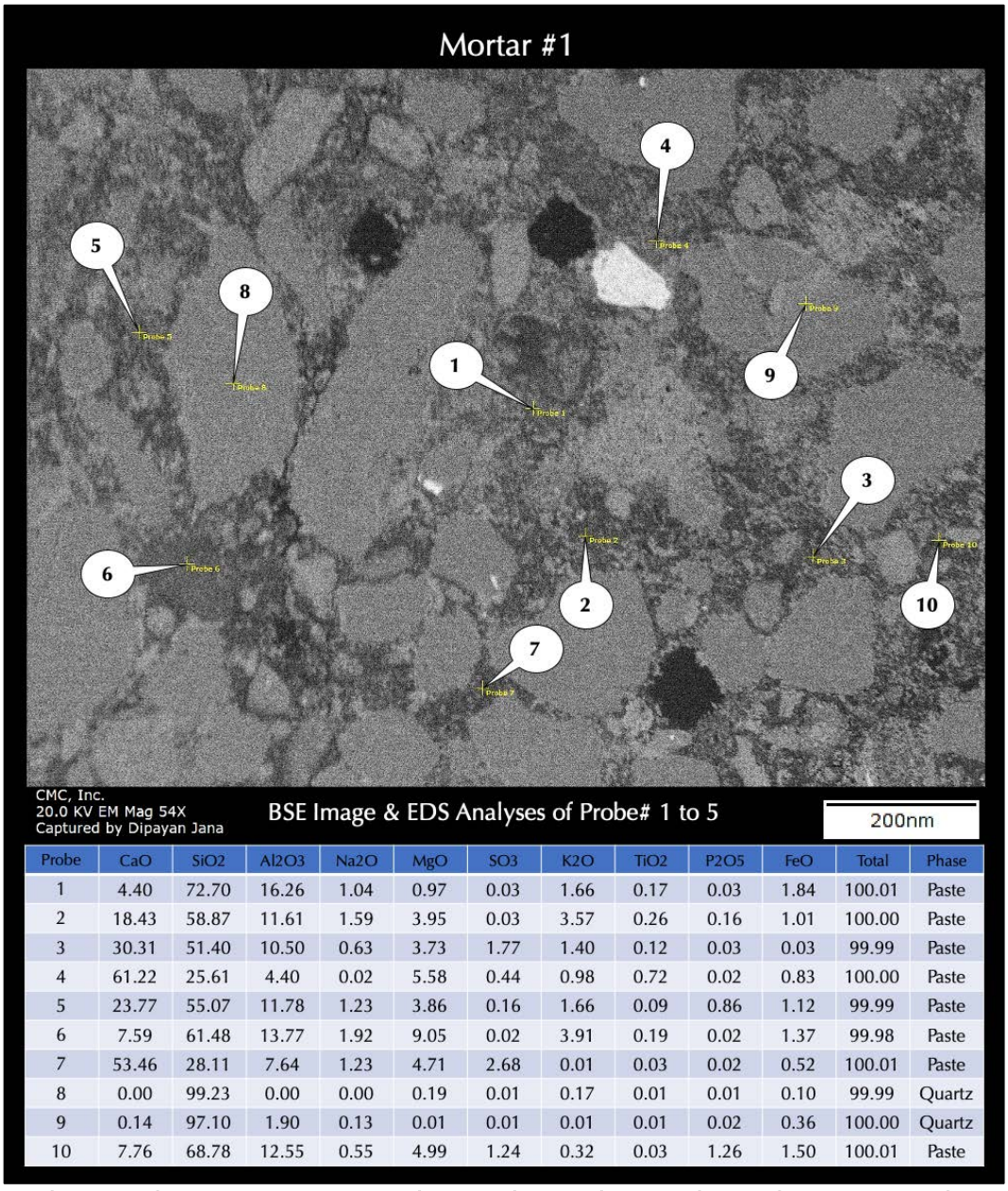

Probe	CaO	SiO2	Al2O3	Na2O	MgO	SO3	K2O	TiO2	P2O5	FeO	Total	Phase
1	4.40	72.70	16.26	1.04	0.97	0.03	1.66	0.17	0.03	1.84	100.01	Paste
2	18.43	58.87	11.61	1.59	3.95	0.03	3.57	0.26	0.16	1.01	100.00	Paste
3	30.31	51.40	10.50	0.63	3.73	1.77	1.40	0.12	0.03	0.03	99.99	Paste
4	61.22	25.61	4.40	0.02	5.58	0.44	0.98	0.72	0.02	0.83	100.00	Paste
5	23.77	55.07	11.78	1.23	3.86	0.16	1.66	0.09	0.86	1.12	99.99	Paste
6	7.59	61.48	13.77	1.92	9.05	0.02	3.91	0.19	0.02	1.37	99.98	Paste
7	53.46	28.11	7.64	1.23	4.71	2.68	0.01	0.03	0.02	0.52	100.01	Paste
8	0.00	99.23	0.00	0.00	0.19	0.01	0.17	0.01	0.01	0.10	99.99	Quartz
9	0.14	97.10	1.90	0.13	0.01	0.01	0.01	0.01	0.02	0.36	100.00	Quartz
10	7.76	68.78	12.55	0.55	4.99	1.24	0.32	0.03	1.26	1.50	100.01	Paste

Figure 38: Backscatter electron image (top), and X-ray elemental (as oxide weight percent) analyses of paste in Mortar #1 from exterior east elevation of Castle given in the bottom table measured at the tips of callouts. The inherent hydraulic composition of binder is detected from the high silica compositions of paste, which is also indicative of use of natural cement. Lime contents are reflection of both natural cement and lime binder. The magnesia contents also indicate use of natural cement and perhaps a magnesian lime binder. Alumina and iron contents are additional indications of incorporation of natural cement binder, which is positively identified during optical microscopy. Paste compositions reflect calcination of an impure magnesian limestone feed that had resulted in production of both natural cement and lime.

Figure 39 shows backscatter electron image (BSE, top), and, X-ray elemental analyses (as oxide weight percentages) of paste in Mortar #2 from interior north elevation of Castle where paste compositions provided in the Table are from various areas across the image measured at the tips of callouts.

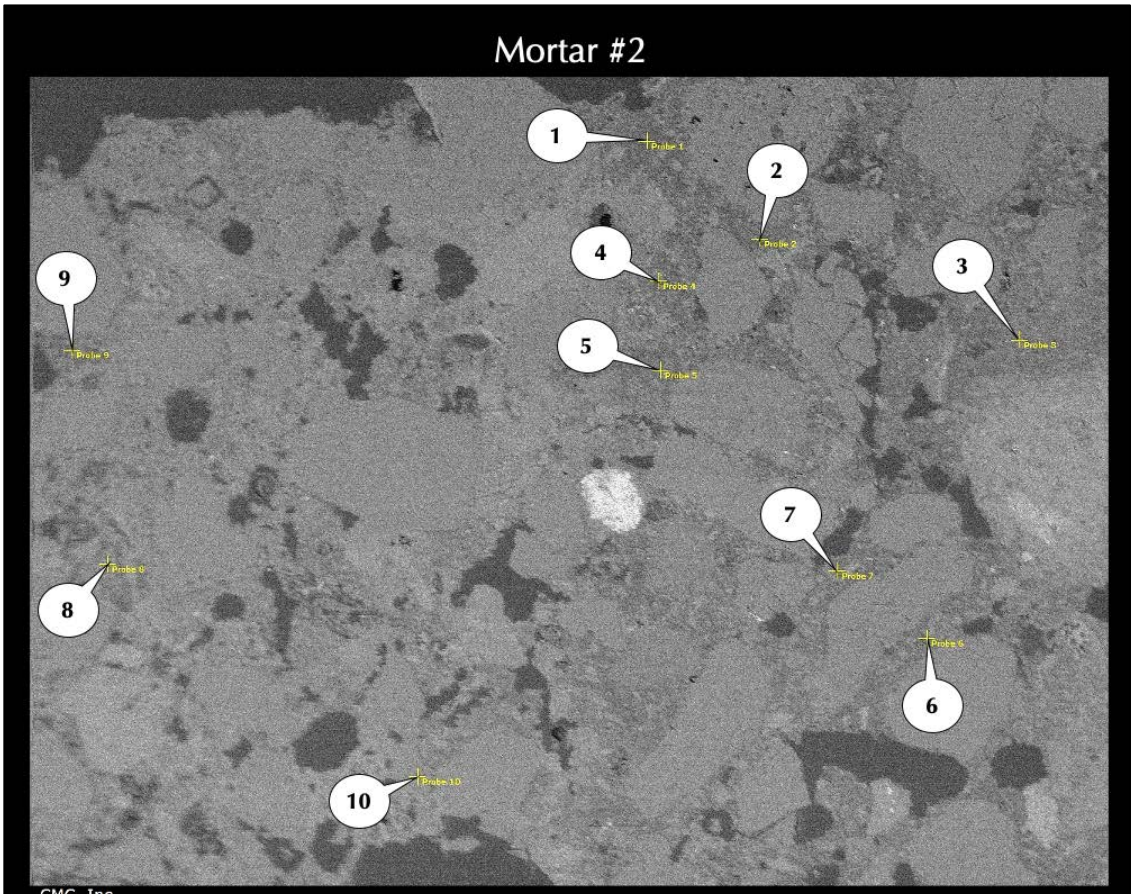

Probe	CaO	SiO2	Al2O3	Na2O	MgO	SO3	K2O	TiO2	P2O5	FeO	Total	Phase
1	20.09	52.27	11.53	2.01	5.70	0.77	5.78	0.59	0.02	0.84	100.00	Paste
2	24.78	51.99	11.34	0.23	4.66	0.56	4.58	0.02	0.02	1.11	100.00	Paste
3	50.08	30.32	9.32	0.24	4.06	1.44	3.68	0.25	0.01	0.48	100.00	Paste
4	32.64	48.00	9.79	1.26	3.83	0.02	3.33	0.15	0.02	0.58	100.00	Paste
5	29.52	48.52	10.40	0.85	4.10	1.58	3.76	0.26	0.02	0.94	100.01	Paste
6	84.10	3.70	7.72	0.03	0.37	1.62	0.01	0.02	1.32	0.23	100.00	Calcite
7	61.09	24.98	6.60	0.41	2.56	1.34	2.25	0.02	0.02	0.69	100.01	Paste
8	43.05	33.88	9.54	0.72	6.88	2.00	2.66	0.28	0.02	0.53	100.01	Paste
9	8.69	64.46	14.28	0.01	1.17	0.42	10.02	0.45	0.02	0.28	100.00	Paste
10	0.17	98.86	0.00	0.12	0.16	0.01	0.05	0.01	0.01	0.19	99.99	Quartz

Figure 39: Backscatter electron image (top), and X-ray elemental (as oxide weight percent) analyses of paste in Mortar #2 from interior north elevation of Castle given in the bottom table measured at the tips of callouts. The inherent hydraulic composition of binder is detected from the high silica compositions of paste, which is also indicative of use of natural cement. Lime contents are reflection of both natural cement and lime binder. The magnesia contents also indicate use of natural cement and perhaps a magnesian lime binder. Alumina and iron contents are additional indications of incorporation of natural cement binder, which is positively identified during optical microscopy. Paste compositions reflect calcination of an impure magnesian limestone feed that had resulted in production of both natural cement and lime.

Figure 40 shows backscatter electron image (BSE, top), and, X-ray elemental analyses (as oxide weight percentages) of paste in Mortar #3 from North Dome of Meigs Vault where paste compositions provided in the Table are from various areas across the image measured at the tips of callouts.

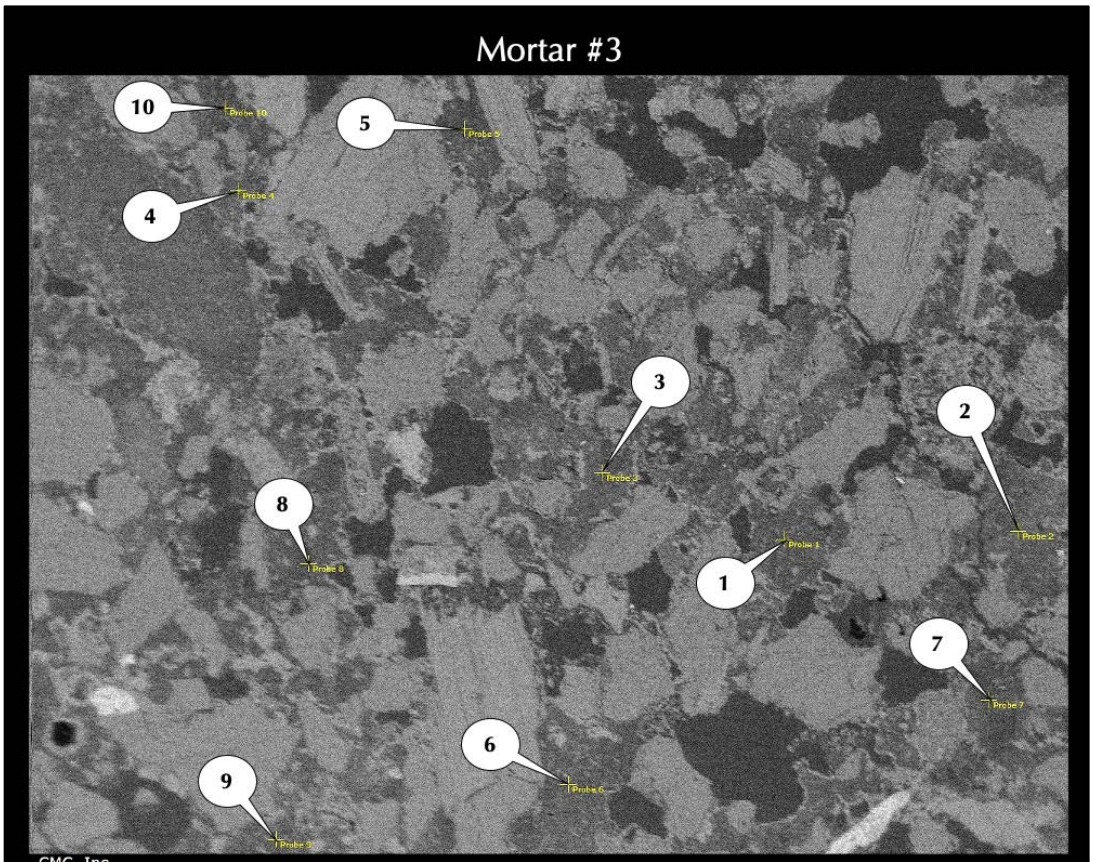

Probe	CaO	SiO2	Al2O3	Na2O	MgO	SO3	K2O	TiO2	P2O5	FeO	Total	Phase
1	5.31	62.30	22.25	1.45	6.46	0.03	0.22	0.43	0.03	1.30	100.01	Paste
2	2.17	90.19	4.86	0.03	0.97	0.01	0.91	0.28	0.02	0.35	100.00	Quartz
3	10.62	71.81	5.51	0.19	3.97	0.02	6.31	0.42	0.01	0.47	100.00	Paste
4	10.68	53.48	14.38	0.30	3.17	14.86	0.81	0.02	0.67	0.71	100.00	Paste
5	5.50	62.40	22.59	1.19	4.64	0.90	0.33	0.41	0.22	1.62	99.99	Paste
6	9.64	58.69	23.34	0.57	3.10	0.75	1.36	0.19	0.04	1.22	100.01	Paste
7	10.31	63.38	18.20	0.02	5.66	0.04	0.67	0.03	0.04	1.10	100.00	Paste
8	6.06	62.99	22.41	0.02	5.74	0.03	0.20	0.03	0.04	1.90	100.01	Paste
9	4.87	85.31	7.03	0.01	0.91	0.25	0.01	0.02	0.03	1.19	100.01	Paste
10	3.47	59.89	24.22	0.76	5.26	1.15	0.22	1.02	0.05	3.22	100.00	Paste

Figure 40: Backscatter electron image (top), and X-ray elemental (as oxide weight percent) analyses of paste in Mortar #3 from North Dome of Meigs Vault given in the bottom table measured at the tips of callouts. The inherent leached and altered nature of the paste are highlighted in the compositions. The hydraulic nature of binder is detected from the high silica compositions of paste (alteration also increases silica content), which is also indicative of use of natural cement. Low lime contents are reflection of both lime leaching of an original lime-rich binder. The magnesia contents also indicate use of natural cement and perhaps a magnesian lime binder. Alumina and iron contents are additional indications of incorporation of natural cement binder, which is positively identified during optical microscopy.

Figure 41 shows backscatter electron image (BSE, top), and, X-ray elemental analyses (as oxide weight percentages) of paste in Mortar #4 from interior of Meigs Vault where paste compositions provided in the Table are from various areas across the image measured at the tips of callouts.

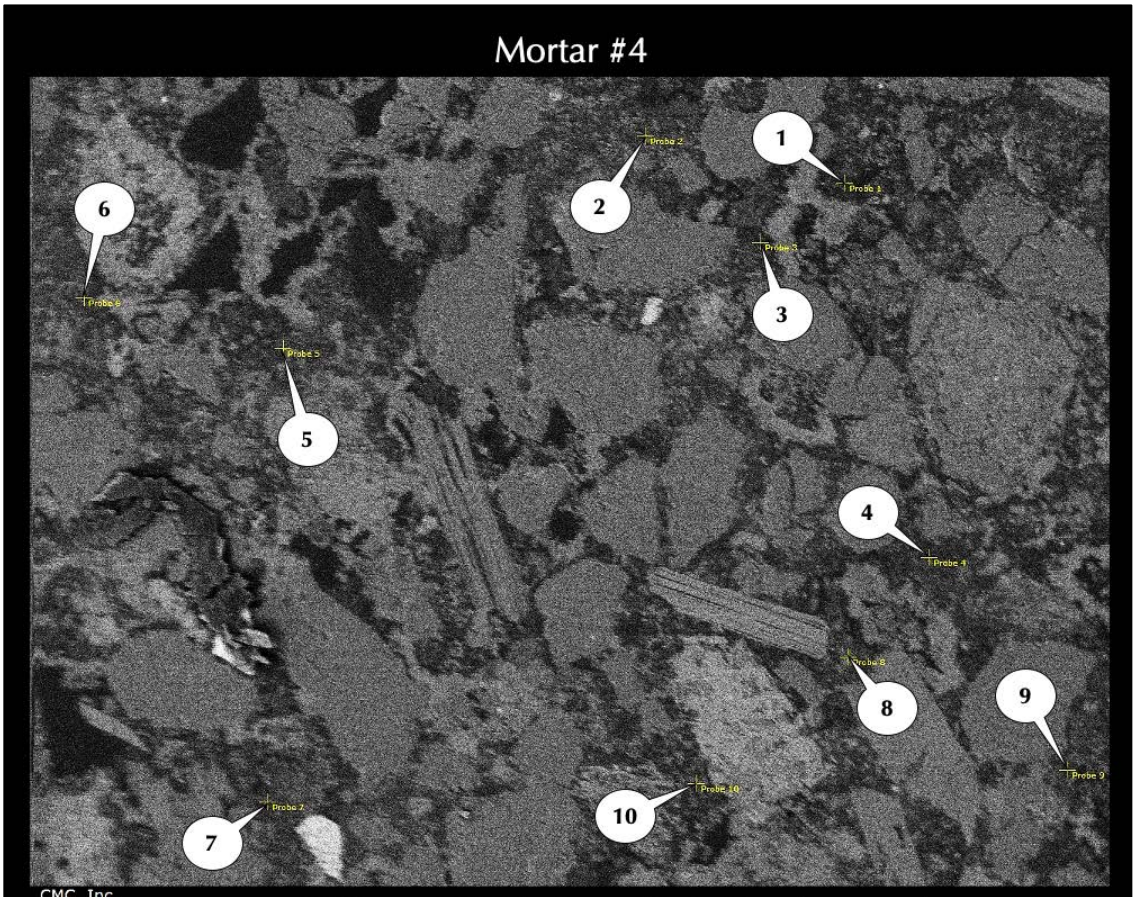

Probe	CaO	SiO2	Al2O3	Na2O	MgO	SO3	K2O	TiO2	P2O5	FeO	Total	Phase
1	3.10	64.07	13.76	3.23	10.48	0.03	1.09	1.08	0.04	2.98	100.01	Paste
2	39.12	41.83	11.69	0.01	4.33	0.02	1.26	0.36	0.02	1.16	100.01	Paste
3	5.39	67.35	15.61	0.02	5.40	0.04	1.90	1.53	1.67	0.81	100.00	Paste
4	7.89	67.61	14.83	1.46	2.69	0.02	2.46	0.02	0.03	1.56	100.00	Paste
5	5.20	69.97	15.84	0.53	4.76	0.57	1.30	0.50	0.05	0.92	99.99	Paste
6	18.62	57.99	14.31	0.39	5.69	0.03	1.82	0.45	0.03	0.45	100.00	Paste
7	2.30	72.45	16.27	0.55	2.42	1.51	2.42	0.02	0.03	1.42	100.02	Paste
8	34.44	47.81	10.64	0.01	3.78	0.21	2.20	0.02	0.02	0.79	99.99	Paste
9	13.98	66.90	10.14	0.51	3.98	0.14	1.40	0.83	0.02	1.85	99.98	Paste
10	44.57	34.98	12.84	0.02	2.11	1.61	2.32	0.11	0.02	1.05	99.99	Paste

Figure 41: Backscatter electron image (top), and X-ray elemental (as oxide weight percent) analyses of paste in Mortar #4 from interior of Meigs Vault given in the bottom table measured at the tips of callouts. The inherent hydraulic composition of binder is detected from the high silica compositions of paste, which is also indicative of use of natural cement. Lime contents are reflection of both natural cement and lime binder. The magnesia contents also indicate use of natural cement and perhaps a magnesian lime binder. Alumina and iron contents are additional indications of incorporation of natural cement binder, which is positively identified during optical microscopy. Paste compositions reflect calcination of an impure magnesian limestone feed that had resulted in production of both natural cement and lime.

Mineralogy of Mortars From XRD

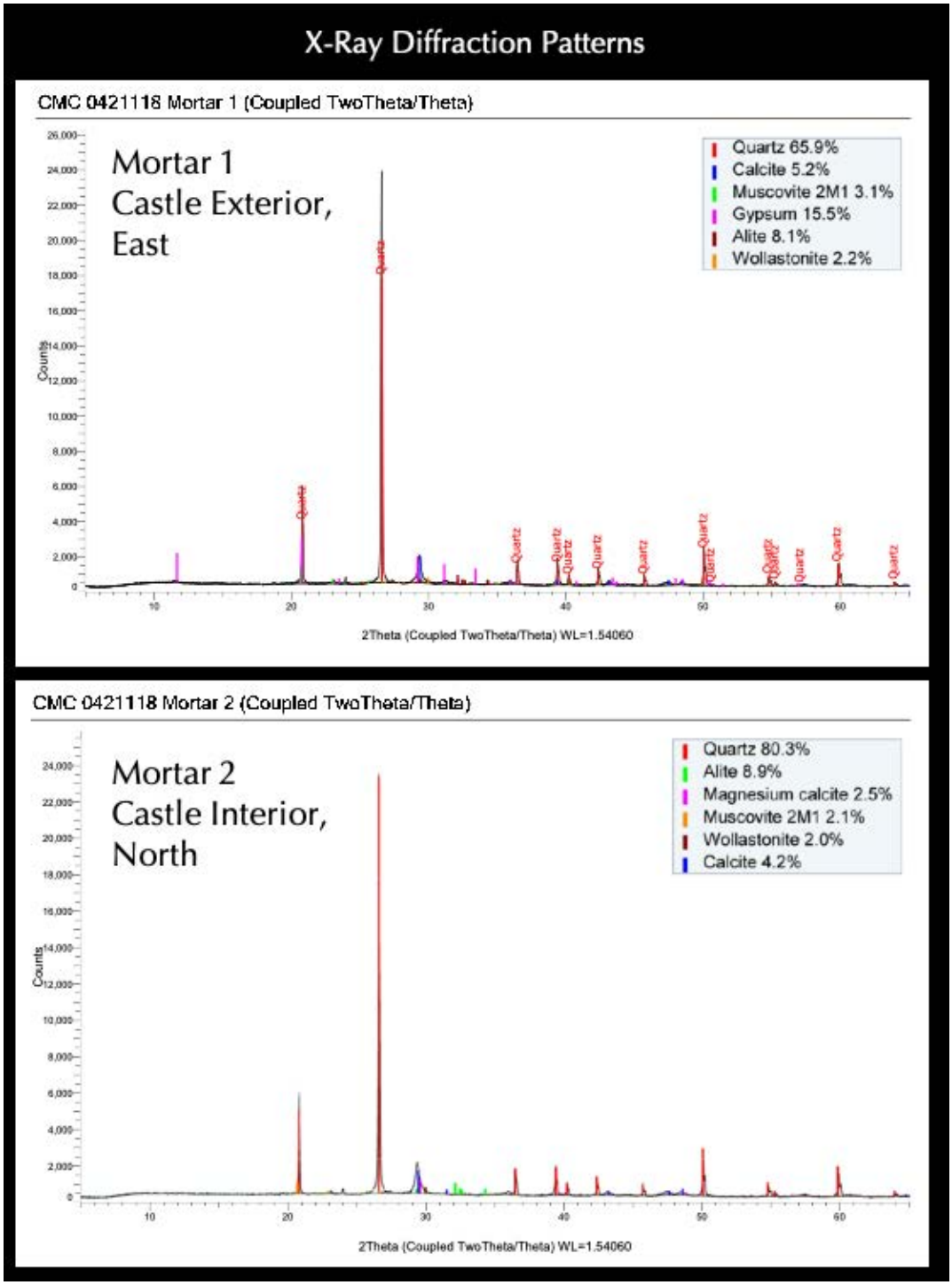

Figure 42: X-ray diffraction patterns of bulk mortar samples Nos. 1 and 2 from the Castle showing the main quartz peak from the dominant quartz sand composition of mortar and peaks for other subordinate phases. Gypsum is detected only in Mortar #1 from exterior east elevation of the Castle. Calcite is from carbonated paste. Alite is from the product of calcination of original raw feed even though natural cement does not contain alite as a main phase unless it is locally produced at the hot zone in the cement kiln. Wollastonite is also a product of calcination of raw feed for the production of natural cement.

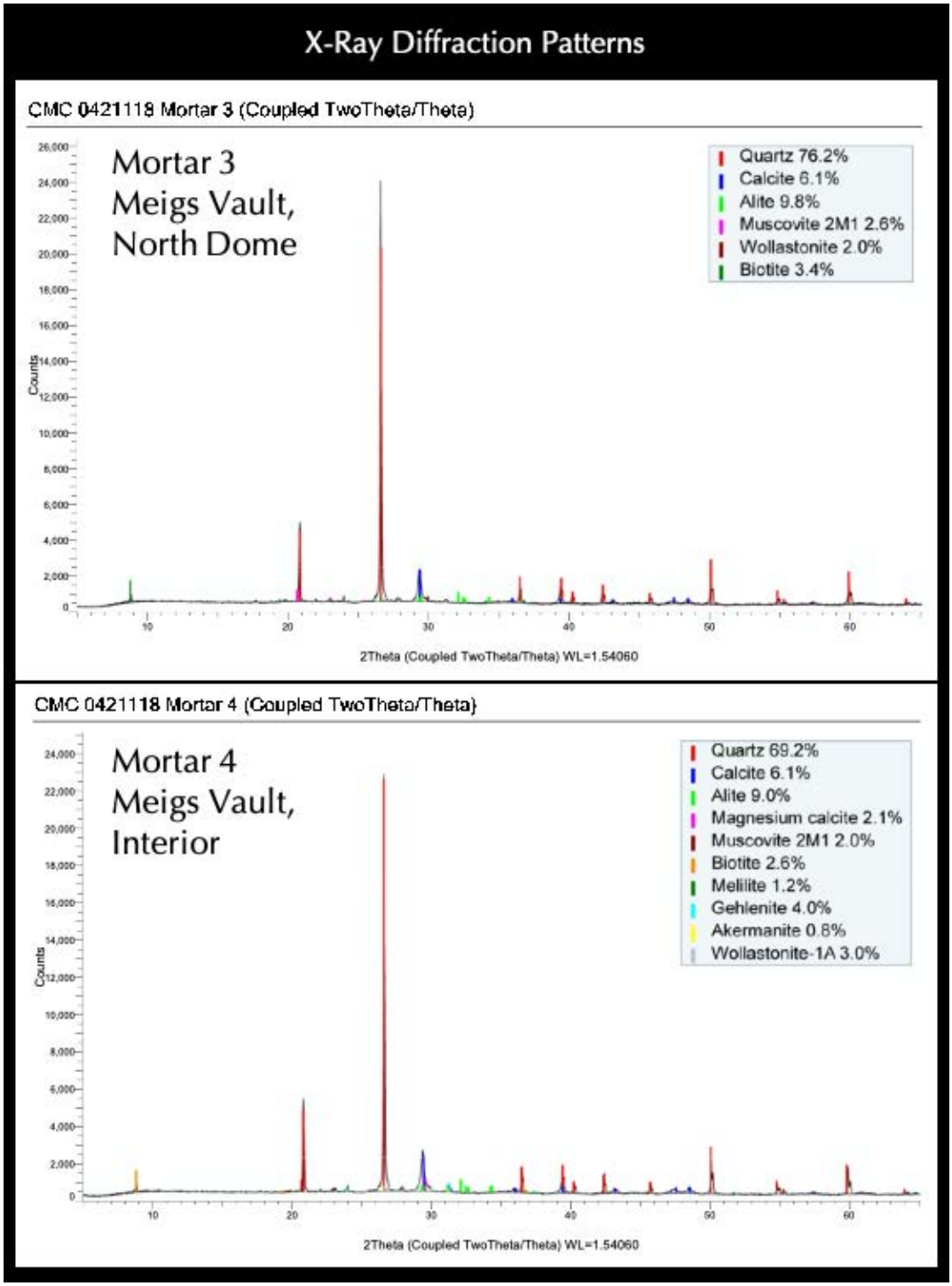

Figure 43: X-ray diffraction patterns of bulk mortar samples Nos. 3 and 4 from Meigs Vault showing the main quartz peak from the dominant quartz sand composition of mortar and peaks for other subordinate phases. Calcite is from carbonated paste. Alite is from the product of calcination of original raw feed even though natural cement does not contain alite as a main phase unless it is locally produced at the hot zone in the cement kiln. Wollastonite is also a product of calcination of raw feed for the production of natural cement. Melilite, gehlenite, and akermenite in Mortar #4 are typical phases of natural cement. Mica is from the muscovite flakes detected in these mortars from optical microscopy.

Composition of Mortars From XRF (Major Element Oxides), Acid & Alkali Digestion (Soluble Silica), Loss on Ignition (Free Water, Combined Water, Carbonation), and Acid-Insoluble Residue Content (Siliceous Sand Contents)

Table 1 shows oxide compositions of mortars determined from pressed pellet of pulverized (< 45 micron size) bulk mortar in XRF. Dominance of silica in all samples is a reflection of dominance of quartz in sand as seen in the XRD analysis of the mortars.

Lime is contributed from carbonated paste, and alumina, iron, and alkalis are contributed from both sand and paste. Balance includes volatiles (combined H_2O, CO_2) not measured in XRF.

Magnesia content is a testament of use of natural cement and magnesian lime binder.

Hydraulic component in the cement was responsible for the soluble silica contents in the XRF analysis of filtrates after digestions in cold-HCl and hot-NaOH.

The high sulfate content in Mortar #1 is consistent with the detection of gypsum salt in the XRD pattern of this sample.

Acid-insoluble residue contents of 67 to 93% are determined after digesting pulverized (<0.3 mm size) fragments of mortars in hydrochloric acid. Due to the presence of mostly siliceous components in the sand (as determined from petrography), the determined acid-insoluble residue contents are considered corresponding to the siliceous sand contents of the mortars.

Chemical Analyses (XRF & Gravimetric) of Mortars

Mortar#	1	2	3	4	Methods
Silica - SiO_2	55.4	67.7	67.5	66.1	XRF
Alumina - Al_2O_3	3.58	4.22	6.05	5.71	XRF
Iron - Fe_2O_3	3.22	2.51	3.65	3.13	XRF
Lime - CaO	11.4	14.0	12.1	14.6	XRF
Magnesia - MgO	2.81	1.45	1.39	1.42	XRF
Sodium - Na_2O	1.06	ND	0.37	0.38	XRF
Potassium - K_2O	1.34	1.94	1.08	1.61	XRF
Titanium - TiO_2	1.06	0.36	0.42	0.45	XRF
Phosphorus - P_2O_5	0.025	0.077	0.087	0.068	XRF
Sulfate - SO_3	5.38	0.051	ND	ND	XRF
Balance (LOI)	14.7	7.62	7.69	6.82	XRF
Total	100				XRF
Soluble Silica in filtrates of Cold-HCl and Hot-NaOH digested mortar	1.91	2.12	2.02	1.87	Gravimetry + XRF
Acid-Insoluble Residue	75.78	66.93	77.36	93.11	Gravimetry
Loss on Ignition @ 110°C	1.70	0.90	1.10	0.70	Gravimetry
Loss on Ignition @ 550°C	6.00	1.50	2.90	1.50	Gravimetry
Loss on Ignition @ 950°C	6.50	8.70	8.10	7.90	Gravimetry

Table 1: Bulk oxide compositions and soluble silica contents of mortars from XRF, and acid-insoluble residue contents and losses on ignition from gravimetry.

Losses on ignition of a separate aliquot of pulverized mortars to 110°C, 550°C, and 950°C correspond to free water, combined (hydrate) water, and degree of carbonation, respectively. The loss at 110°C is due to the loss of free moisture. The loss on ignition at 550°C corresponds to the water content from dehydration of hydraulic paste. The loss on ignition at 950°C corresponds to degree of carbonation of carbonated lime. The results are consistent with the results originated from thermal analyses of mortars (discussed later).

Thermal Analyses of Mortars

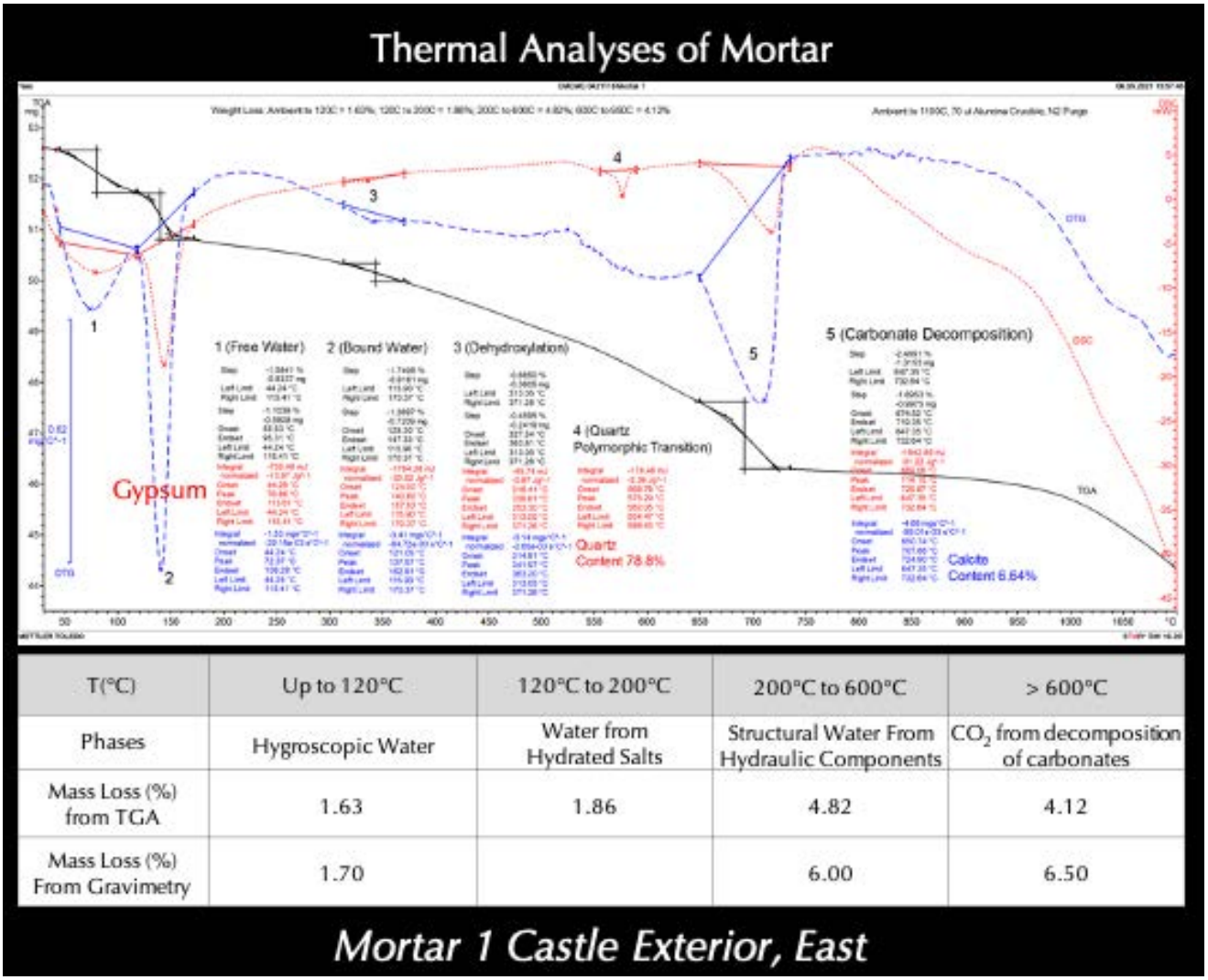

T(°C)	Up to 120°C	120°C to 200°C	200°C to 600°C	> 600°C
Phases	Hygroscopic Water	Water from Hydrated Salts	Structural Water From Hydraulic Components	CO_2 from decomposition of carbonates
Mass Loss (%) from TGA	1.63	1.86	4.82	4.12
Mass Loss (%) From Gravimetry	1.70		6.00	6.50

Figure 44: TGA (in bold black), DSC (in dotted red), and DTG (in dashed blue) curves of Mortar #1 showing losses in weight due to decompositions (loss of water and carbon dioxide) of various phases during controlled heating in a Mettler-Toledo's simultaneous TGA/DSC 1 unit from 30ºC to 1000ºC in a ceramic crucible (alumina 70µl, no lid) at a heating rate of 10ºC/min in a nitrogen purge at a rate of 75 mL/min. Dehydration and decarbonation reactions are marked as endothermic peaks in the DTG curve, whereas alpha to beta-form polymorphic transition of quartz is marked at the characteristic temperature of 573ºC in the DSC curve.

In the DTG curve, losses in weights are detected at (i) Peak #1 from the loss of water, and (ii) Peak #2 from bound water. Peak #3 shows dehydroxylation of hydrated phases. DSC curve in Peak #4 shows polymorphic transition from alpha to beta form of quartz around 575ºC from silica (quartz) sand. Semi-quantitative estimates of quartz and calcite are determined from DSC results. Calcite content is consistent with carbonated nature of the mortar from its carbonated natural cement-lime composition. Results of thermal analyses are therefore consistent with the results obtained from microscopy and XRD studies.

Notice similar results obtained from thermal analysis and gravimetry for mass losses from loss of free water (up to 120ºC), structural water (200 to 600ºC), and carbonation (600 to 950 ºC), respectively.

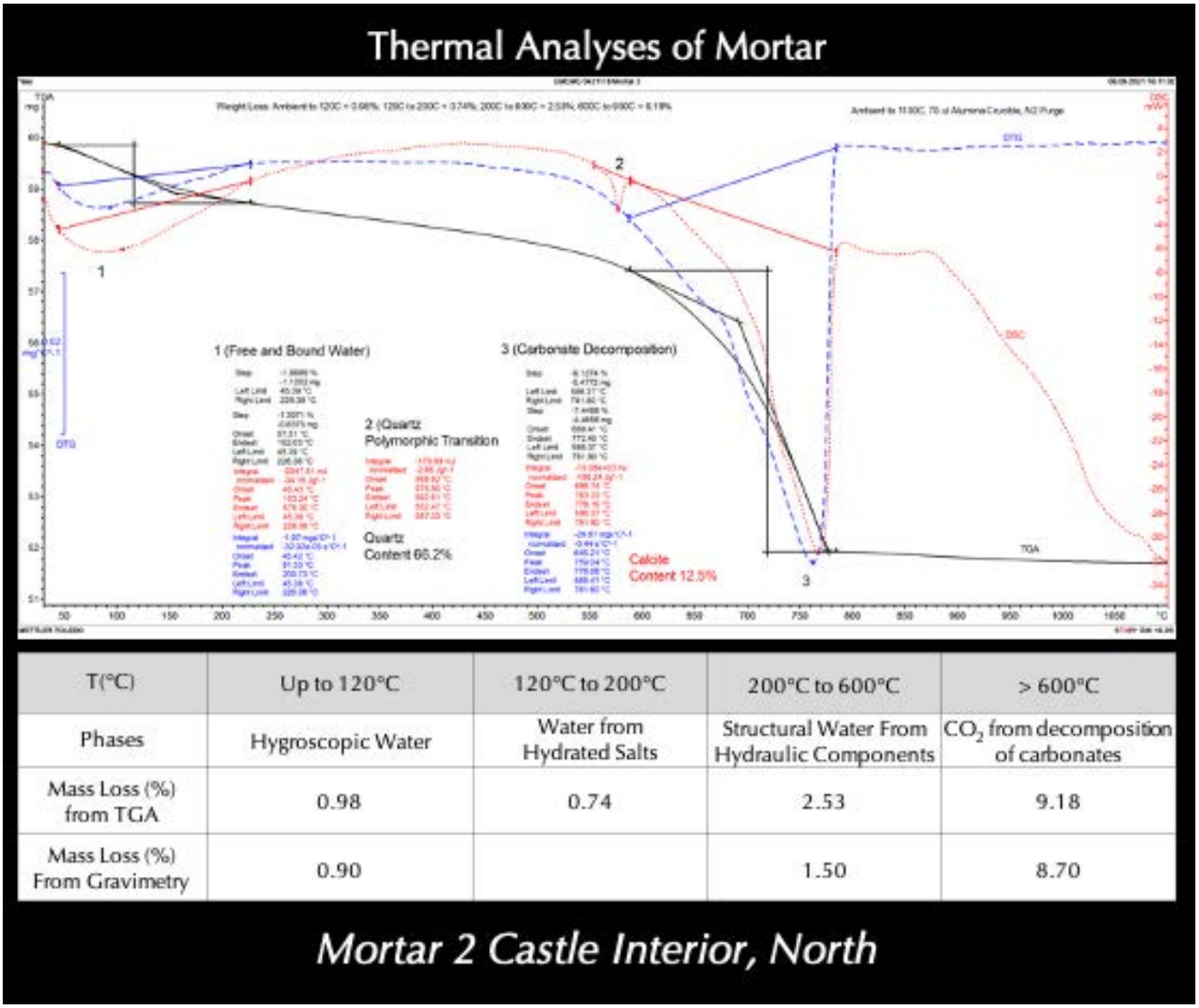

T(°C)	Up to 120°C	120°C to 200°C	200°C to 600°C	> 600°C
Phases	Hygroscopic Water	Water from Hydrated Salts	Structural Water From Hydraulic Components	CO_2 from decomposition of carbonates
Mass Loss (%) from TGA	0.98	0.74	2.53	9.18
Mass Loss (%) From Gravimetry	0.90		1.50	8.70

Mortar 2 Castle Interior, North

Figure 45: TGA (in bold black), DSC (in dotted red), and DTG (in dashed blue) curves of Mortar #2 showing losses in weight due to decompositions (loss of water and carbon dioxide) of various phases during controlled heating in a Mettler-Toledo's simultaneous TGA/DSC 1 unit from 30ºC to 1000ºC in a ceramic crucible (alumina 70µl, no lid) at a heating rate of 10ºC/min in a nitrogen purge at a rate of 75 mL/min. Dehydration and decarbonation reactions are marked as endothermic peaks in the DTG curve, whereas alpha to beta-form polymorphic transition of quartz is marked at the characteristic temperature of 573ºC in the DSC curve.

In the DTG curve, losses in weights are detected at (i) Peak #1 from the loss of water, and (ii) Peak #2 from bound water. Peak #3 shows dehydroxylation of hydrated phases. DSC curve in Peak #4 shows polymorphic transition from alpha to beta form of quartz around 575ºC from silica (quartz) sand. Semi-quantitative estimates of quartz and calcite are determined from DSC results. Calcite content is consistent with carbonated nature of the mortar from its carbonated natural cement-lime composition. Results of thermal analyses are therefore consistent with the results obtained from microscopy and XRD studies.

Notice similar results obtained from thermal analysis and gravimetry for mass losses from loss of free water (up to 120ºC), structural water (200 to 600ºC), and carbonation (600 to 950 ºC), respectively.

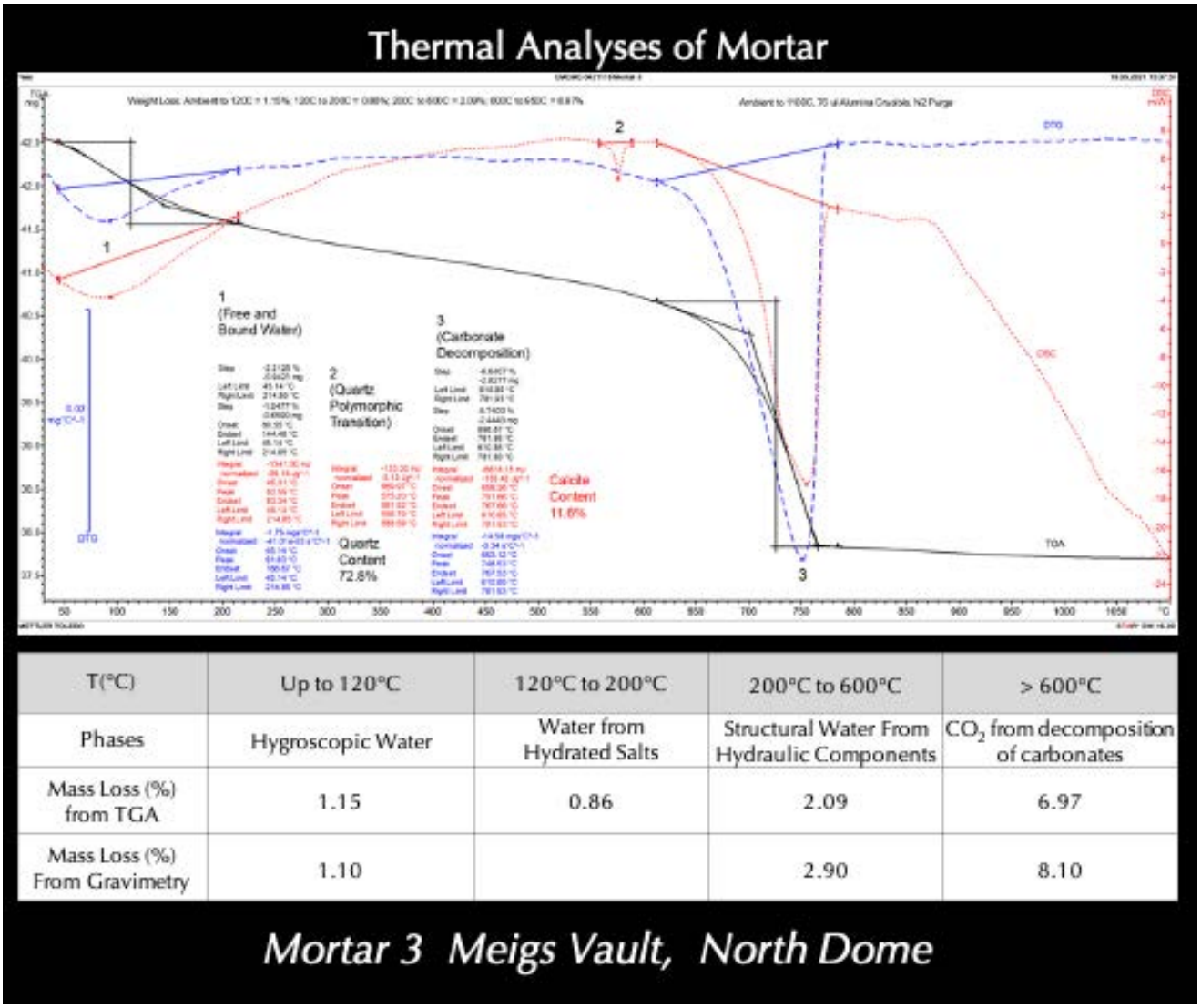

T(°C)	Up to 120°C	120°C to 200°C	200°C to 600°C	> 600°C
Phases	Hygroscopic Water	Water from Hydrated Salts	Structural Water From Hydraulic Components	CO_2 from decomposition of carbonates
Mass Loss (%) from TGA	1.15	0.86	2.09	6.97
Mass Loss (%) From Gravimetry	1.10		2.90	8.10

Figure 46: TGA (in bold black), DSC (in dotted red), and DTG (in dashed blue) curves of Mortar #3 showing losses in weight due to decompositions (loss of water and carbon dioxide) of various phases during controlled heating in a Mettler-Toledo's simultaneous TGA/DSC 1 unit from 30ºC to 1000ºC in a ceramic crucible (alumina 70µl, no lid) at a heating rate of 10ºC/min in a nitrogen purge at a rate of 75 mL/min. Dehydration and decarbonation reactions are marked as endothermic peaks in the DTG curve, whereas alpha to beta-form polymorphic transition of quartz is marked at the characteristic temperature of 573ºC in the DSC curve.

In the DTG curve, losses in weights are detected at (i) Peak #1 from the loss of water, and (ii) Peak #2 from bound water. Peak #3 shows dehydroxylation of hydrated phases. DSC curve in Peak #4 shows polymorphic transition from alpha to beta form of quartz around 575ºC from silica (quartz) sand. Semi-quantitative estimates of quartz and calcite are determined from DSC results. Calcite content is consistent with carbonated nature of the mortar from its carbonated natural cement-lime composition. Results of thermal analyses are therefore consistent with the results obtained from microscopy and XRD studies.

Notice similar results obtained from thermal analysis and gravimetry for mass losses from loss of free water (up to 120ºC), structural water (200 to 600ºC), and carbonation (600 to 950 ºC), respectively.

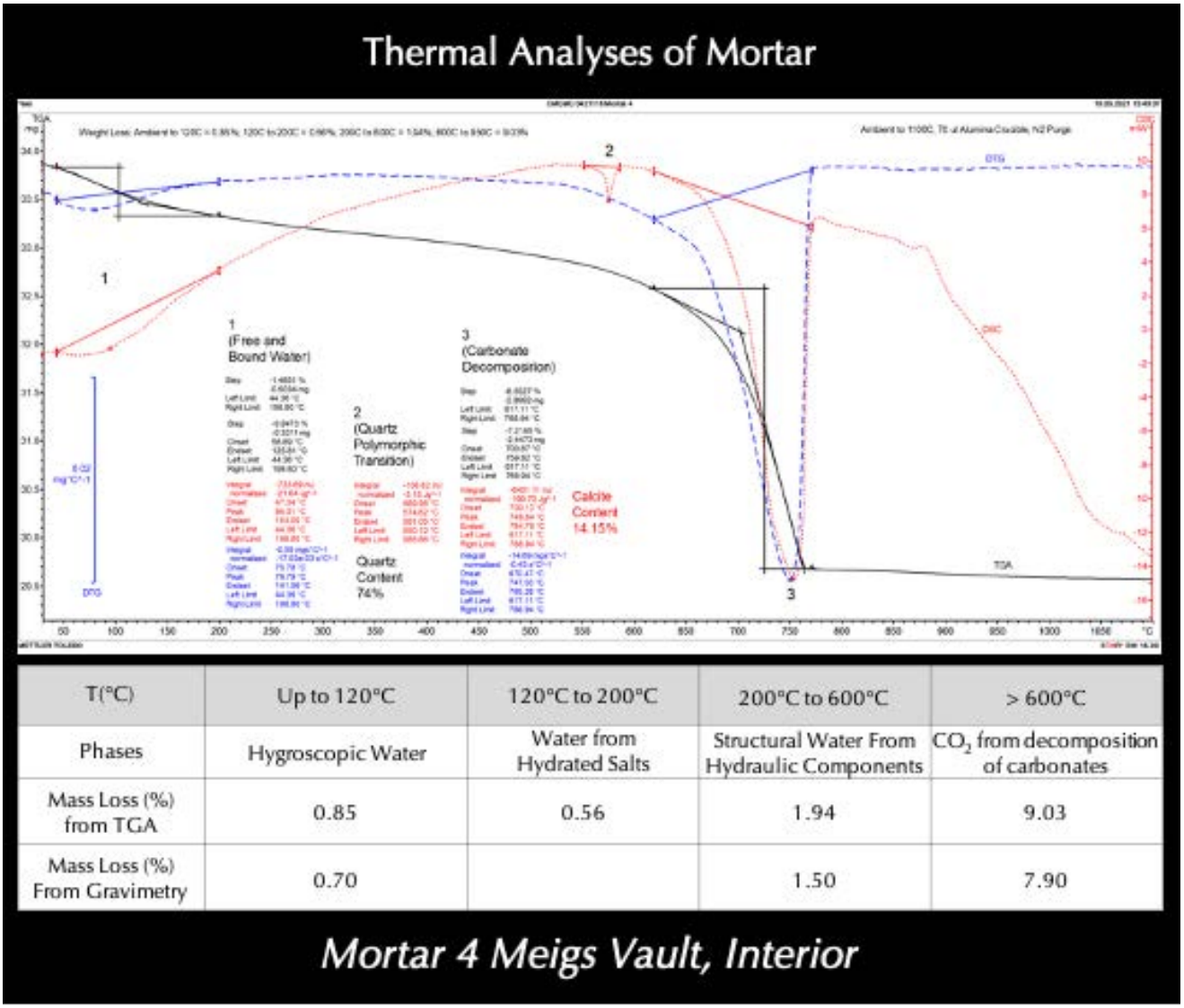

T(°C)	Up to 120°C	120°C to 200°C	200°C to 600°C	> 600°C
Phases	Hygroscopic Water	Water from Hydrated Salts	Structural Water From Hydraulic Components	CO_2 from decomposition of carbonates
Mass Loss (%) from TGA	0.85	0.56	1.94	9.03
Mass Loss (%) From Gravimetry	0.70		1.50	7.90

Figure 47: TGA (in bold black), DSC (in dotted red), and DTG (in dashed blue) curves of Mortar #4 showing losses in weight due to decompositions (loss of water and carbon dioxide) of various phases during controlled heating in a Mettler-Toledo's simultaneous TGA/DSC 1 unit from 30ºC to 1000ºC in a ceramic crucible (alumina 70µl, no lid) at a heating rate of 10ºC/min in a nitrogen purge at a rate of 75 mL/min. Dehydration and decarbonation reactions are marked as endothermic peaks in the DTG curve, whereas alpha to beta-form polymorphic transition of quartz is marked at the characteristic temperature of 573ºC in the DSC curve.

In the DTG curve, losses in weights are detected at (i) Peak #1 from the loss of water, and (ii) Peak #2 from bound water. Peak #3 shows dehydroxylation of hydrated phases. DSC curve in Peak #4 shows polymorphic transition from alpha to beta form of quartz around 575ºC from silica (quartz) sand. Semi-quantitative estimates of quartz and calcite are determined from DSC results. Calcite content is consistent with carbonated nature of the mortar from its carbonated natural cement-lime composition. Results of thermal analyses are therefore consistent with the results obtained from microscopy and XRD studies.

Notice similar results obtained from thermal analysis and gravimetry for mass losses from loss of free water (up to 120ºC), structural water (200 to 600ºC), and carbonation (600 to 950 ºC), respectively.

Ion Chromatography of Mortars

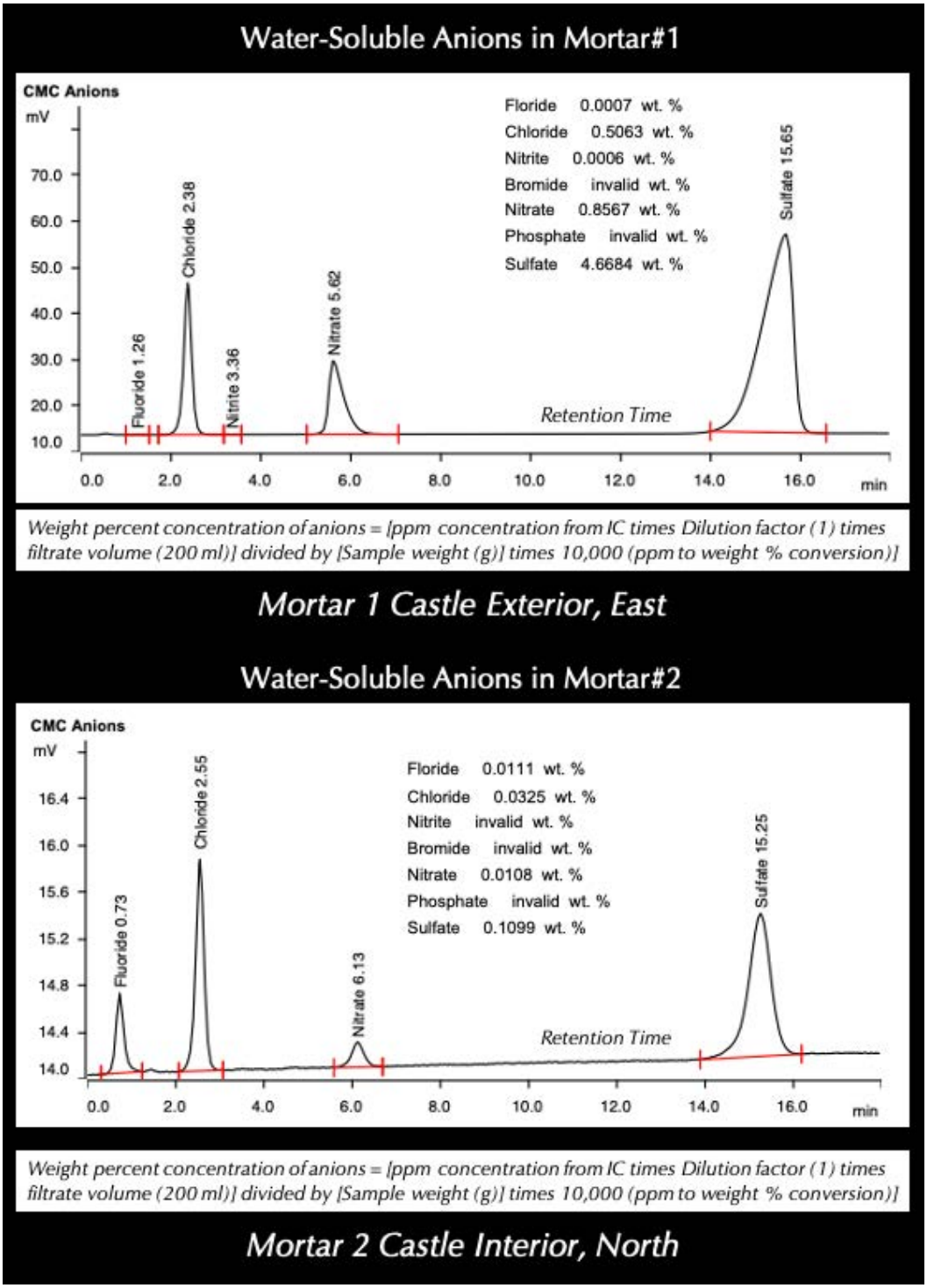

Figure 48: Anion chromatograms of water-soluble salts in Mortar #1 and 2 from the Castle after digesting about a gram of pulverized mortar from each sample in deionized water for 30 minutes at a temperature below boiling, followed by continued digestion in water at the ambient laboratory condition for 24 hours. The filtrate was analyzed by ion chromatography. Results showed measurable anions, particularly of chloride and sulfate, especially in Mortar #1 for sulfate, which is consistent with detection of gypsum salt in the XRD analysis of this mortar.

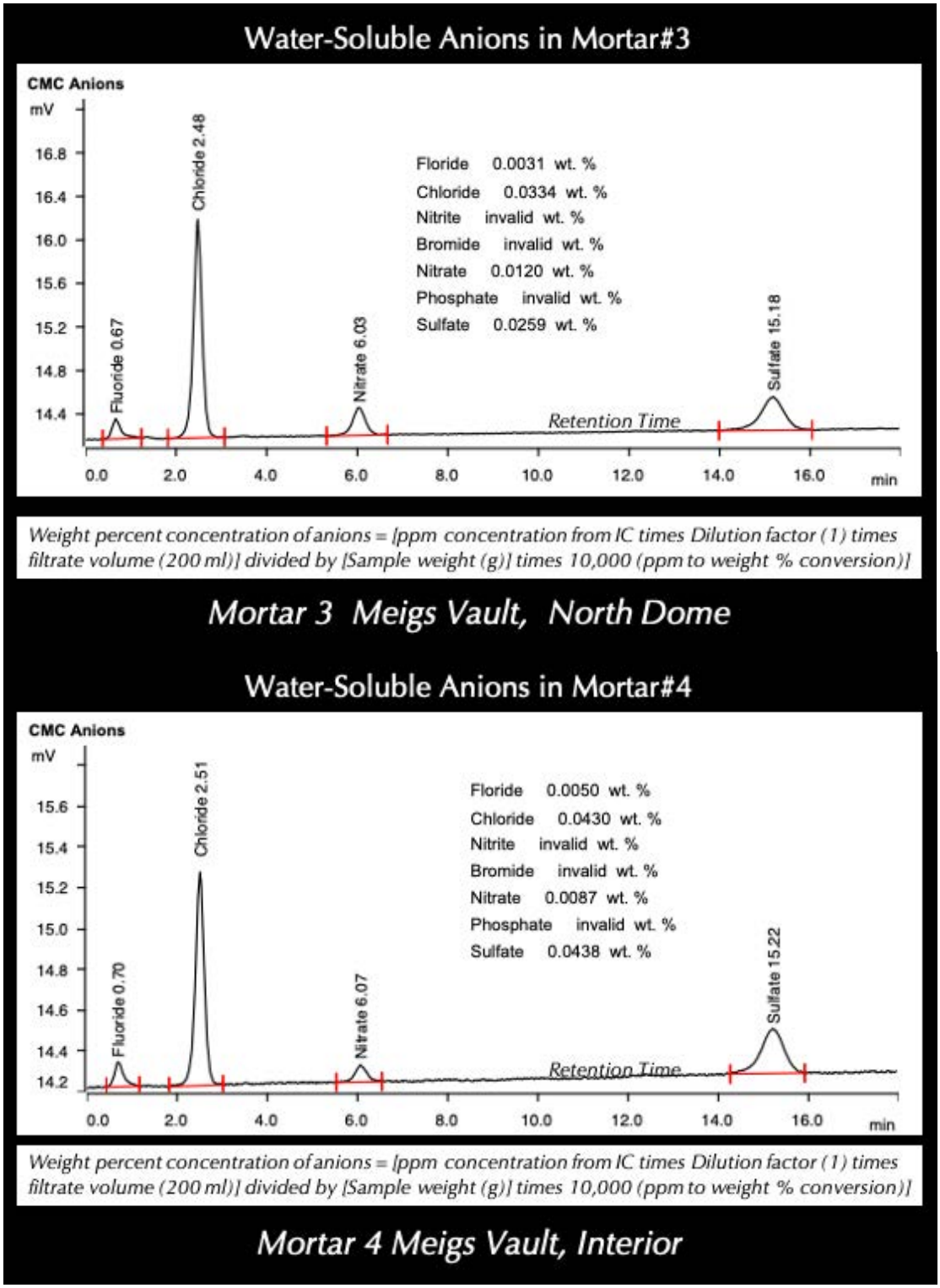

Figure 49: Anion chromatograms of water-soluble salts in Mortar #1 and 2 from the Castle after digesting about a gram of pulverized mortar from each sample in deionized water for 30 minutes at a temperature below boiling, followed by continued digestion in water at the ambient laboratory condition for 24 hours. The filtrate was analyzed by ion chromatography.

DISCUSSIONS

Types of Mortars & Ingredients

Optical microscopy of four mortar samples from Castle and Meigs Vault have determined dominantly natural cement and magnesian lime compositions of mortars, particles of the ones from Castle and the interior of Meigs Vault whereas severely altered and leached dominantly lime based composition of the mortar rom North Dome of Meigs Vault. Sand compositions are similar, consistent between all four mortars, and are all excessively fine-grained, close to the silt-size fractions (mostly 0.2 mm or less of the entire sand size range of 2 mm and 0.05 mm), and made using major amount of quartz and subordinate amounts of quartzite, feldspar, and other siliceous components. Sand in the two mortars from the Meigs Vault contained muscovite and biotite flakes from use of micaeous schist grains that are not found in the mortar from the Castle. The siliceous sand, natural cement, and lime compositions of all four mortars are determined from: (a) the characteristic mineralogies of sands and binders; (b) microstructures and compositions of paste having overall variably dense and carbonated paste having scattered grains of incompletely calcined residual raw feeds of natural cements showing the typical original argillaceous limestone composition of the natural cement feed; and (c) dominantly quartz-based compositions from optical microsocpy, XRD, and acid-insoluble residue content analyses. Sand was probably derived from the nearby Potomac river, which was excessviely finer than the typical ASTM C 144 masonry sand. SEM-EDS analyses of interstitial paste fractions of mortars have confirmed the presence of a natural cement and a magnesian lime binder as well as the hydraulic nature of the binder from the silica contents of paste. XRD analysis has confirmed dominant quartz from quartz sand and subordinate calcite from carbonated lime paste along with phases contributed from natural cement. XRF studies of acid and alkali-digested filtrates of mortars showed detectable soluble silica from the hydraulic binders. Results obtained from microscopy, and chemical analyses are all consistent, confirmatory to each other, and provided a comprehensive understanding of mortars, which was determined to be prepared from mixing natural cement, magnesian lime, and excessively fine-grained silica sand. Mortar from Castle is slightly different from that from Meigs Vault in lacking mica in sand and having an overall higher proportion of natural cement binder. The high lime and severely altered (leached) nature of Mortar #3 from North Dome of Meigs Vault is indicative of corrosive action of water in the mortar.

Stucco Coats

Contrary to the mortars, the stucco sample received is made using Portland cement and silica sand. Stucco contains three distinct layers: (a) an interior medium gray scratch coat, approximately 18 mm in nominal thickness applied over the brick masonry, which contains expanded metal lath reinforcement present as large voids (circled) mostly at the upper end of the scratch coat as opposed to the more common installation of mesh at the lower end, i.e. closest to the brick wall on which the coat was applied; (b) a thin dark gray intermediate brown coat, approximately 3 to 5 mm in nominal thickness, well-bonded to the scratch coat but is noticeably denser and darker gray in color tone due to lower water-cement ratio of the coat compared to the underlying scratch coat; and, finally, (c) a thin finish coat, approximately 4 mm in nominal thickness, which is also well-bonded to the intermediate dark gray brown coat but is lighter gray in color tone, indicating an inherently higher water-cement ratio, more similar to the innermost scratch coat. The finish coat has a sand-texture finish. Although all three coats are well-bonded to each other in the small fragment received, such differential water-cement ratios of three coats can potentially led to differential drying shrinkage and potential shrinkage-related cracking and debonding of the coats.

Mix Calculations of Mortars

Information obtained from: (a) chemical analyses of mortars to determine the soluble silica contents, water contents, and insoluble residue contents, and, (b) determination of use of natural cement and magnesian lime composition of binders in the mortars from microscopy and chemical analyses are useful for calculation of the natural cement and lime and sand contents, and, eventually, the volumetric proportions of ingredients of mortars. However, due to the extreme variability of compositions of natural cements conventional calculations of mix proportions according

to the procedures of ASTM C 1324 recommended for modern-day cement-lime or masonry cement mortars is not feasible. Therefore, the natural cement, lime and sand contents are estimated from the combined approach of microstructural and chemical analyses, which indicate use of natural cement to lime to sand at 1 to 1/2 to 5-7 proportions, respectively for the two mortars from Castle and 1 to 1 1/2 to 7 for the mortar from North Dome of Meigs Vault, and 1 to 1/2 to 10 for the mortar from interior of Meigs Vault, which is essentially an over-sanded mortar.

Conditions of Mortars

Extensive leaching and carbonation is noticed for the Mortar #3 from the North Dome of Meigs Vault. Gypsum salt precipitation is found in Mortar #1 from the exterior of east elevation of Castle, which was also confirmed by excessively high sulfate in the water-soluble filtrate in ion chromatography. No freezing-related distress is found in the samples. Sand was present in sound condition without any deleterious reactions with the binder.

Condition of Stucco

Contrary to reported cracking and delamination of stucco, the sample received showed no evidence of cracking or de-bonding where all three coats are well-bonded and present in sound condition. However, the detected differential water-cement ratios of three coats along with very different thickness of the scratch coat as opposed to similar thinner brown and finish coats (which are each less than half the thickness of scratch coat) can potentially lead to differential drying shrinkage and shrinkage-related cracking and debonding of the coats.

Replacement Mix For Mortars

Based on: (i) the determined natural cement, lime, and siliceous sand compositions of mortars from microscopy and chemical analyses; and (ii) 'estimated' volumetric proportions, a possible replacement mortar mix for the Castle could be made using: (a) 1-part natural cement to 1/2 part magnesian lime or a natural hydraulic lime (e.g., NHL 3.5), and (b) a modern ASTM C 144 masonry sand at 2 1/2 to 3 times the sum of volumetric proportions of cement and lime. Similar mix can be used for the Meigs Vault mortars even at the location of North Dome where a lime-rich highly altered mortar was detected. Sand to be used should match in color to the color of sand in the present mortars, preferably from a similar source, free of any debris, certainly not of as fine-grained as found in the samples, unsound, free of clay particles, or any potentially deleterious constituents, should conform to the size requirements of ASTM C 144 for masonry sand, and should be durable. Due to years of atmospheric weathering and alterations, an exact match in color to the existing mortars may not be possible, which, even if possible, could alter in future due to continued atmospheric weathering in the presence of oxygen, moisture, and other elements.

REFERENCES

ASTM C 10, "Standard Specification for Natural Cement," In Annual Book of ASTM Standards, Section Four Construction, Vol. 04.01 Cement; Lime; Gypsum; ASTM Committee C01 on Cement, 2017.

ASTM C 91, "Standard Specification for Masonry Cement," In Annual Book of ASTM Standards, Section Four Construction, Vol. 04.01 Cement; Lime; Gypsum; ASTM Committee C01 on Cement, 2017.

ASTM C 144, "Standard Specification for Aggregate for Masonry Mortar," In Annual Book of ASTM Standards, Section Four Construction, Vol. 04.05 Chemical-Resistant Nonmetallic Materials; Vitrified Clay Pipe; Concrete Pipe; Fiber-Reinforced Cement Products; Mortars or mortars and Grouts; Masonry; Precast Concrete; ASTM Committee C12 on Mortars or mortars for Unit Masonry, 2017.

ASTM C 1324, "Standard Test Method for Examination and Analysis of Hardened Masonry Mortar," In Annual Book of ASTM Standards, Section Four Construction, Vol. 04.05 Chemical-Resistant Nonmetallic Materials; Vitrified Clay Pipe; Concrete Pipe; Fiber-Reinforced Cement Products; Mortars or mortars and Grouts; Masonry; Precast Concrete; ASTM Committee C12 on Mortars or mortars for Unit Masonry, 2017.

ASTM C 270, "Standard Specification for Mortar for Unit Masonry," In Annual Book of ASTM Standards, Section Four Construction, Vol. 04.05 Chemical-Resistant Nonmetallic Materials; Vitrified Clay Pipe; Concrete Pipe; Fiber-Reinforced Cement Products; Mortars or mortars and Grouts; Masonry; Precast Concrete; ASTM Committee C12 on Mortars or mortars and Grouts for Unit Masonry, 2017.

ASTM C 1713, "Standard Specification for Mortars or mortars for the Repair of Historic Masonry," In Annual Book of ASTM Standards, Section Four Construction, Vol. 04.05 Chemical-Resistant Nonmetallic Materials; Vitrified Clay Pipe; Concrete Pipe; Fiber-Reinforced Cement Products; Mortars or mortars and Grouts; Masonry; Precast Concrete; ASTM Committee C12 on Mortars or mortars and Grouts for Unit Masonry, 2017.

ASTM C 51, "Standard Terminology Relating to Lime and Limestone (as used by the Industry)'" In Annual Book of ASTM Standards, Section Four Construction, Vol. 04.01 Cement; Lime; Gypsum; ASTM Committee C07 on Lime, 2017.

ASTM C 856, "Standard Practice for Petrographic Examination of Hardened Concrete," In Annual Book of ASTM Standards, Section Four Construction, Vol. 04.02; ASTM Subcommittee C 9.65, 2017.

ASTM C 1723, "Standard Guide for Examination of Hardened Concrete Using Scanning Electron Microscopy," In Annual Book of ASTM Standards, Section Four Construction, Vol. 04.02; ASTM Subcommittee C 9.65, 2017.

ASTM C 1329, "Standard Specification for Mortar Cement," In Annual Book of ASTM Standards, Section Four Construction, Vol. 04.01; ASTM Subcommittee C01.11, 2016.

ASTM C 150, "Standard Specification for Portland Cement," In Annual Book of ASTM Standards, Section Four Construction, Vol. 04.01; ASTM Subcommittee C01.10, 2018.

ASTM C 1489, "Standard Specification for Lime Putty for Structural Purposes," In Annual Book of ASTM Standards, Section Four Construction, Vol. 04.01; ASTM Subcommittee C07.02, 2015.

ASTM C 207, "Standard Specification for Hydrated Lime for Masonry Purposes," In Annual Book of ASTM Standards, Section Four Construction, Vol. 04.01; ASTM Subcommittee C07.02, 2011.

Bartos, P. Groot, C., and Hughes, J.J. (eds.), "Historic Mortars or mortars: Characteristics and Tests", Proceedings PRO12, RILEM Publications, France, 2000.

Boynton, R., *Chemistry and Technology of Lime and Limestone, 2nd edition*, John Wiley & Sons, Inc. 1980.

Brosnan, Denis, A., Characterization of Rosendale Mortars or mortars For Fort Sumter National Monument and Degradation of Mortars or mortars by Sea Water and Frost Action, Final Report, April 19, 2012.

Callebaut, K., Elsen, J., Van Balen, K., and Viaene, W., "Nineteenth century hydraulic restoration mortars or mortars in the Saint Michael's Church (Leuven, Belgium) Natural hydraulic lime or cement?" Cement and Concrete Research, V 31, pp 397-403, 2001.

Callebaut, K., Elsen, J., Van Balen, K., and Viaene, W., Historical and scientific study of hydraulic mortars or mortars from the 19th century. In International RILEM workshop on historic mortars or mortars: Characterization and Tests; Paisley, Scotland, 12th to 14th May 1999, Edited by Barton, P., Groot, C., and Hughes, J.J., Cachan, France, RILEM Publications, 2000.

Charloa, A.E., "Mortar analysis: A comparison of European procedures." US/ICOMOS Scientific Journal: Historic Mortars or mortars & Acidic Deposition on Stone, 3 (1), pp. 2-5, 2001.

Charola, A.E., and Lazzarin, L., Deterioration of Brick Masonry Caused by Acid Rain, ACS Symposium Series, Vol. 318, pp. 250-258, 2009.

Chiari, G., Torraca, G., and Santarelli, M.L., "Recommendations for Systematic Instrumental Analysis of Ancient Mortars or mortars: The Italian Experience", *Standards for Preservation and Rehabilitation*, ASTM STP 1258, S.J. Kelley, ed., American Society for Testing and Materials, pp. 275-284, 1996.

Doebley, C.E., and Spitzer, D., "Guidelines and Standards for Testing Historic Mortars or mortars", *Standards for Preservation and Rehabilitation*, ASTM STP 1258, S.J. Kelley, ed., American Society for Testing and Materials, pp. 285-293, 1996.

Eckel, Edwin, C., *Cements, Limes, and Plasters*, John Wiley & Sons, Inc. 655 pp, 1922.

Edison, M.P. (Editor), *Natural Cement*, ASTM STP 1494, American Society for Testing and Materials, 2008.

Elsen, J., "Microscopy of Historic Mortars or mortars – A Review", *Cement and Concrete Research 36*, 1416-1424, 2006.

Elsen, J., Mertens, G., and Van Balen, K., Raw materials used in ancient mortars or mortars from the Cathedral of Notre-Dame in Tournai (Belgium), Eur. J. Mineral., Vol. 23, pp. 871-882, 2011.

Elsen, J., Van Balen, K., and Mertens, G., Hydraulicity in Historic Lime Mortars or mortars: A Review, In, Valek, J, Hughes, J.J., and Groot, W.P. (Eds.), Historic Mortars or mortars Characterization, Assessment and Repair, RILEM Book series, Volume 7, pp. 125-139, Springer, 2012.

Erlin, B., and Hime, W.G., "Evaluating Mortar Deterioration", *APT Bulletin*, Vol. 19, No. 4, pp. 8-10+54, 1987.

Goins E.S., "Standard Practice for Determining the Components of Historic Cementitious Materials," National Center for Preservation Technology and Training, Materials Research Series, NCPTT 2004.

Goins, E.S., "A standard method for the characterization of historic cementitious materials." US/ICOMOS Scientific Journal: Historic Mortars or mortars & Acidic Deposition on Stone, # (1), pp. 6-7, 2001.

Groot, C., Ashall, G., and Hughes, J., Characterization of Old Mortars or mortars with Respect to their Repair, State-of-the-art Report of RILEM Technical Committee 167-COM, 2004.

Hughes, D.C., Jaglin, D., Kozlowski, R., Mayr, N., Mucha, D., and Weber, J., "Calcination of Marls to Produce Roman Cement", pp. 84-95, In, Edison, M.P. (Editor), *Natural Cement*, ASTM STP 1494, American Society for Testing and Materials, 2007.

Hughes, J.J., Cuthbert, S., and, Bartos, P., "Alteration Textures in Historic Scottish Lime Mortars or mortars and the Implications for Practical Mortar Analysis", *Proceedings of the 7th Euroseminar on Microscopy Applied to Building Materials*, Delft, pp. 417-426, 1999.

Hughes, R.E., and Bargh, B.L., The weathering of brick: Causes, Assessment and Measurement, A Report of the Joint Agreement between the U.S. Geological Survey and the Illinois State Geological Survey, 1982.

Jana, D., "Application of Petrography In Restoration of Historic Masonry Structures", In: Hughes, J.J., Lesie, A.B. and Walsh, J.A., eds. *Proceedings of 10th Euroseminar on Microscopy Applied to Building Materials*, Paisley, 2005.

Jana, D., "Sample Preparation Techniques in Petrographic Examinations of Construction Materials: A State-of-the-art Review", *Proceedings of the 28th Conference on Cement Microscopy*, International Cement Microcopy Association, Denver, Colorado, pp. 23-70, 2006.

Jedrzejewska, H., Old mortars or mortars in Poland: a new method of investigation, Studies in Conservation 5, pp. 132-138, 1960.

Leslie, A.B., and Hughes, J.J., "Binder Microstructure in Lime Mortars or mortars: Implications for the Interpretation of Analysis Results", *Quarterly Journal of Engineering Geology & Hydrogeology*, V. 35, No. 3, pp. 257-263, 2001.

Lubell, B., van Hees, Rob. P.J., and Groot, Casper J.W.P., The role of sea salts in the occurrence of different damage mechanisms and decay on brick masonry, Construction and Building Materials, Vol. 18, pp. 119-124, 2004.

Martinet, G., Quenee, B., Proposal for a useful methodology for the study of ancient mortars or mortars, Proceedings of the International RILEM workshop "Historic Mortars or mortars: Characteristics and tests," Paisley, pp. 81-91, 2000.

Mack, Robert, and Speweik, John P., *Preservation Briefs 2*, U.S. Department of the Interior, National Park Service Cultural Resources, Heritage Preservation Services, pp. 1-16, 1998.

Middendorf, B., Baronio, G., Callebaut, K, and Hughes, J.J., "Chemical-mineralogical and physical-mechanical investigation of old mortars or mortars, Proceedings of the International RILEM workshop "Historic Mortars or mortars: Characteristics and tests," Paisley, pp. 53-61, 2000.

Middendorf, B., Hughes, J.J., Callebaut, K., Baronio, G., and Papayanni, I., Mineralogical characterization of historic mortars or mortars, In. Groot, C., et al. (eds), Characterization of Old Mortars or mortars with Respect to their Repair, State-of-the-art Report of RILEM Technical Committee 167-COM, pp. 21-36, 2004a.

Middendorf, B., Hughes, J.J., Callebaut, K., Baronio, G., and Papayanni, I., Chemical characterization of historic mortars or mortars, In. Groot, C., et al. (eds), Characterization of Old Mortars or mortars with Respect to their Repair, State-of-the-art Report of RILEM Technical Committee 167-COM, pp. 37-53, 2004b.

Middendorf, B., Hughes, J.J., Callebaut, K., Baronio, G., and Papayanni, I., "Investigative Methods for the Characterization of Historic Mortars or mortars – Part 1: Mineralogical Characterization," *Materials and Structures*, Vol. 38, 2005a.

Middendorf, B., Hughes, J.J., Callebaut, K., Baronio, G., and Papayanni, I., "Investigative Methods for the Characterization of Historic Mortars or mortars – Part 2: Chemical Characterization," *Materials and Structures*, Vol. 38, pp 771-780, 2005b.

Sarkar, S.L., Aimin, Xu, and Jana, Dipayan, Scanning electron microscopy and X-ray microanalysis of Concretes, pp. 231-274, In, Ramachandran, V.S. and Beaudoin, J.J. Handbook of Analytical Techniques in Concrete Science and Technology, Noyes Publications, Park Ridge, New Jersey, 2000.

Speweik, J.P., *The History of Masonry Mortar in America 1720-1995*, 2010.

Stewart, J., and Moore, J., Chemical techniques of historic mortar analysis, Proceedings of the ICCROM Symposium "Mortars or mortars, Cements, and Grouts used in the Conservation of Historic Buildings," Rome, ICCROM, Rome, pp. 297-310, 1981.

Valek, J., Hughes, J.J., and Groot, C. (eds.), *Historic Mortars or mortars: Characterization, Assessment and Repair*, Springer, RILEM Book series Vol. 7, p. 464, 2012.

Valek, J., Hughes, J.J., and Groot, C. (eds.), Historic Mortars or mortars: Characterization, Assessment and Repair, Springer, RILEM Book series Vol. 7, 2012.

Van Balen, K., Toumbakari, E.E., Blanco, M.T., Aguilera, J., Puertas, F., Sabbioni, C., Zappia, G., Riontino, C., and Gobbi, G., "Procedures for mortar type identification: A proposal." In International RILEM workshop on historic mortars or mortars: Characteristics and Tests; Paisley, Scotland, 13th to 14th May 1999, edited by Barton, P., Groot, C., and Hughes, J.J., Cachan, France: RILEM Publications, 2000.

Vyskocilova, R., W. Schwarz, D. Mucha, D. Hughes, R. Kozlowski, and J. Weber, "Hydration processes in pastes of roman and American natural cements," *ASTM STP*, vol. 4, no. 2, 2007.

Weber, J., Gadermayr, N., Kozlowski, R., Mucha, D., Hughes, D., Jaglin, D., and Schwarz, W., Microstructure and mineral composition of Roman cements produced at defined calcination conditions, Materials Characterization, Vol. 58, pp. 1217-1228, 2007.

✪ ✪ ✪ END OF TEXT ✪ ✪ ✪

END OF REPORT[2]

[2] The CMC logo is made using a lapped polished section of a 1930's concrete from an underground tunnel in the U.S. Capitol.